NAVAL POSTGRADUATE SCHOOL

MONTEREY, CALIFORNIA

THESIS

AN EXPERIMENTAL INVESTIGATION OF THE PERFORMANCE OF STAGGERED PIN-FIN ARRAY LAMINAR FLOW HEAT EXCHANGERS

by

Matthew T. Harding

March 2005

Thesis Advisor: Ashok Gopinath

Approved for public release; distribution is unlimited

THIS PAGE INTENTIONALLY LEFT BLANK

REPORT DOCUMENTATION PAGE			Form Approved OMB No. 0704-0188
Public reporting burden for this collection of information is estimated to average 1 hour per response, including the time for reviewing instruction, searching existing data sources, gathering and maintaining the data needed, and completing and reviewing the collection of information. Send comments regarding this burden estimate or any other aspect of this collection of information, including suggestions for reducing this burden, to Washington headquarters Services, Directorate for Information Operations and Reports, 1215 Jefferson Davis Highway, Suite 1204, Arlington, VA 22202-4302, and to the Office of Management and Budget, Paperwork Reduction Project (0704-0188) Washington DC 20503.			
1. AGENCY USE ONLY ***(Leave blank)***	**2. REPORT DATE** March 2005	**3. REPORT TYPE AND DATES COVERED** Master's Thesis	
4. TITLE AND SUBTITLE: **An Experimental Investigation of the Performance of Staggered Pin-Fin Array Laminar Flow Heat Exchangers**			**5. FUNDING NUMBERS**
6. AUTHOR(S) Matthew T. Harding			
7. PERFORMING ORGANIZATION NAME(S) AND ADDRESS(ES) Naval Postgraduate School Monterey, CA 93943-5000			**8. PERFORMING ORGANIZATION REPORT NUMBER**
9. SPONSORING /MONITORING AGENCY NAME(S) AND ADDRESS(ES) Naval Air Systems Command Patuxent River, MD			**10. SPONSORING/MONITORING AGENCY REPORT NUMBER**
11. SUPPLEMENTARY NOTES The views expressed in this thesis are those of the author and do not reflect the official policy or position of the Department of Defense or the U.S. Government.			
12a. DISTRIBUTION / AVAILABILITY STATEMENT Approved for public release; distribution is unlimited			**12b. DISTRIBUTION CODE**

ABSTRACT *(maximum 200 words)*

This study concentrates on the empirical characterization of a staggered pin-fin array heat exchanger placed in a modular, rectangular wind tunnel. A full analysis of the heat transfer and pressure drop behavior was conducted on various pin-fin shapes, sizes, and configurations. The study was based on airflow over a wide range of Reynolds numbers in the laminar regime. The empirical data gathered can be used to corroborate and develop better numerical models to characterize the performance of such heat exchangers as well as scale down to the micro level for comparison with micro-heat exchangers.

14. SUBJECT TERMS compact heat exchanger, experimental study, pin-fin array			**15. NUMBER OF PAGES** 127
			16. PRICE CODE
17. SECURITY CLASSIFICATION OF REPORT Unclassified	**18. SECURITY CLASSIFICATION OF THIS PAGE** Unclassified	**19. SECURITY CLASSIFICATION OF ABSTRACT** Unclassified	**20. LIMITATION OF ABSTRACT** UL

NSN 7540-01-280-5500 Standard Form 298 (Rev. 2-89)
Prescribed by ANSI Std. 239-18

THIS PAGE INTENTIONALLY LEFT BLANK

Approved for public release; distribution is unlimited

AN EXPERIMENTAL INVESTIGATION OF THE PERFORMANCE OF STAGGERED PIN-FIN ARRAY LAMINAR FLOW HEAT EXCHANGERS

Matthew T. Harding
Lieutenant, United States Navy
B.S.M.E., Auburn University, 1998

Submitted in partial fulfillment of the
requirements for the degree of

MASTER OF SCIENCE IN MECHANICAL ENGINEERING

from the

NAVAL POSTGRADUATE SCHOOL
March 2005

Author: Matthew T. Harding

Approved by: Ashok Gopinath
Thesis Advisor

Anthony J. Healey
Chairman, Department of Mechanical Engineering

THIS PAGE INTENTIONALLY LEFT BLANK

ABSTRACT

This study concentrates on the empirical characterization of a staggered pin-fin array heat exchanger placed in a modular, rectangular wind tunnel. A full analysis of the heat transfer and pressure drop behavior was conducted on various pin-fin shapes, sizes, and configurations. The study was based on airflow over a wide range of Reynolds numbers in the laminar regime. The empirical data gathered can be used to corroborate and develop better numerical models to characterize the performance of such heat exchangers as well as scale down to the micro level for comparison with micro-heat exchangers.

THIS PAGE INTENTIONALLY LEFT BLANK

TABLE OF CONTENTS

LIST OF FIGURES

THIS PAGE INTENTIONALLY LEFT BLANK

LIST OF TABLES

THIS PAGE INTENTIONALLY LEFT BLANK

ACKNOWLEDGMENT

Without the guidance, assistance and patience of those who helped me complete my thesis; I wouldn't be writing this acknowledgement. I would like to thank Professor Ashok Gopinath for his dedication and time in advising me, as well as dealing with my constant and persistent nagging for more equipment and money throughout the thesis process.

I would also like to thank Tom Christian whose expertise with anything in the realm of data collection programs and devices was instrumental in the completion of my thesis.

Perhaps the one person who made the successful completion of my thesis a reality more than anyone else was Jim Lefler. Of course it is Jim's job at the machine shop to help build the pieces and parts necessary for students to complete their theses, but there is no doubt in my mind that Jim went above and beyond that which is expected. Jim spent hours, days and even weeks on properly building the Plexiglas enclosure for my heat exchanger section so that we could ensure airtight integrity and collect meaningful pressure drop data. Thanks for all the help, Jim.

Finally, I would like to thank my wonderful and beautiful wife Shel and my best little buddy Aidan, who have been at home enduring the long days at school. Without their patience and understanding, the thesis process would have been even more difficult than it was.

THIS PAGE INTENTIONALLY LEFT BLANK

I. INTRODUCTION

Compact heat exchangers (CHE's) have numerous applications that range from microelectronics to gas turbine blade cooling. CHE's have been studied extensively for years to try to maximize the heat transfer rate with minimal pressure drop to the fluid cooling the desired component. A common heat exchanged design is a short pin fin staggered array assembly. Ultimately, the goal of the CHE is to accumulate empirical data that can be used to verify numerical models, which are easier to implement and much more cost effective.

A rectangular shaped, short pin-fin heat exchanger consisting of 10 rows was developed by Ramthun (2003). All though this heat exchanger was not by definition a compact heat exchanger, it does have dimensions that are of the same magnitude as CHE's, and by use of the hydraulic diameter, this heat exchanger can be scaled down to the compact or micro level. The purpose of this heat exchanger was to validate numerical models developed by Boulares (2003) and Hamilton (2003). Initial testing showed that the heat exchanger data correlated well with these 3-D numerical models.

This thesis will further expand the experimental database established by Ramthun (2003) as well as Summers (2003). This thesis focused on pressure drop and heat transfer through the heat exchanger in laminar flow. The heat exchanger section was re-designed and encapsulated by Plexiglas plates to ensure airtight integrity. When dealing with low laminar flow, any air leak will exacerbate the error in the results. This thesis will also be used to validate results from Summers (2003), specifically his low laminar flow pressure drop data.

THIS PAGE INTENTIONALLY LEFT BLANK

II. BACKGROUND AND OBJECTIVES

A. BACKGROUND DISCUSSION

Shah (International Centre for Heat and Mass Transfer, Session 13) indicated that in order for a heat exchanger to be compact, its heat transfer area per unit volume needed to exceed 600-700 m^2/m^3. As previously stated, this heat exchanger is not a CHE, but is on the same order of magnitude and therefore this research is very relevant to previous studies in the field. Another defining ratio of a CHE is the height to diameter ratio (H/D). This heat exchanger uses short pins, which correspond to an H/D of less than five.

CHE study is of great importance due to its small size and weight as well as its ability to remove great amounts of heat with a smaller per unit volume density. Research is continuously being conducted on pin size, shape and geometry to maximize the heat transfer with minimum pressure drop. This research will ultimately be used to create numerical models that can be flexible to adjust to any size application. Numerical models are much more time and cost effective than empirical studies, but there must be enough empirical data first to corroborate the results of the numerical models. Also, since Reynolds number and Nusselt number are based on hydraulic diameter, the results at the macro level can be scaled down to the micro level. This research will also be used to compare results at the micro level to verify the validity of scaling down.

B. PREVIOUS WORK

There has been a great deal of study in the area of CHE's since the early 1980's. One of the pioneers of CHE study was VanFossen. His study in 1982 concluded that heat transfer coefficients from channels with short pin fins were much greater than those of plain channels with no fins. This is expected due to the significant increase in heat transfer surface area. He estimated the heat transfer coefficients on the pin surface were about 35% greater than the endwalls. These results were later corroborated by Sparrow (1984) in his study of cylinders attached to walls in a cross flow.

Metzger (1982), another forerunner in CHE study, experimented with a ten row staggered short pin-fin array CHE, similar to the one used in this thesis, with a specific focus on row-by-row analysis. He showed that the majority of the heat transfer occurred

in the first three to five rows of the assembly, and the peak heat transfer also occurred in this region.

Arora (1985) conducted research efforts toward varying pin geometry and showed that using elliptical pins would result in higher heat transfer rates with lower frictional losses, as long as the pins were perfectly aligned with the flow path.

Chyu (1990) conducted research on a CHE with an in-line and staggered array configuration. He used the naphthalene sublimation mass transfer technique, which measures the heat transfer at various points in the heat exchanger based on the amount of erosion of the naphthalene fillets. The results verified the row-by-row results obtained by Metzger (1982). The fillets however resulted in the undesirable side effects of higher friction and lower heat transfer.

Research conducted by Al Dabagh in 1992, contradicted results from VanFossen (1982) in regards to pin vs. endwall heat transfer contributions. Al Dabagh showed that the endwall heat transfer coefficients were 15-35% higher than the pins, whereas the earlier research showed that the pins heat transfer coefficients were 35% higher than the endwalls. This discrepancy was the focus of research done by Chyu in 1999. His results corroborated the earlier results of VanFossen (1982) vice the newer results of Al Dabagh (1992). Chyu's (1999) results showed that the pins heat transfer coefficients were 10-20% higher than the endwalls.

Early 1990's research conducted by Jurban (1993) focused on optimization of the pin-fin array. Ultimately, his results showed that staggered arrays always outperformed in-line arrays regardless of changing shroud clearance-to-height ratio. His results also showed that the optimum X/D and S/D were both 2.5. His experiments involved long pins however, making it difficult to compare with short pin results.

In 1998 Li conducted research that compared elliptical pins to cylindrical. His conclusions support the results of Arora (1989) in which the elliptical pins showed higher heat transfer rate and lower pressure drop than the cylindrical pins. The elliptical pins however, showed a decrease in Nusselt number compared to the elliptical pins.

With the turn of the century, numerical modeling became the focus of heat exchanger research and design. Donahoo (2001) developed a 2-D numerical model to

optimize a staggered pin-fin array. His results agreed with the earlier work by Metzger (1982) that showed that maximum heat transfer occurred between the third and fifth row. The 2-D model showed promise, however, did not take into account the effect of pin height.

In 2001, Adametz developed a 3-D numerical model. This model simulated conditions in a rectangular, staggered short pin-fin array heat exchanger to analyze heat transfer and differential pressure characteristics. His results showed that the endwall's heat transfer coefficients were 20-100% higher than that of the pins. This opposed the work of VanFossen (1982) and Chyu (1999) and supported the findings of Al Dabagh (1992). His results also showed that X/D = 1.5 and S/D = 1.75-2.0 produced the maximum heat transfer coefficient.

Hamilton (2003) used a 3-D numerical model to simulate the conditions of the heat exchanger Ramthun (2003) built. He successfully simulated the heat exchanger and investigated it over many pin shapes and configurations. The model worked well at predicting Nusselt numbers; however, significant errors occurred in the pressure drop and friction factor analysis.

Boulares (2003) also used a 3-D numerical model, but his research focused on optimizing a heat exchanger with teardrop shaped pins. He ultimately found that a configuration of S/D=X/D=1.5 was the optimum configuration. Similar to Hamilton (2003), experimental and numerical friction factors were not in agreement.

Summers (2003) did extensive experimentation on the heat exchanger Ramthun (2003) built. His research involved both laminar and turbulent flows for various pin diameters and configurations. His experiments showed good comparison to the numerical models in regards to heat transfer parameters, however, his results for friction factor did not match the numerical results. There was some concern about the heat exchanger test section having air leaks significant enough to corrupt the low laminar pressure drop data.

Rose (2004) and Roussakies (2004) designed, built and conducted experiments on a micro-heat exchanger. This micro-heat exchanger, along with numerical models, is the focus of heat exchanger work at the Naval Postgraduate School. Experiments conducted

on the heat exchanger Ramthun (2003) built are significant since they can be scaled down to the micro level and compared to the results of the micro-heat exchanger.

C. HEAT EXCHANGER RE-DESIGN

The heat exchanger section as originally designed had two major issues that needed to be corrected. The first issue was the placement of the thermocouples. The original design had the thermocouple wire placed under the heaters in a slot that was machined in the plate (Figure 1). The wire was routed through the screw holes in the heater strip as shown in Figure (2). This was initially a desirable place to put the thermocouple wire due to ease of replacement if necessary. However, as the heat exchanger was repeatedly taken apart to alter the pin configuration, the screwing and un-screwing of the screws that held the heat exchanger together began to wear on the thermocouple wires. This became so excessive that during Summers (2003) thesis data collection, it was common to have to replace a thermocouple before each run. The thermocouples could be easily repaired, but it became evident that the loss of operational time to repair and replace the thermocouples was too high. An alternative placement of the thermocouples needed to be investigated.

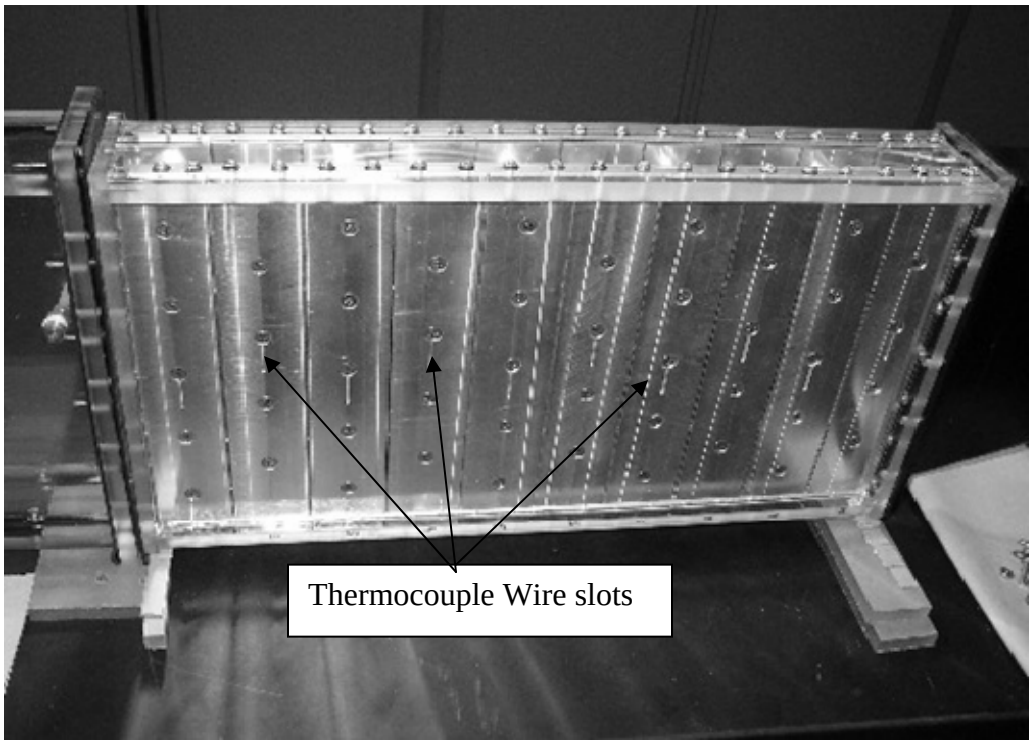

Figure 1. Old heat exchanger design

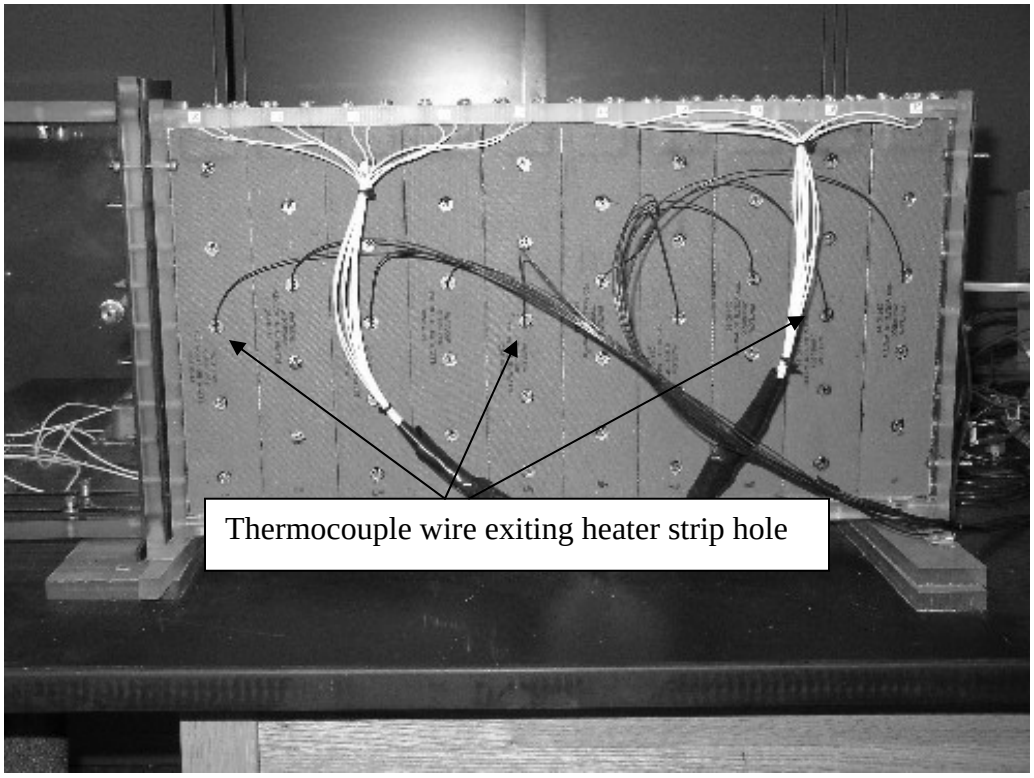

Figure 2. Old heat exchanger design

The second and most significant issue with the old heat exchanger design was its airtight integrity. As previously stated, any air leaks at very low flows greatly intensify the associated errors. At high Reynolds numbers, small air leaks are insignificant to the large flows through the test section. However, very small air leaks can be a significant portion of the flow through the test section in low laminar flows. The low laminar pressure drop data obtained by Summers is suspect due to this specific reason. That is the primary reason that a new design for the test section was planned and implemented.

The airtight integrity issue needed to be addressed first. A Plexiglas enclosure for the test section was deemed the most feasible and cost effective means to ensure the integrity of the system. The Plexiglas enclosure would consist of two halves (Figure 3) held together by the screws that hold the pins in contact to the plates. Once the two halves were put together, they would be connected to the inlet and exit sections of the assembly (Figure 4).

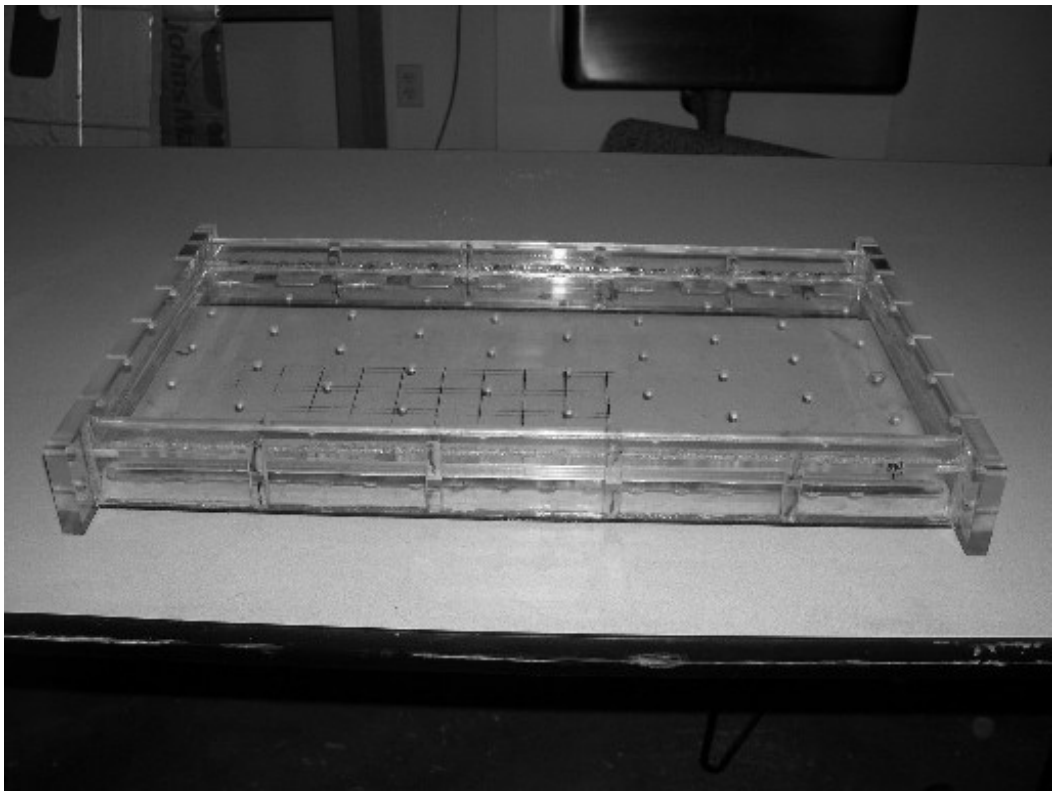

Figure 3. One half of Plexiglas enclosure

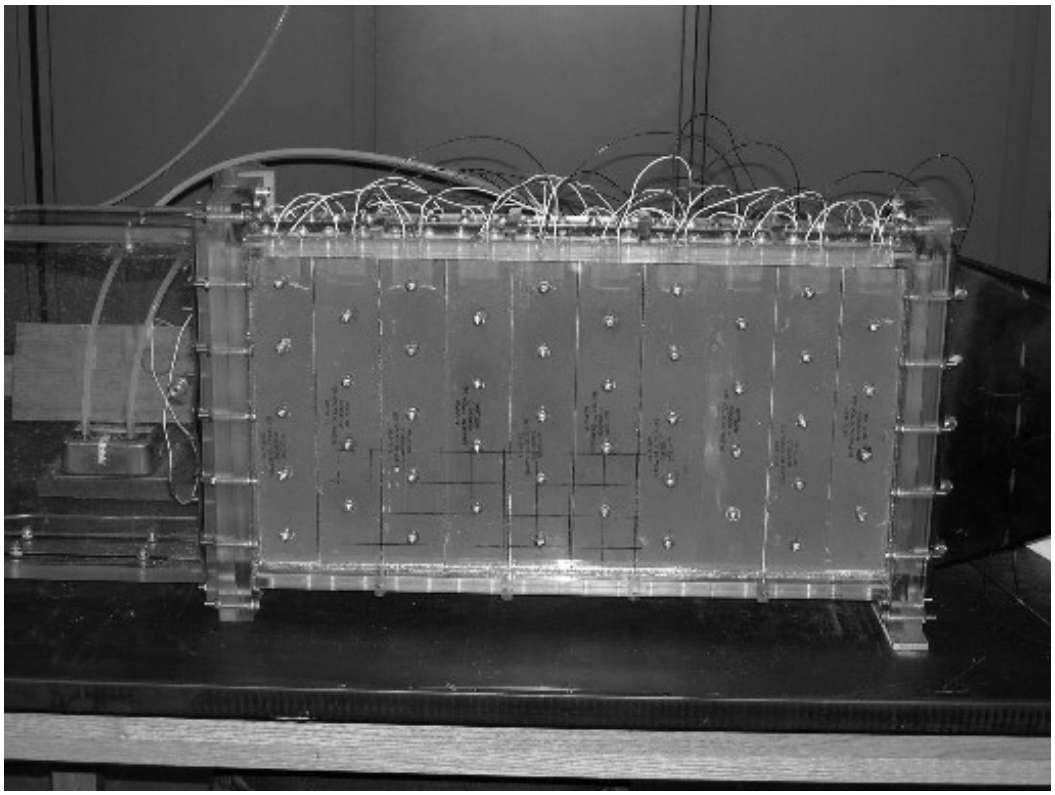

Figure 4. Complete test section

Due to the frequency at which the pin-fin array needed to be altered, the ease of disassembly and reassembly was also an important consideration. Once the entire assembly is together and connected to the inlet and exit sections, alteration of the pin-fin array is not difficult. One half of the test section would remain connected to the inlet and exit sections (Figure 5), while the other half would be removed. From here, it is simple to remove all or some of the pins and reassemble the heat exchanger section as necessary for the next pin configuration.

One of the biggest concerns with this new design was the placement of the thermocouple wires and the heater wires. It was determined that the slot in the two sidewalls (Figure 6) would be the best place for the wires to exit the test section. Similarly to the original design, an o-ring would be placed in a slot at the end of each plate to ensure that air would not leak past and out of the slot where the wires exited the test section.

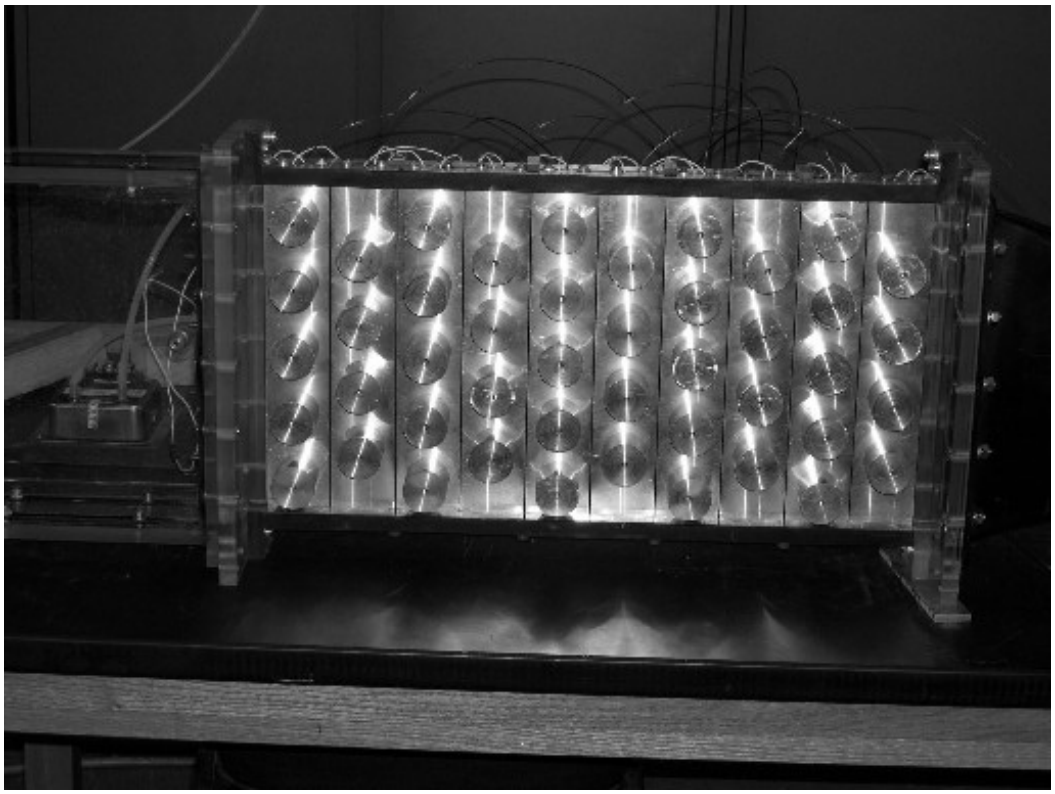

Figure 5. One half of test section

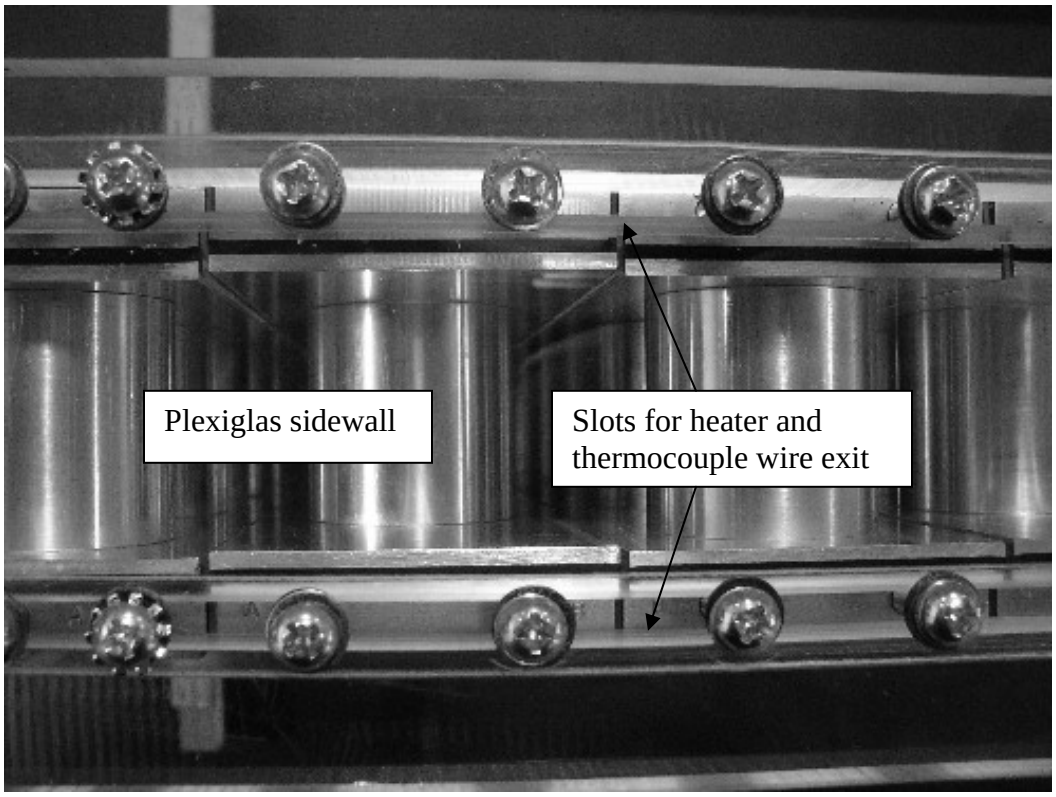

Figure 6. Slots in test section sidewalls

The original design had a slot cut into each plate for thermocouple wire placement. An extension to this slot (Figure 7) needed to be machined into each plate so that the thermocouple wire could exit the test section where the heater wires did. Once this slot was machined, the thermocouple wire was placed in the slot under the heater and routed along with the heater wires out of the test section.

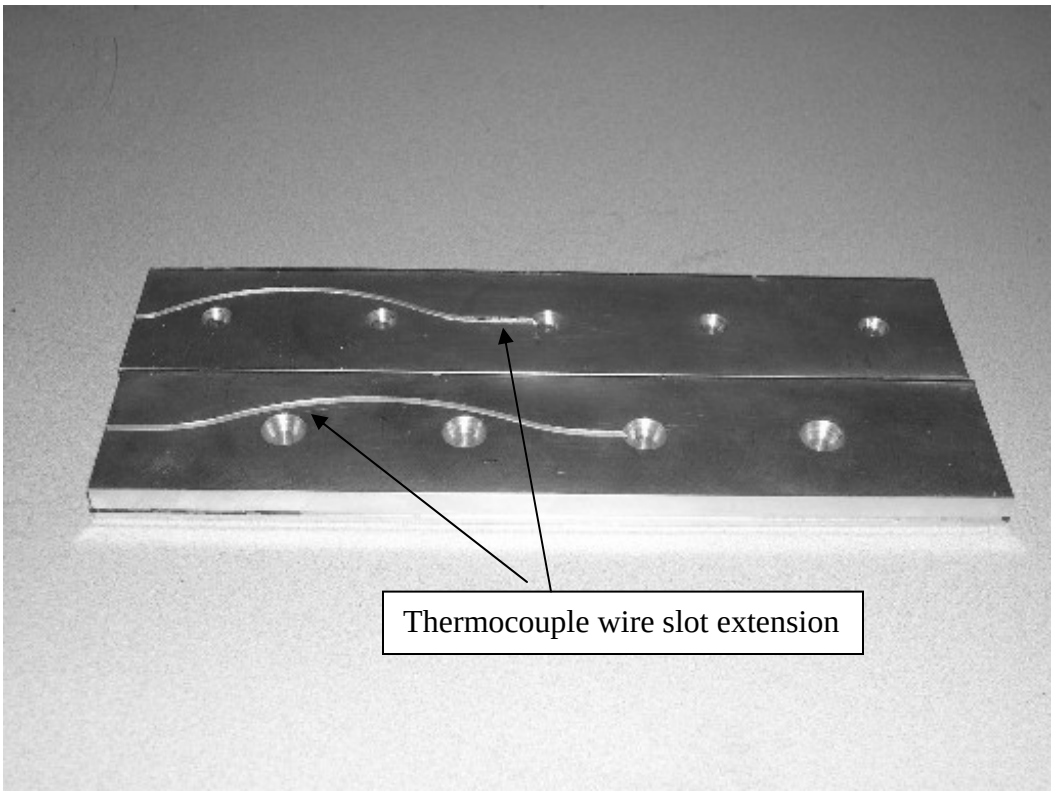

Figure 7. Plate slots for thermocouple wire

In the original design, the plates were thermally isolated from each other by using 1 mm Plexiglas strips. However, these spacers needed to be replaced frequently and were deemed inefficient. Instead of the strips, 1/32nd inch gasket material was used to provide thermal isolation as well as provide some cushion between the plates, which was desirable due to the very tight confines of the Plexiglas enclosure. The cushion of the gasket material between the plates allowed for easier installation of the plates into the Plexiglas enclosure.

D. OBJECTIVES

Ultimately, this heat exchanger was designed and built to verify numerical models, which are much more cost effective and flexible. The specific goals of this thesis are as follows:

1. Redesign and rebuild the heat exchanger text section to ensure airtight integrity.
2. Continue to collect and build upon the empirical database that has previously been collected on the following pin geometries: 10, 16.5, 33, and 66 mm circular pins as well as teardrop shaped pins.

3. Continue to collect and build upon the empirical database that has previously been collected on the following pin configurations: full ten-row analysis, X/D doubled and S/D the same, S/D doubled and X/D the same, and both X/D and S/D doubled.
4. Use the data collected to verify numerical models.
5. Compare results to micro-heat exchangers based on hydraulic diameter.
6. Validate low laminar flow pressure drop data previously collected.
7. Determine the optimum heat exchanger (for pin size, shape and configuration) based on fluid friction power per unit surface area (E (W/m^2)).

III. EXPERIMENTAL SETUP

A. OVERVIEW

Initially, the design of the test apparatus developed by Ramthun (2003) was as shown in Figure (8). The entrance duct was of sufficient length to allow for fully developed turbulent flow to enter the test section. The entrance duct, as well as the test section, was rectangular, and the downstream piping transitioned to circular. A blower drew air through the system and bypass valves were positioned to regulate flow through the test section. Summers (2003) made alterations to the initial apparatus to include low turbulent and laminar flows. For the laminar flows that this thesis deals with, the system setup was identical to Figure (8) with the exception of a throttle valve and a new mass flow meter being installed in place of the airflow meter.

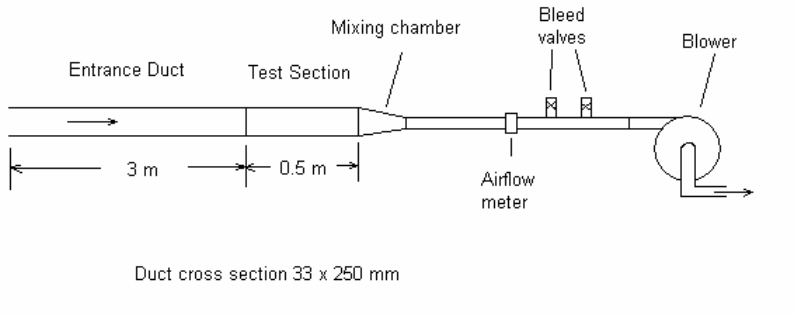

Figure 8. Original design of test apparatus

B. SYSTEM COMPONENTS

1. Inlet Section

The inlet section (Figure 9) was originally designed to accommodate both laminar and turbulent flows. This thesis deals only with laminar flow with Reynolds numbers between 100 and 2000. The inlet section is comprised of 3, meter long sections of a Plexiglas duct. Each section is 1 meter long, with a rectangular cross-section of 250mm by 33mm.

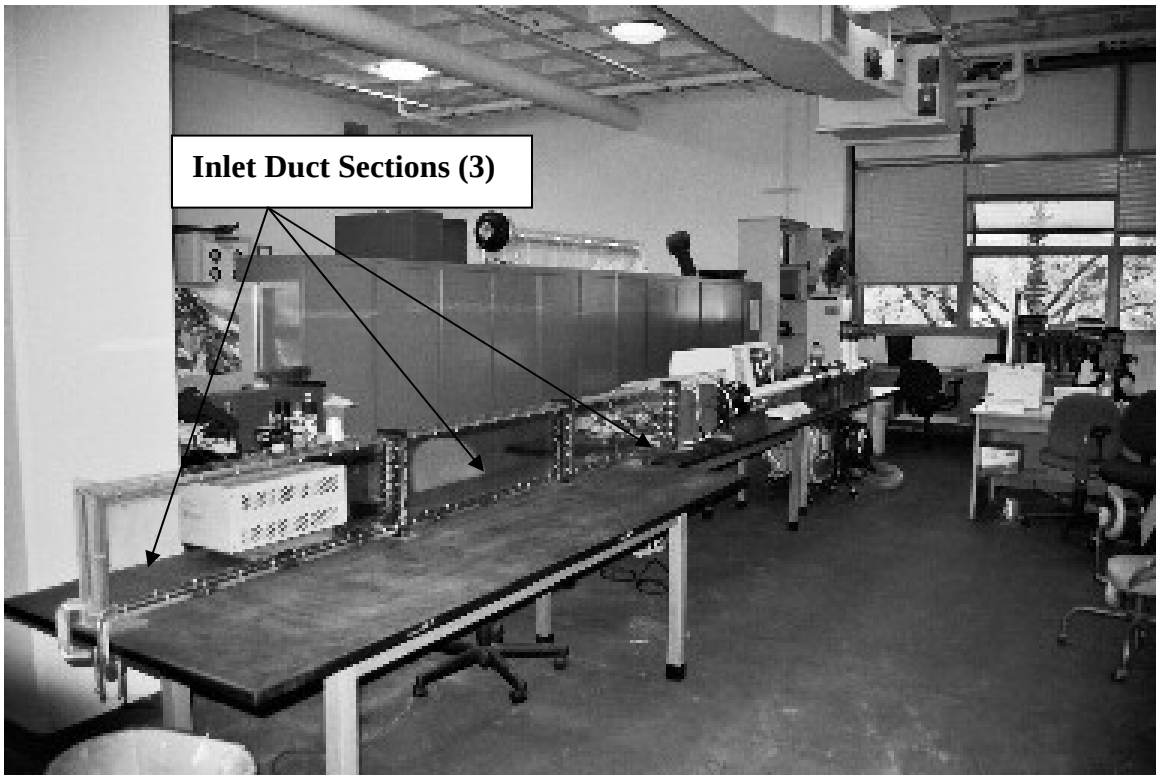

Figure 9. Inlet duct section

2. Heat Transfer Test Section

As previously discussed, the heat transfer test section was redesigned to ensure airtight integrity as well as allow for new thermocouple placement. The test section consisted of ten rows with each row having two 6061 T6 aluminum plates (Figure 10), four or five pins, two heaters and two thermocouples. Separating the plates were aluminum pins of various size and shape. One type E thermocouple (Figure 10) wire was placed in the slot machined in each plate. One 50-watt heater (Figure 10) was mounted over the thermocouple on each plate, and the thermocouple and heater wires were routed through the slot in the Plexiglas sidewalls. The thermocouples and heater were used to provide the heat input (up to 1000 watts) as well as temperature monitoring and control.

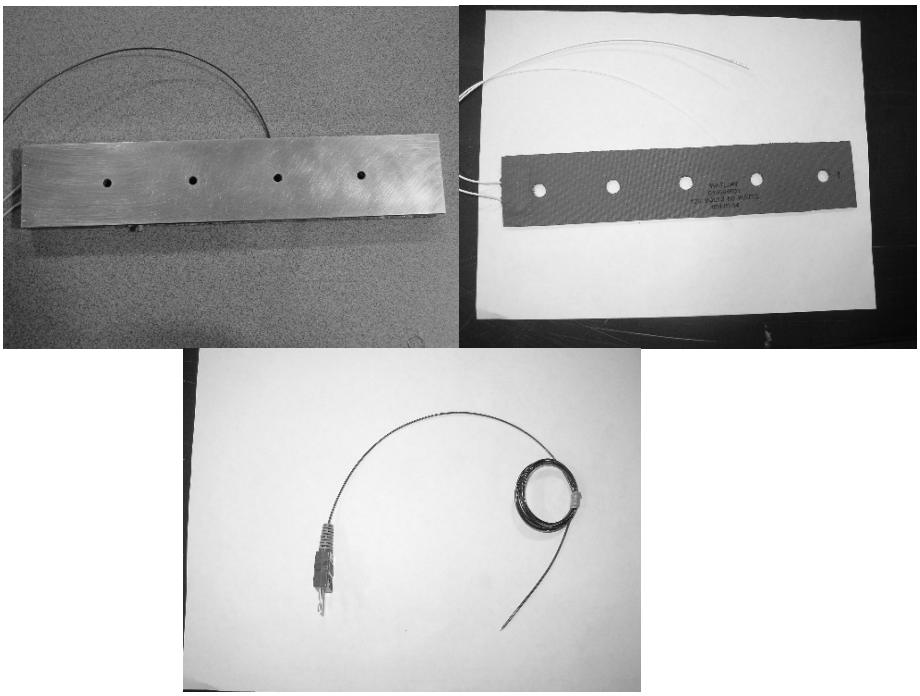

Figure 10. Aluminum plate, heating element and type E thermocouple

3. Heat Exchanger Pin-Fins

As shown in Figure (11), four different diameter (66, 33, 16.5 and 10 mm) cylindrical pins as well as a teardrop shaped pin (Figure 12) were used for data collection. These pins were constructed of the same aluminum as the plates. The pins were fastened to the plates by screws to ensure positive surface contact between the plates and the pins. Each pin had a height of 33mm therefore establishing the H/D ratio for each specific pin.

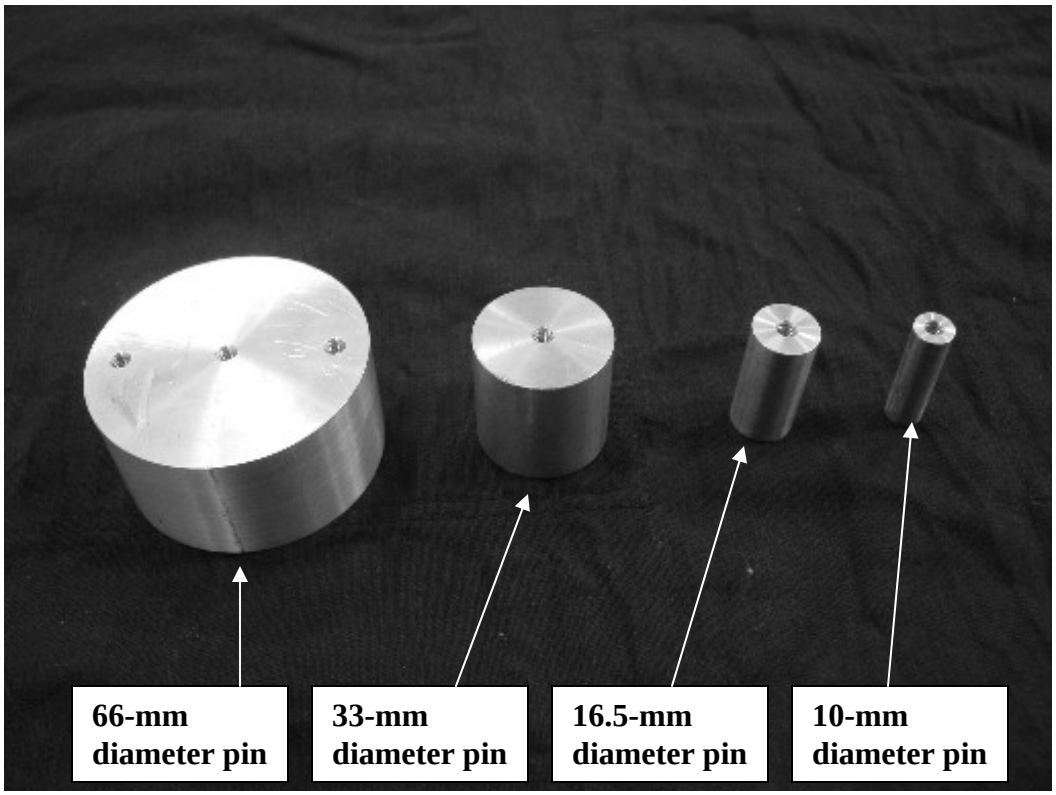

Figure 11. Cylindrical shaped pin-fins

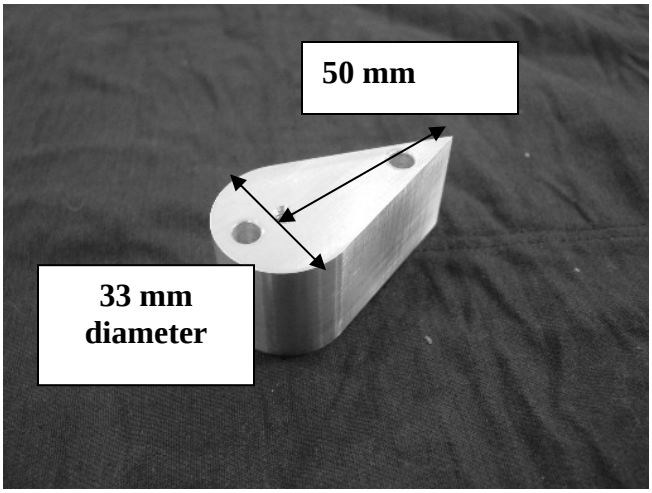

Figure 12. Teardrop shaped pin-fin

Throughout the thesis, pins would need to be removed and replaced frequently to achieve the necessary ratios of S/D, X/D and H/D as shown in Table (1). These ratios are defined in Figure (13). When pins were removed, non-fluted wooden dowels (Figure 14) were inserted in the plate holes vacated by the pin's associated screw. This was done to

maintain airtight integrity as well as to prevent any flow disruption through the test section.

Table 1. Pin configuration table

Diameter	Set 1	Set 2	Set 3	Set 4
10 mm	**S/D = 5.0 X/D = 5.0 H/D = 3.3 D_h=49.7mm**	**S/D = 10.0 X/D = 10.0 H/D = 3.3 D_h=53.6mm**	**S/D = 5.0 X/D = 10.0 H/D = 3.3 D_h=52.9mm**	**S/D = 10.0 X/D = 5.0 H/D = 3.3 D_h=53.3mm**
16.5 mm	**S/D = 3.0 X/D = 3.0 H/D = 2.0 D_h=44.7mm**	**S/D = 6.1 X/D = 6.0 H/D = 2.0 D_h=50.7mm**	**S/D = 3.0 X/D = 6.1 H/D = 2.0 D_h=49.5mm**	**S/D = 6.1 X/D = 3.0 H/D = 2.0 D_h=50.1mm**
33 mm	**S/D = 1.5 X/D = 1.5 H/D = 1.0 D_h=31.7mm**	**S/D = 3.0 X/D = 3.0 H/D = 1.0 D_h=43.1mm**	**S/D = 1.5 X/D = 3.0 H/D = 1.0 D_h=40.9mm**	**S/D = 3.0 X/D = 1.5 H/D = 1.0 D_h=42.0mm**
66 mm	**S/D = 1.89 X/D = 0.76 H/D = 0.5 D_h=39.2mm**	**Not Possible**	**S/D = 1.89 X/D = 1.5 H/D = 0.5 D_h=48.7mm**	**Not Possible**
Tear Drop	**S/D = 1.5 X/D = 1.5 H/D = 1.0 D_h=22.4mm**	**S/D = 3.0 X/D = 3.0 H/D = 1.0 D_h=36.8mm**	**S/D = 1.5 X/D = 3.0 H/D = 1.0 D_h=33.9mm**	**S/D = 3.0 X/D = 1.5 H/D = 1.0 D_h=35.3mm**
Two configurations were completed with the 66mm pins. Heat exchanger cannot accommodate set number two or four.				

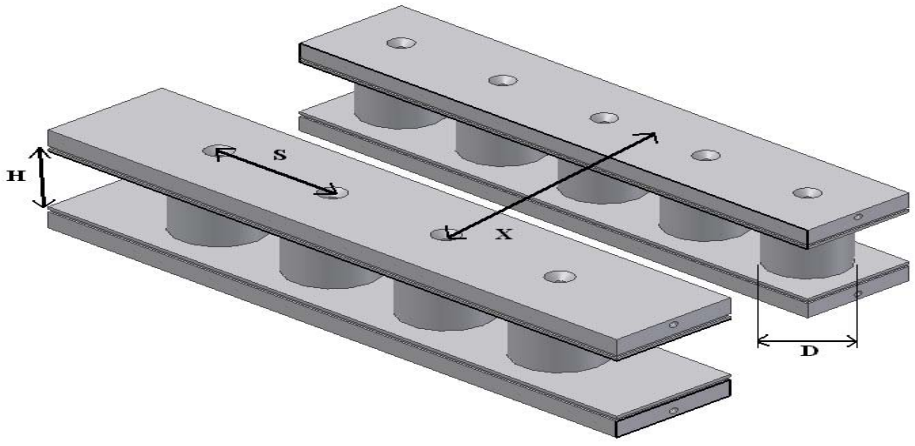

Figure 13. Schematic of a staggered pin-fin array

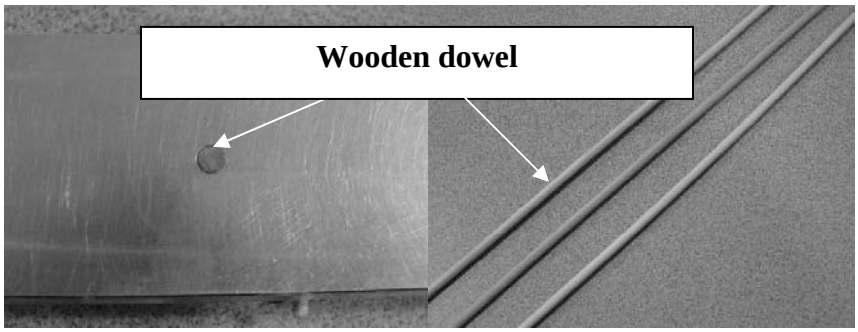

Figure 14. Non-fluted wooden dowel

4. Exit Duct

The exit duct transition piece (Figure 15) provided a smooth transition from the rectangular test section to the 2.5-inch diameter circular piping downstream. At the exit of this transition piece, four thermocouples were installed (Figure 16) to provide the heat exchanger outlet temperature. This temperature was obtained by averaging the temperature of the four thermocouples.

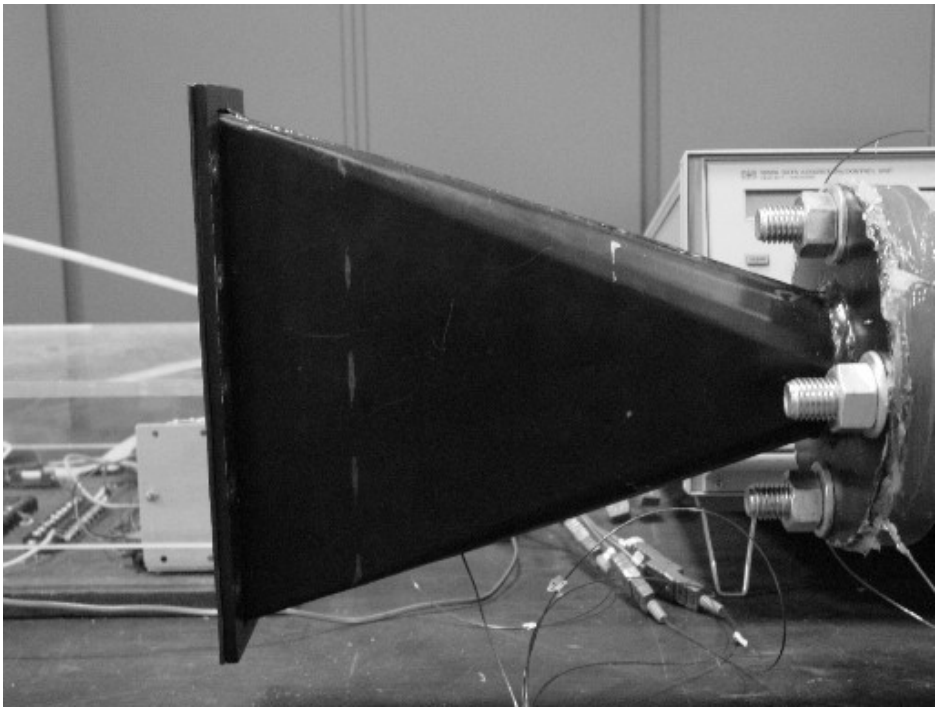

Figure 15. Exit duct transition piece

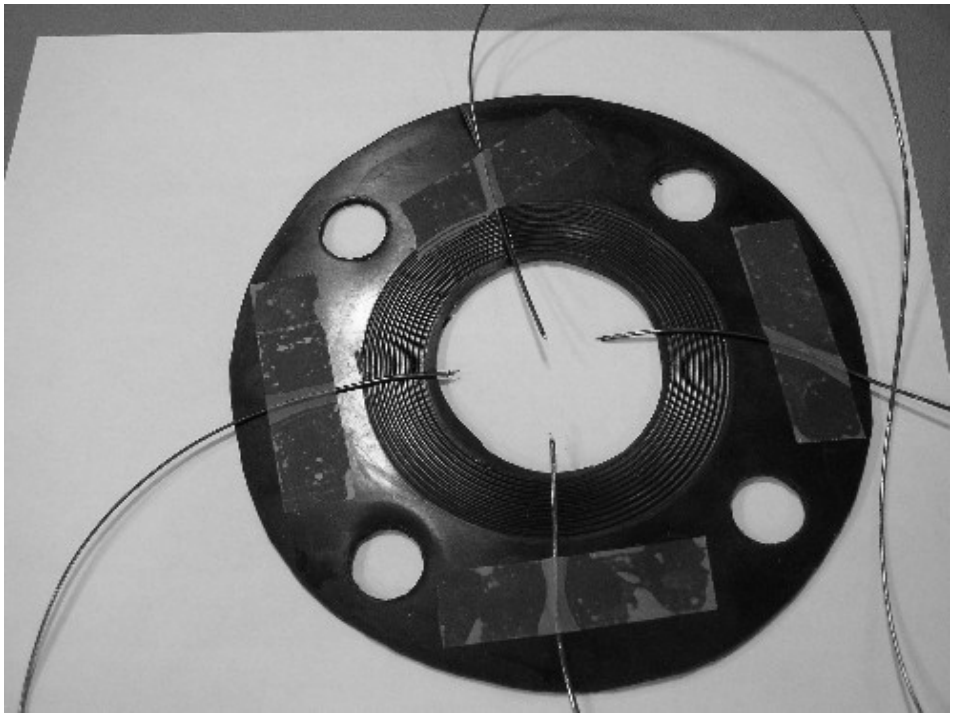

Figure 16. Exit duct thermocouple arrangement

As previously stated, the exit duct initially consisted of the 2.5-inch diameter piping connected to a turbine flow meter for turbulent flows. This thesis deals only with laminar flow; therefore, the turbine flow meter was replaced by the Omega FMA-1844 mass flow meter (Figure 17), a throttle valve (Figure 18), and the subsequent .5-inch piping. Figure (19) shows the transition from rectangular to 2.5-inch circular, and from 2.5-inch to .5-inch.

The new flow meter was needed to accurately measure the lower flow rates required for this detailed laminar flow analysis. The flow meter had a range of 0-500 SLPM, which was deemed ideal for Reynolds numbers between 100-2000.

The throttle valve was required to achieve the very low flow rates associated with Reynolds numbers between 100 and 300. These flow rates ranged between 15 and 45 SLPM depending on the test section configuration, and could only be achieved by adjusting the throttle valve.

Figure 17. Omega FMA-1844 mass flow meter

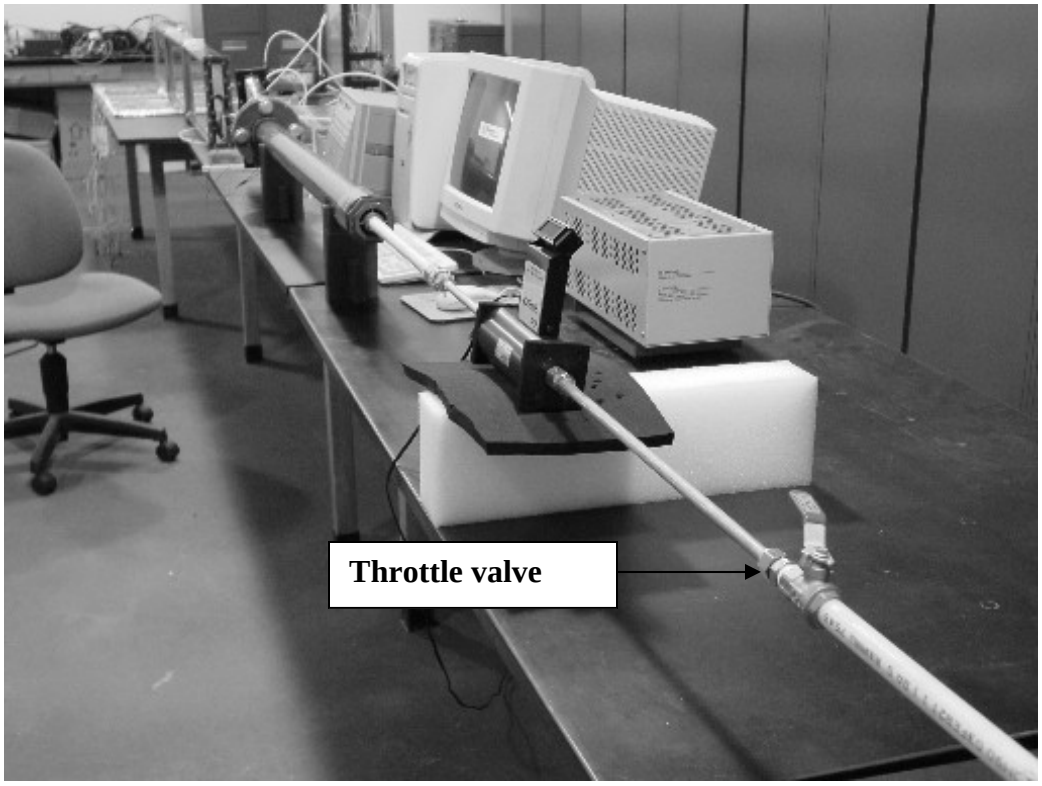

Figure 18. System throttle valve

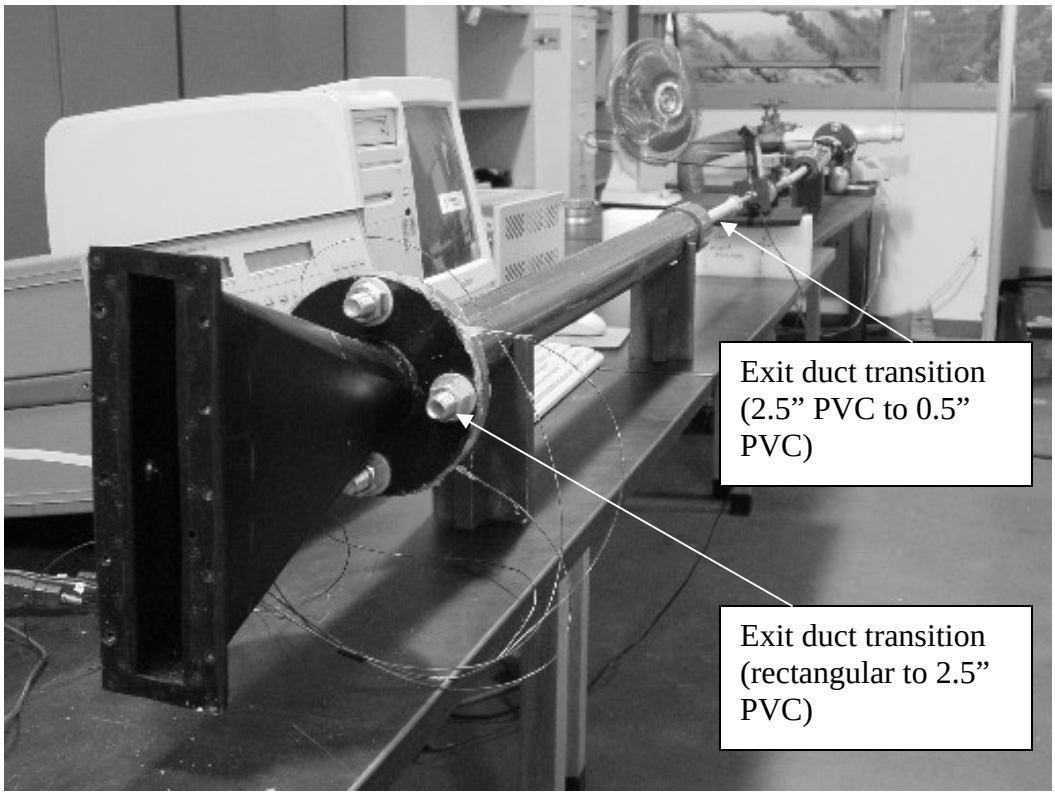

Figure 19. Exit duct

At the very end of the exit duct were three bypass valves (Figure 20) and the system blower (Figure 21). The three bypass valves could be manipulated to achieve the Reynolds numbers in the upper laminar region (500-2000). To achieve the lower laminar flow rates, all three bypass valves would be open while adjusting the throttle valve to achieve the desired flow rate.

The blower was selected based on a differential pressure and flow analysis conducted by Ramthun (2003). The blower was selected primarily to ensure a fully developed flow profile prior to entering the heat transfer test section. The blower’s pump curve is located in Appendix F.

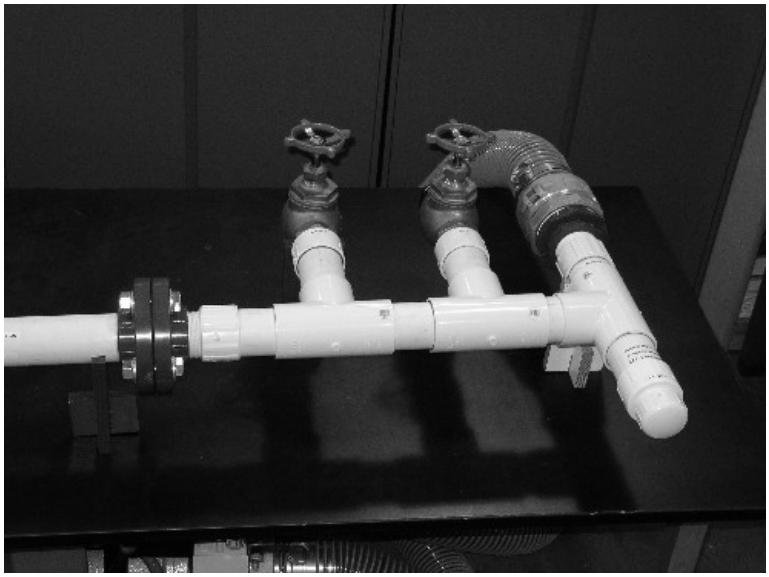

Figure 20. Exit duct bypass valves

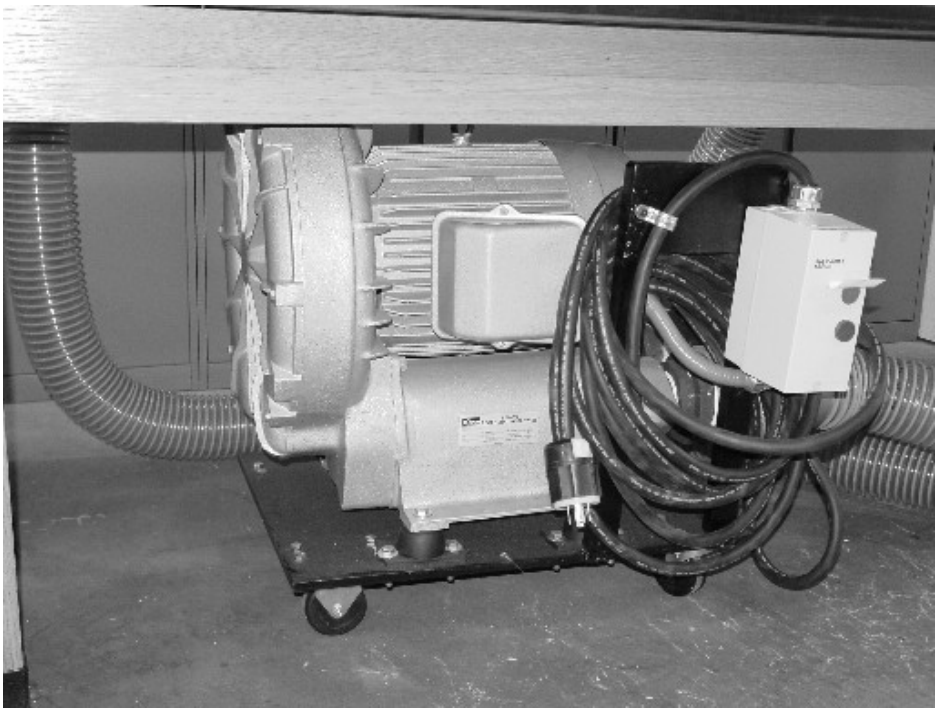

Figure 21. System blower

5. Monitoring Equipment

Throughout this research, a wide range of parameters had to be monitored and controlled. A micro-manometer, a differential pressure transducer, a mass flow meter, a digital power meter (Figure 22), which was used to determine the total power delivered to the heaters, and twenty-five thermocouples were used to monitor and collect the required

data. As described earlier, twenty thermocouples were used, one for each plate, to monitor the temperature of each plate, and control its associated heater. Four thermocouples were used to monitor heat exchanger outlet temperature. The other thermocouple was used to monitor heat exchanger inlet temperature (ambient).

Figure 22. Digital power meter

The micro-manometer (Figure 23) had a full-scale range of 0-4 inches of water readable in .005-inch increments. This differential pressure device was also compared to a differential pressure transducer (Figure 24) that converted the differential pressure to a DC voltage that corresponded to that pressure. These two devices were used to verify proper operation of the other.

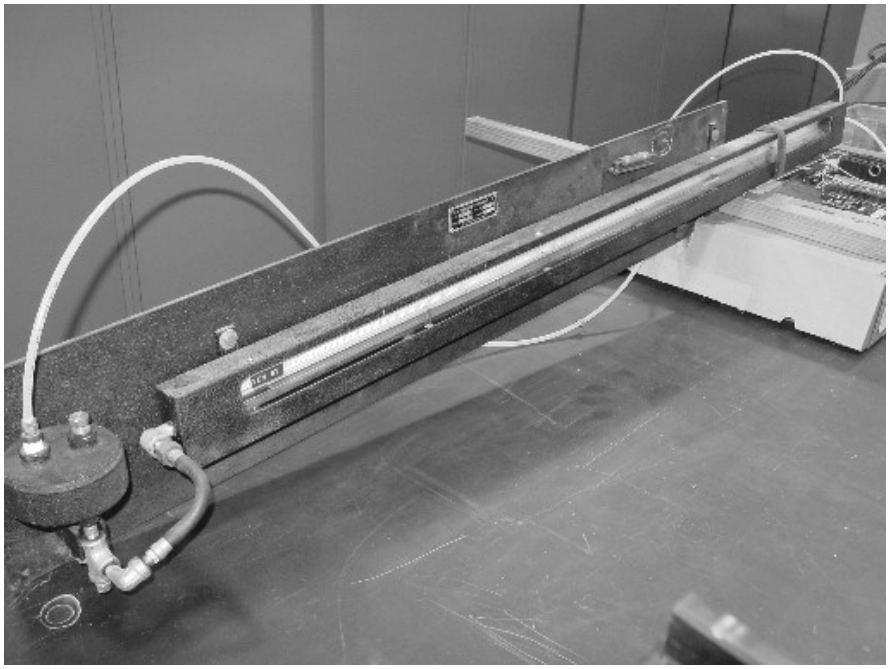

Figure 23. 0 – 4 inch inclined micro-manometer

Figure 24. Pressure transducer (VDC)

An electronics board (Figure 25) was used to house the relays that were used to control the twenty heaters as well as the differential pressure transducer. The data from the thermocouples and pressure transducer were collected by a Hewlett Packard 3852 Data Acquisition/Control Unit (Figure 26) and delivered to a computer program called LabVIEW developed by National Instruments. As LabVIEW cycles through each channel corresponding to a thermocouple or the pressure transducer, it records the data in a Microsoft Excel file. System temperature is established by the user based on ambient temperature and input into LabVIEW.

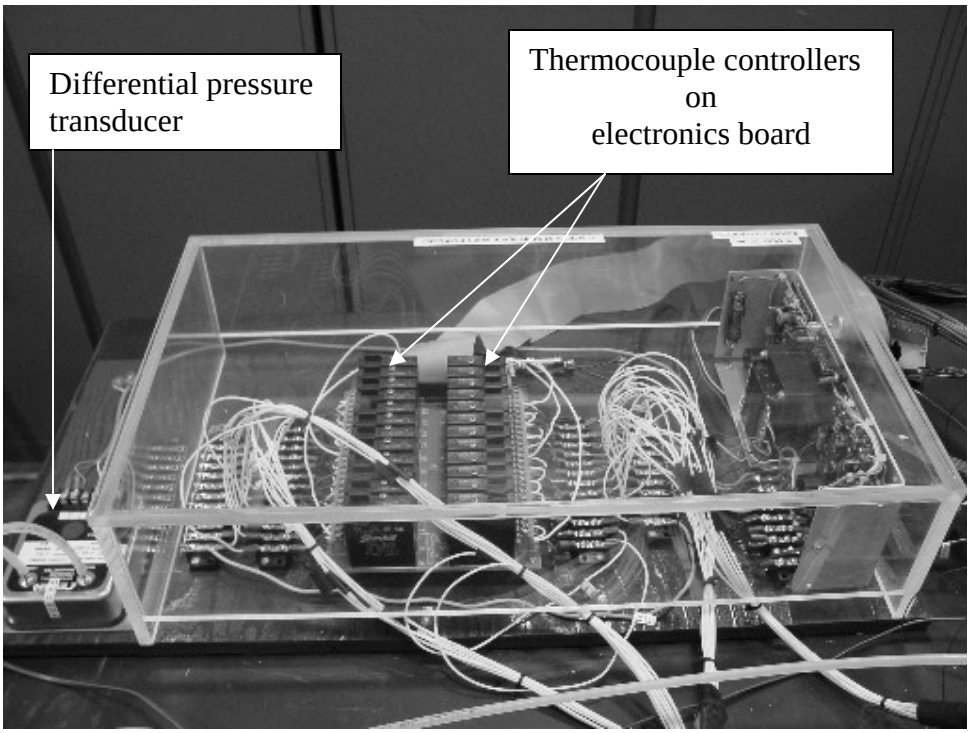

Figure 25. Electronics Board

Figure 26. HP 3852A Data Acquisition/Control Unit

THIS PAGE INTENTIONALLY LEFT BLANK

IV. EXPERIMENTAL TESTING

A. TESTING PROCEDURE

1. Test Matrix - Pin Configuration Table

This research involves diverse pin diameters, shapes and configurations tested over several Reynolds numbers in the laminar regime. Table (1) is re-introduced as Table (2) to aid the reader in understanding the various configurations. Table (2) shows that for every pin diameter, with the exception of the 66 mm pins, there are four configurations for which data will be collected. The 66 mm pins are too large to accommodate sets 2 and 4. Set 1 is the configuration that contains the maximum number of pins for that pin diameter. In set 1, all pin diameters have 45 total pins with the exception of the 66 mm pins, which have 12. In set 2, X/D and S/D are doubled and thus, 22 pins are removed to achieve these new ratios. In set 3, X/D is doubled from the set 1 values and S/D remains the same as the set 1 values. Set 3 contains 27 pins for all pin diameters with the exception of the 66 mm pins, which have 6. Set 4 doubles S/D from the set 1 values and leaves the X/D unchanged from the set 1 values. Set 4 has 25 pins for all pin diameters. The only exception to the above pin configurations was the use of 33 mm diameter pins in the last row of the heat exchanger for the teardrop sets. This was done to prevent the tail of the teardrop pin from protruding into the exit duct.

Table 2. Pin configuration table

Diameter	Set 1	Set 2	Set 3	Set 4
10 mm	**S/D = 5.0 X/D = 5.0 H/D = 3.3 D_h=49.7mm**	**S/D = 10.0 X/D = 10.0 H/D = 3.3 D_h=53.6mm**	**S/D = 5.0 X/D = 10.0 H/D = 3.3 D_h=52.9mm**	**S/D = 10.0 X/D = 5.0 H/D = 3.3 D_h=53.3mm**
16.5 mm	**S/D = 3.0 X/D = 3.0 H/D = 2.0 D_h=44.7mm**	**S/D = 6.1 X/D = 6.0 H/D = 2.0 D_h=50.7mm**	**S/D = 3.0 X/D = 6.1 H/D = 2.0 D_h=49.5mm**	**S/D = 6.1 X/D = 3.0 H/D = 2.0 D_h=50.1mm**
33 mm	**S/D = 1.5 X/D = 1.5 H/D = 1.0 D_h=31.7mm**	**S/D = 3.0 X/D = 3.0 H/D = 1.0 D_h=43.1mm**	**S/D = 1.5 X/D = 3.0 H/D = 1.0 D_h=40.9mm**	**S/D = 3.0 X/D = 1.5 H/D = 1.0 D_h=42.0mm**
66 mm	**S/D = 1.89 X/D = 0.76 H/D = 0.5 D_h=39.2mm**	**Not Possible**	**S/D = 1.89 X/D = 1.5 H/D = 0.5 D_h=48.7mm**	**Not Possible**
Tear Drop	**S/D = 1.5 X/D = 1.5 H/D = 1.0 D_h=22.4mm**	**S/D = 3.0 X/D = 3.0 H/D = 1.0 D_h=36.8mm**	**S/D = 1.5 X/D = 3.0 H/D = 1.0 D_h=33.9mm**	**S/D = 3.0 X/D = 1.5 H/D = 1.0 D_h=35.3mm**
Two configurations were completed with the 66mm pins. Heat exchanger cannot accommodate set number two or four.				

2. Test Matrix – Data Runs

For each pin configuration listed in Table (2), a full data run was conducted. A full data run consisted of 7 laminar flow rates with Reynolds numbers ranging from 100 to 2000. Initially, only 6 flow rates were used; however, as testing continued, it was deemed desirable to have a 1500 Reynolds number added to bridge the gap between 1000 and 2000. Table (3) shows the expected flow rates in SLPM to achieve each of the specified Reynolds numbers for each pin configuration.

Table 3. Full data run with Reynolds number and corresponding flow rate

	Set 1		Set 2		Set 3		Set 4	
10 mm	**Re**	**Flowrate**	**Re**	**Flowrate**	**Re**	**Flowrate**	**Re**	**Flowrate**
	100	15 SLPM	100	15 SLPM	100	15 SLPM	100	15 SLPM
	200	30 SLPM	200	30 SLPM	200	30 SLPM	200	30 SLPM
	300	45 SLPM	300	45 SLPM	300	45 SLPM	300	45 SLPM
	500	75 SLPM	500	70 SLPM	500	75 SLPM	500	75 SLPM
	1000	150 SLPM	1000	140 SLPM	1000	145 SLPM	1000	145 SLPM
	1500	Not done	1500	220 SLPM	1500	215 SLPM	1500	215 SLPM
	2000	300 SLPM	2000	290 SLPM	2000	290 SLPM	2000	290 SLPM
16.5 mm	**Re**	**Flowrate**	**Re**	**Flowrate**	**Re**	**Flowrate**	**Re**	**Flowrate**
	100	20 SLPM	100	15 SLPM	100	15 SLPM	100	15 SLPM
	200	35 SLPM	200	30 SLPM	200	30 SLPM	200	30 SLPM
	300	50 SLPM	300	45 SLPM	300	45 SLPM	300	45 SLPM
	500	80 SLPM	500	75 SLPM	500	75 SLPM	500	75 SLPM
	1000	165 SLPM	1000	145 SLPM	1000	150 SLPM	1000	150 SLPM
	1500	Not done	1500	225 SLPM	1500	Not done	1500	Not done
	2000	300 SLPM	2000	290 SLPM	2000	300 SLPM	2000	300 SLPM
33 mm	**Re**	**Flowrate**	**Re**	**Flowrate**	**Re**	**Flowrate**	**Re**	**Flowrate**
	100	20 SLPM	100	15 SLPM	100	15 SLPM	100	15 SLPM
	200	35 SLPM	200	30 SLPM	200	30 SLPM	200	30 SLPM
	300	50 SLPM	300	45 SLPM	300	45 SLPM	300	45 SLPM
	500	90 SLPM	500	80 SLPM	500	80 SLPM	500	75 SLPM
	1000	170 SLPM	1000	155 SLPM	1000	155 SLPM	1000	155 SLPM
	1500	Not done	1500	Not done	1500	Not done	1500	Not done
	2000	300 SLPM	2000	300 SLPM	2000	300 SLPM	2000	300 SLPM
66 mm	**Re**	**Flowrate**	**Not Possible**		**Re**	**Flowrate**	**Not Possible**	
	100	15 SLPM			100	15 SLPM		
	200	30 SLPM			200	25 SLPM		
	300	40 SLPM			300	40 SLPM		
	500	65 SLPM			500	64 SLPM		
	1000	135 SLPM			1000	135 SLPM		
	1500	Not done			1500	Not done		
	2000	270 SLPM			2000	270 SLPM		
Tear Drop	**Re**	**Flowrate**	**Re**	**Flowrate**	**Re**	**Flowrate**	**Re**	**Flowrate**
	100	20 SLPM	100	15 SLPM	100	15 SLPM	100	15 SLPM
	200	35 SLPM	200	35 SLPM	200	30 SLPM	200	35 SLPM
	300	50 SLPM	300	45 SLPM	300	45 SLPM	300	45 SLPM
	500	85 SLPM	500	75 SLPM	500	80 SLPM	500	80 SLPM
	1000	170 SLPM	1000	160 SLPM	1000	160 SLPM	1000	160 SLPM
	1500	250 SLPM	1500	240 SLPM	1500	240 SLPM	1500	240 SLPM
	2000	320 SLPM	2000	320 SLPM	2000	320 SLPM	2000	320 SLPM

Two configurations were completed with the 66mm pins. Heat exchanger cannot accommodate set number two or four.

B. PROCEDURE

1. Initial Setup

The heat exchanger test section was put in the desired pin configuration based on Table (2). The Omega FMA-1844 mass flow meter was energized first due to its 15-minute warm-up period. The other monitoring and control components were energized next. This included the HP Data Acquisition Unit (HP3852), the circuit board, and the

heater power supply. The LabVIEW program was also started and made ready to collect data and transfer the data to a Microsoft Excel file.

Prior to starting the blower and drawing air through the system, no flow data was collected. This no flow data collection consisted of taking readings on the micro-manometer, differential pressure transducer and the FMA-1844. The National Oceanic and Atmospheric Administration (NOAA) website was consulted for atmospheric pressure. LabVIEW provided inlet or ambient temperature via thermocouple channel 20, and the heaters were energized to 12 degrees Kelvin above this ambient temperature. The system was allowed to reach steady state, which was generally 30 minutes from the time the heaters were energized. Time to reach steady state from one flow rate to the next however, was much faster, taking only about 5 minutes.

2. Full Data Run

After the system was in steady state, the blower was started and the desired flow rate was established. Flow rate was established by monitoring the FMA-1844 while adjusting the three bypass valves and the system throttle valve. Each full data run consisted of seven 10-minute data collection sub-runs. Each sub-run flow rate was determined based on Table (3). The flow rates were determined to achieve the desired Reynolds numbers of 100, 200, 300, 500, 1000, 1500 and 2000. As previously stated, initially, only 6 flow rates were used; however, as testing continued, it was deemed desirable to have a 1500 Reynolds number added to bridge the gap between 1000 and 2000.

Once the desired flow rate was established and steady state was reached, LabVIEW recorded the data, which included the channel it was recording, whether or not that channel's associated heater was on, the parameter value (i.e. temperature or voltage) and the associated time stamp. Figure (27) shows a typical view of the LabVIEW program when it is open. LabVIEW cycles through all channels in approximately 8.4 seconds, therefore every channel and its associated values are recorded in a Microsoft Excel file every 8.4 seconds. After 10 minutes of data collection, the next flow rate was established, steady state reached again, and the process began again for this flow rate. This process continued until data was collected for all seven flow rates.

At this time, the blower was turned off, and the system was allowed to reach steady state with no load on the system. Once steady state was established, a 10-minute no load or zero flow sub-run was collected. This no load data was used to determine the losses from the heat exchanger section as well as compared to the heat transfer rate for each sub-run to determine the net heat transfer rate.

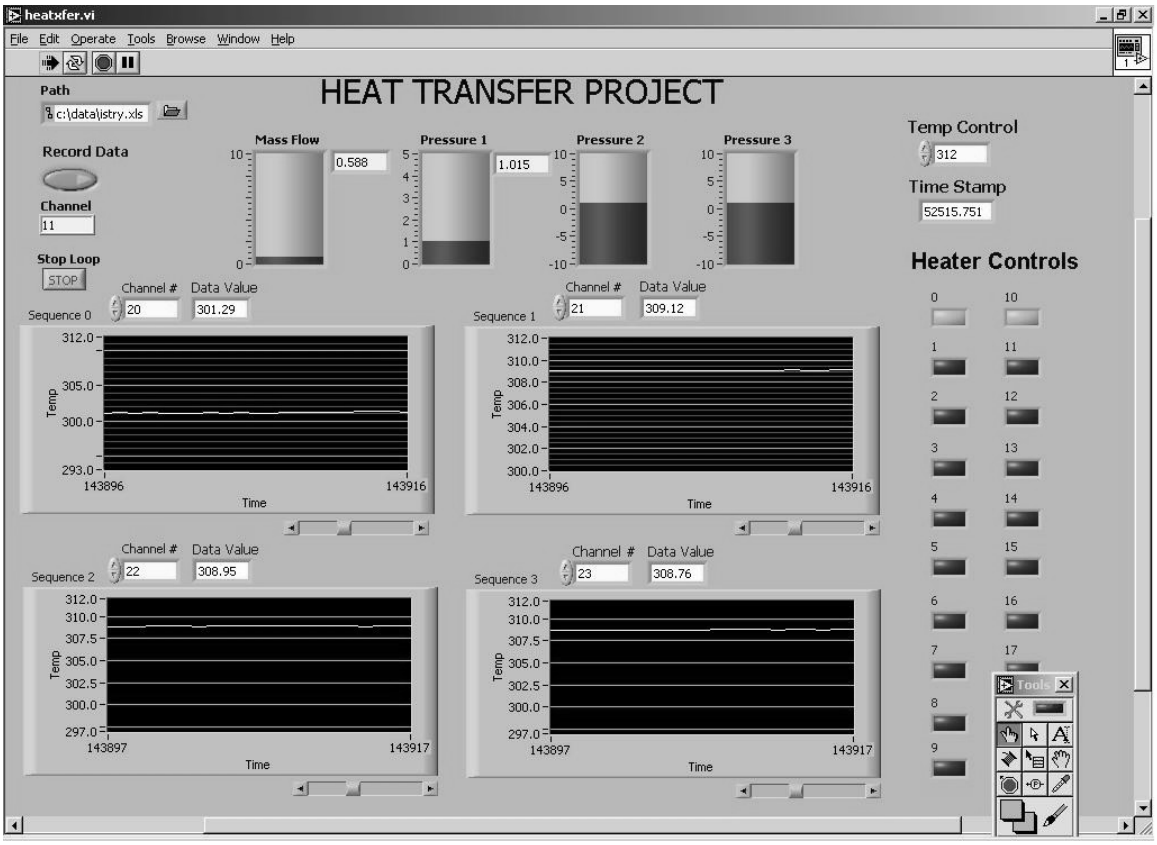

Figure 27. LabVIEW control window

C. DATA COLLECTION

Table (4) shows all the parameters that are measured and how they are used. Appendix A defines the nomenclature for all of the measured parameters. Appendix C shows all the equations that are used to manipulate the various parameters as required.

Table 4. Data collection

Parameter	Data Collection Source	How Used
Individual heater temperatures, 0-19 (k)	LabVIEW channels 0-19 respectively	Row by row analysis of heat transfer rate, T_{wall}, ΔT_{lm}, h, and Nu_{Dh}
Inlet temperature (k)	LabVIEW channel 20	ΔT, ΔT_{lm}, q, h, and Nu_{Dh}.
Four outlet temperatures (k)	LabVIEW channels 21-24	ΔT,ΔT_{lm},HX exit density, f, viscosity, P_{turb}, $\dot{m}$, Re_{Dh}, q, h, Nu_{Dh}, and E.
Differential pressure Transmitter (VDC)	LabVIEW channel 41	HX dp, HX exit density, f, P_{turb}, $\dot{m}$, Re_{Dh}, q, h, Nu_{Dh}, and E.
Manometer 0-4 inches water	Read directly off manometer	Hx dp, Hx exit density, f, P_{turb}, $\dot{m}$, Re_{Dh}, q, h, Nu_{Dh}, and E.
FMA-1844 gas mass flow meter (SLPM)	Read directly off meter	P_{turb}, f, $\bar{U}$, $\dot{m}$, Re_{Dh}, q, h, Nu_{Dh}, and E.
Atmospheric pressure Inches of mercury	www.noaa.com	Reference pressure compared with manometer and pressure transmitter values.
Thermocouple bistable	LabVIEW records when heater is on or off	LabVIEW gives value of 1 for on and 0 for off for each sub-run. Used to calculate q (electric).
Time stamp (seconds)	LabVIEW records time for each data point	Every data point from LabVIEW received a time stamp. Used to calculate q (electric).
Pin diameter (D)	Recorded by data taker	X/D, S/D, V_{open}, A_{wf}, A_{wh}, D_h, and A_{duct}.
Number of pins	Recorded by data taker	V_{open}, A_{wf}, A_{wh}, and D_h.
Value of X in flow direction	Recorded by data taker	X/D determination.
Value of S in span wise direction	Recorded by data taker	S/D determination
LabVIEW Channels 25-39, 42, 43 are reserved for future use. Channel 40 is used for the turbine flow meter for turbulent flows.		

D. DATA ANALYSIS

As shown in the previous section, many parameters are monitored throughout the data collection process. As with any data collection system, there is an amount of uncertainty that can lead to errors. An uncertainty analysis was conducted for all measured and calculated parameters and is located in Appendix D. Once all data for a full data was run was collected, it had to be meticulously analyzed for obvious and potential errors. The heat transfer rate was calculated two different ways and then compared for reasons of accuracy. Any significant errors were further investigated, and if needed, the entire data run was repeated.

THIS PAGE INTENTIONALLY LEFT BLANK

V. RESULTS AND DISCUSSION

A. INTRODUCTION

Collecting and analyzing data for various pin geometries and configurations is the primary objective of this research. Another objective was to use the data collected to validate numerical models. Some of the data collected was compared to prior numerical results. The rest of the data collected can be used in the future to validate results from ongoing numerical work.

Another objective was to compare the current results to the results obtained from a micro-heat exchanger. This can be done by scaling using the hydraulic diameter. The hydraulic diameter is an important characteristic length scale of such a heat exchanger. When certain dimensionless parameters such as Nusselt and Reynolds numbers are based on the hydraulic diameter, they are valid for all length scales from the macro to the micro level. At all times the Nusselt number or Reynolds number used in this research are understood to be based on the hydraulic diameter.

An additional objective was to validate the laminar pressure drop data obtained by Summers (2003). There were concerns that his low laminar pressure drop data was corrupted due to leaks in the heat exchanger test section. That is why there was a need to redesign the heat exchanger test section. Results of Summers (2003) pressure drop data is compared to results obtained from this research and is located in this chapter section D, Friction Factor Analysis.

The final objective was to try to find the optimum heat exchanger pin size and configuration based on an analysis of heat transfer coefficient versus fluid friction power. Table (1) is reintroduced as Table (5) to aid the reader in this section of the thesis.

Table 5. Pin configuration table

Diameter	Set 1	Set 2	Set 3	Set 4
10 mm	**S/D = 5.0 X/D = 5.0 H/D = 3.3 D_h=49.7mm**	**S/D = 10.0 X/D = 10.0 H/D = 3.3 D_h=53.6mm**	**S/D = 5.0 X/D = 10.0 H/D = 3.3 D_h=52.9mm**	**S/D = 10.0 X/D = 5.0 H/D = 3.3 D_h=53.3mm**
16.5 mm	**S/D = 3.0 X/D = 3.0 H/D = 2.0 D_h=44.7mm**	**S/D = 6.1 X/D = 6.0 H/D = 2.0 D_h=50.7mm**	**S/D = 3.0 X/D = 6.1 H/D = 2.0 D_h=49.5mm**	**S/D = 6.1 X/D = 3.0 H/D = 2.0 D_h=50.1mm**
33 mm	**S/D = 1.5 X/D = 1.5 H/D = 1.0 D_h=31.7mm**	**S/D = 3.0 X/D = 3.0 H/D = 1.0 D_h=43.1mm**	**S/D = 1.5 X/D = 3.0 H/D = 1.0 D_h=40.9mm**	**S/D = 3.0 X/D = 1.5 H/D = 1.0 D_h=42.0mm**
66 mm	**S/D = 1.89 X/D = 0.76 H/D = 0.5 D_h=39.2mm**	**Not Possible**	**S/D = 1.89 X/D = 1.5 H/D = 0.5 D_h=48.7mm**	**Not Possible**
Tear Drop	**S/D = 1.5 X/D = 1.5 H/D = 1.0 D_h=22.4mm**	**S/D = 3.0 X/D = 3.0 H/D = 1.0 D_h=36.8mm**	**S/D = 1.5 X/D = 3.0 H/D = 1.0 D_h=33.9mm**	**S/D = 3.0 X/D = 1.5 H/D = 1.0 D_h=35.3mm**
Two configurations were completed with the 66mm pins. Heat exchanger cannot accommodate 66 mm sets number two or four.				

B. HEAT TRANSFER COEFFICIENT

The heat transfer coefficient is calculated based on the equation in Appendix C and is equivalent to the heat transfer rate divided by bulk log mean temperature difference and the wetted surface area for heat transfer. The heat transfer coefficient versus Reynolds number for all pin diameters and configurations is shown in Figures (28-32).

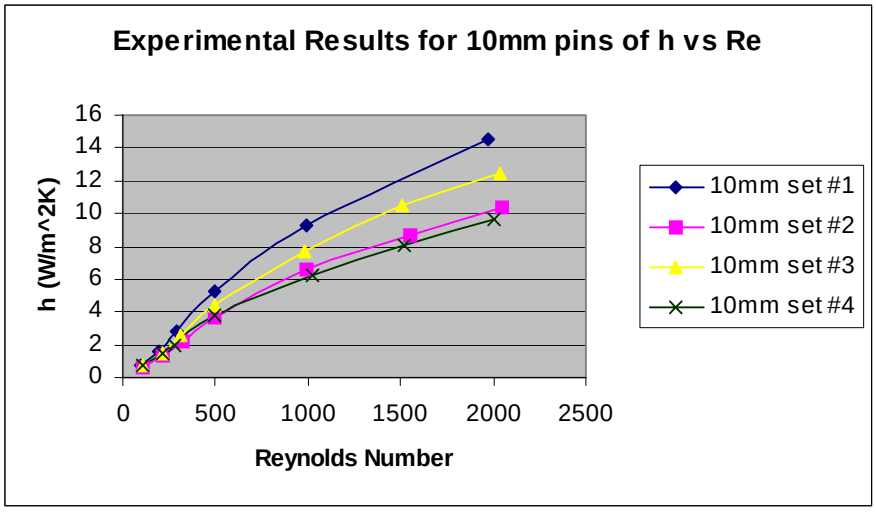

Figure 28. Plot of h vs. Re, 10mm pins

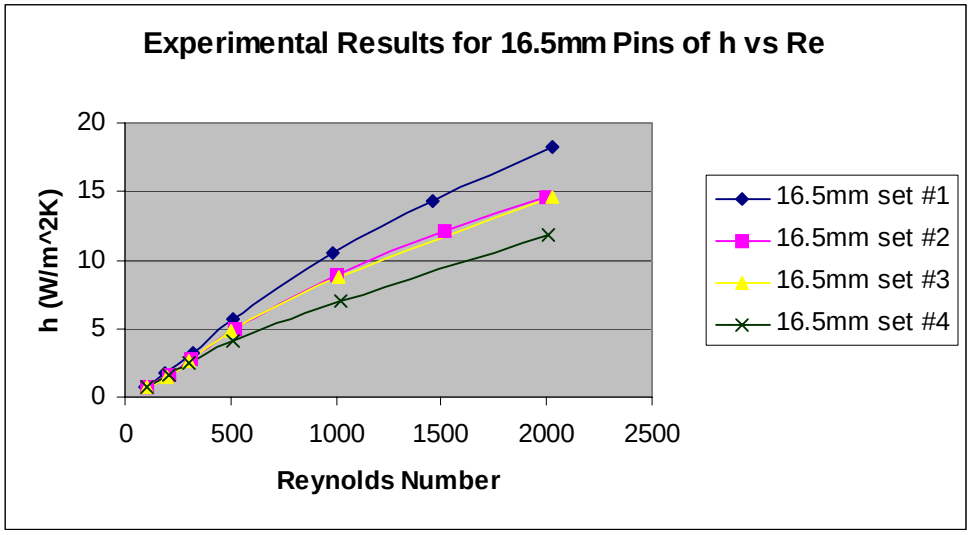

Figure 29. Plot of h vs. Re, 16.5mm pins

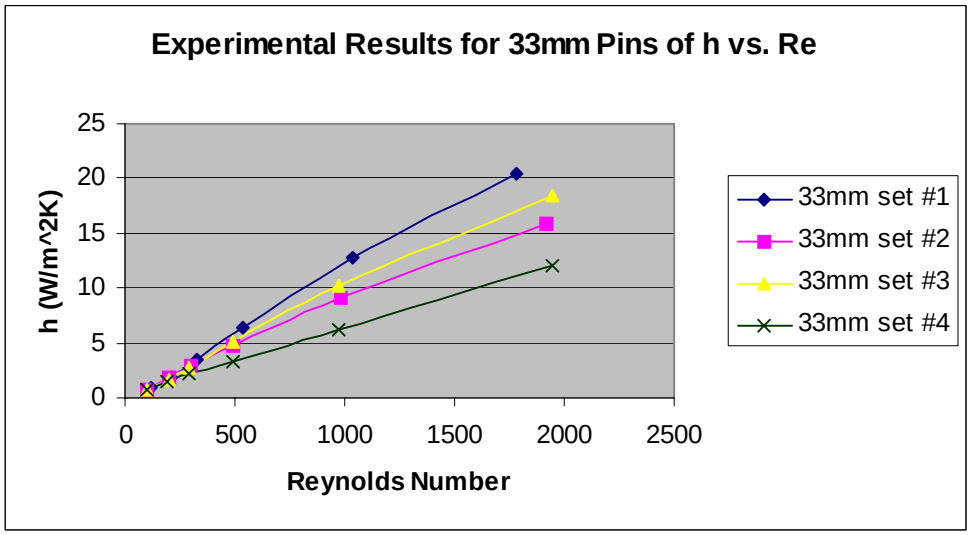

Figure 30. Plot of h vs. Re, 33mm pins

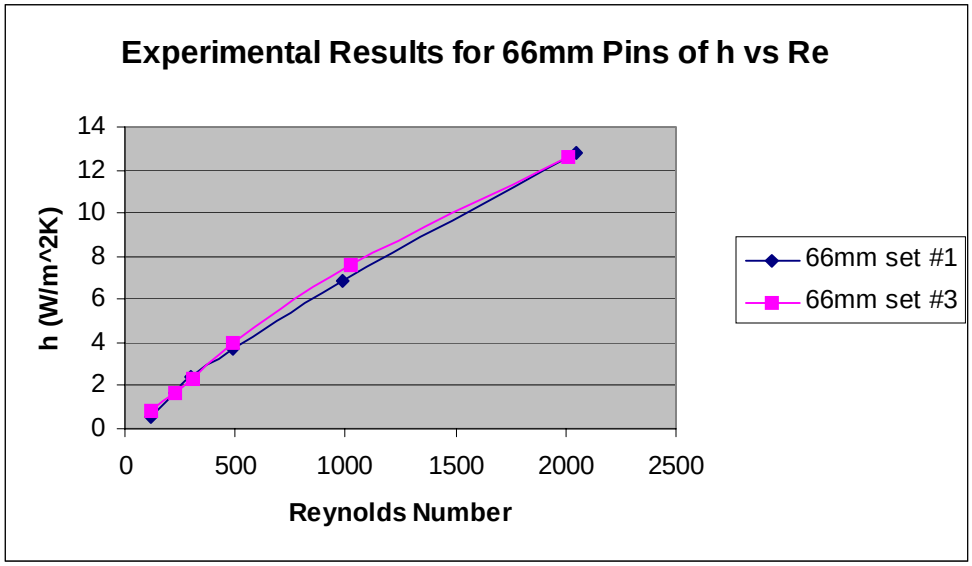

Figure 31. Plot of h vs. Re, 66mm pins

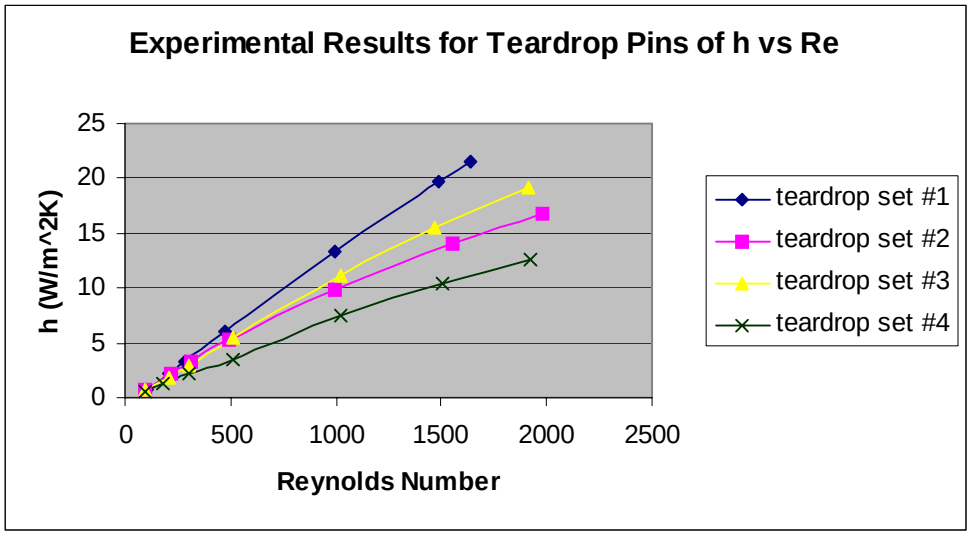

Figure 32. Plot of h vs. Re, teardrop pins

For all cases except the 66mm pins, set #1 provided the highest heat transfer coefficient over the whole laminar range. This is expected since set #1 comprises of the maximum number of pins for each pin diameter. The heat transfer coefficient was relatively the same for both configurations with the 66mm pins. This can probably be attributed to the fact that even though set #1 has twice as many pins as set #3, there are so few pins in the first place (set #1 – 12 pins, set #3 – 6 pins) that the heat transfer coefficient would remain largely the same.

Figures (33-37) show a low Reynolds number analysis for the same parameters, heat transfer coefficient versus Reynolds number. In all cases except for the 10mm and 16.5mm pins, there is virtually no difference in heat transfer coefficient in the low laminar regime. For the 10mm and 16.5mm pins, set #1 has a higher heat transfer coefficient than the other configurations.

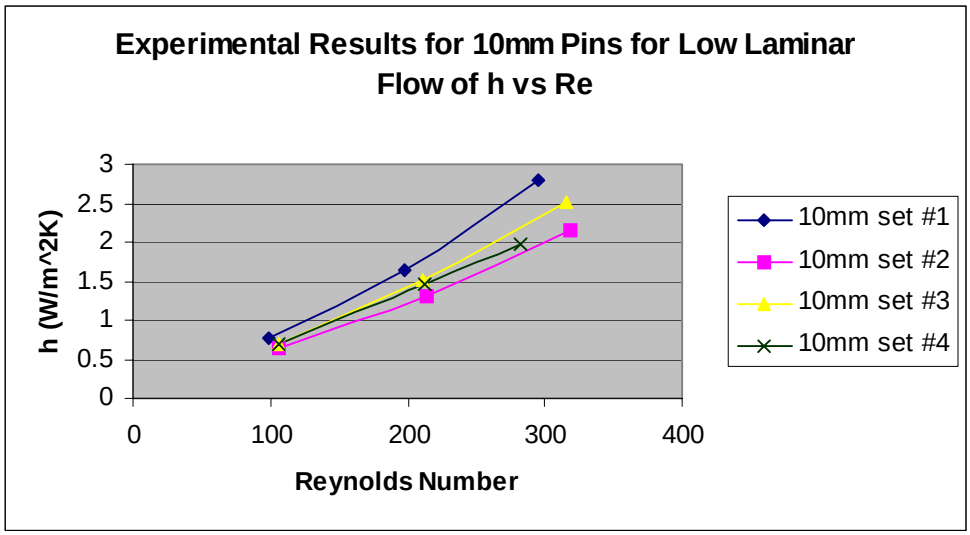

Figure 33. Plot of h vs. Re, 10mm pins, low laminar

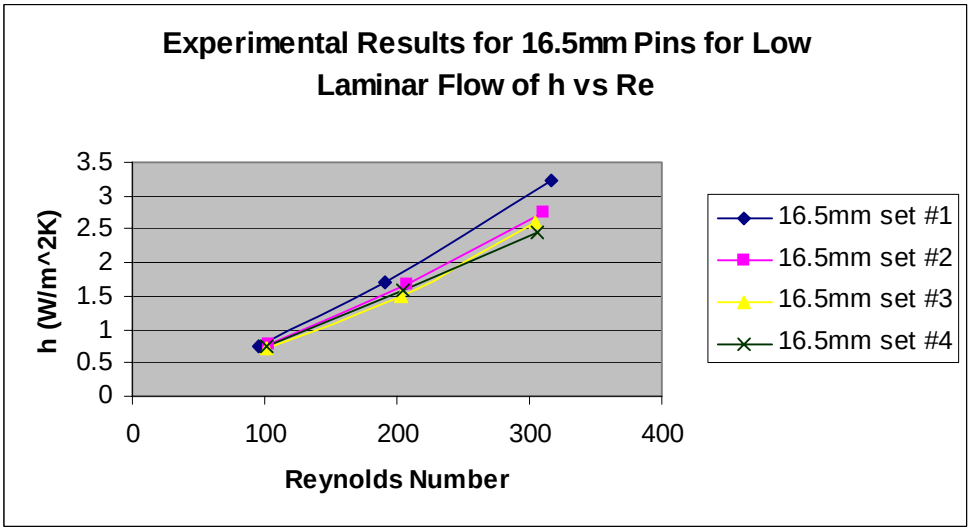

Figure 34. Plot of h vs. Re, 16.5mm pins, low laminar

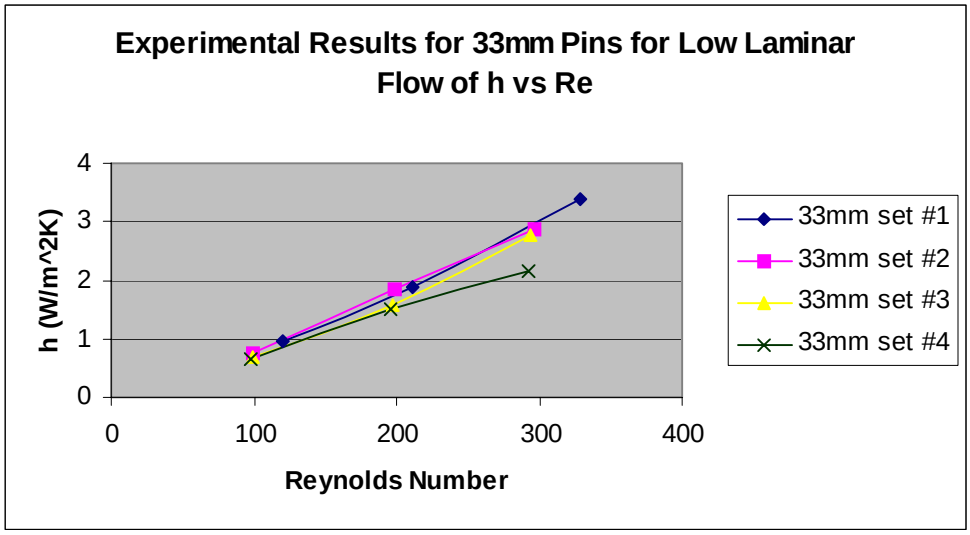

Figure 35. Plot of h vs. Re, 33mm pins, low laminar

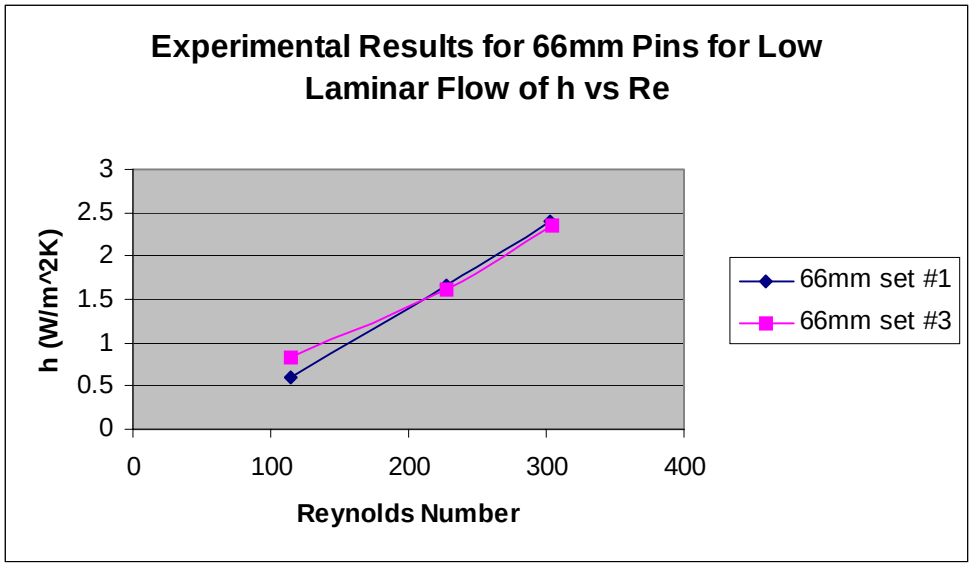

Figure 36. Plot of h vs. Re, 66mm pins, low laminar

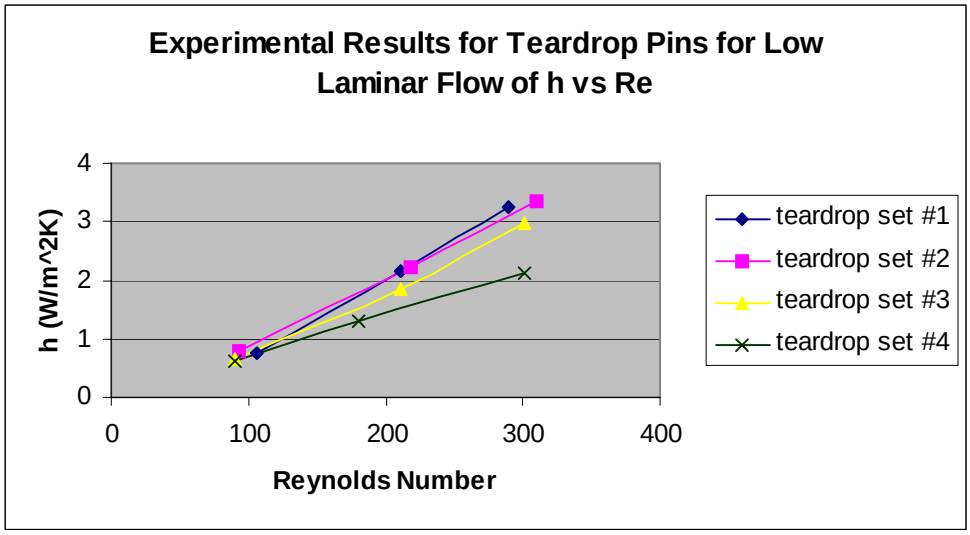

Figure 37. Plot of h vs. Re, teardrop pins, low laminar

Figure (38) shows how the best configurations from the various pin diameters fared against each other. The teardrop shaped pin outperformed the other pins over the entire laminar range in regards to heat transfer coefficient. This result can be expected due to the geometry of the teardrop pin. The tail on the pin increases the effectiveness of the pin to transfer heat as well as minimizing the flow separation compared to the 33mm cylindrical pin. Figure (39) shows similar results with a focus on the top performers in the low laminar regime. Even though flow separation is not as significant at these very low Reynolds numbers, the teardrop pin still outperformed the other pins, although the difference between all pins is much smaller than in the upper laminar regime.

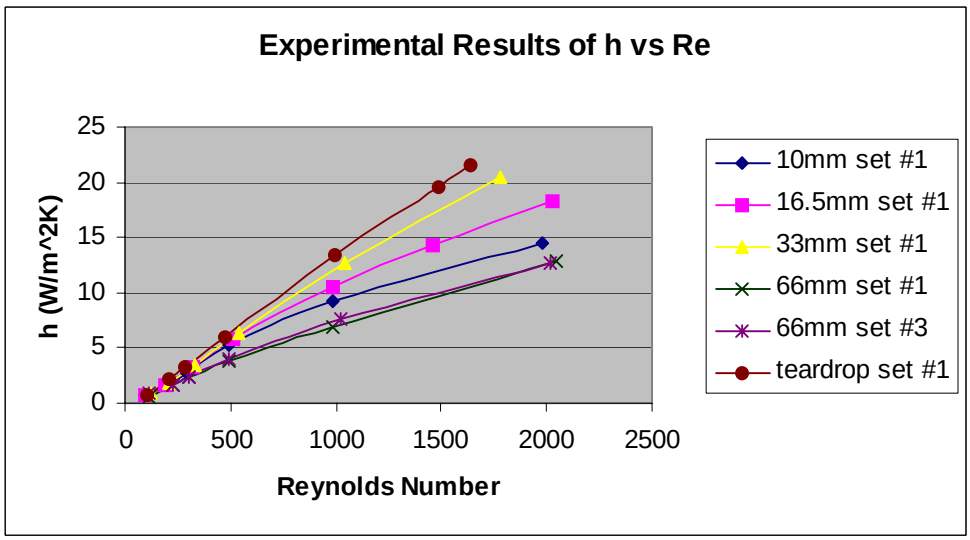

Figure 38. Plot of h vs. Re, top performers

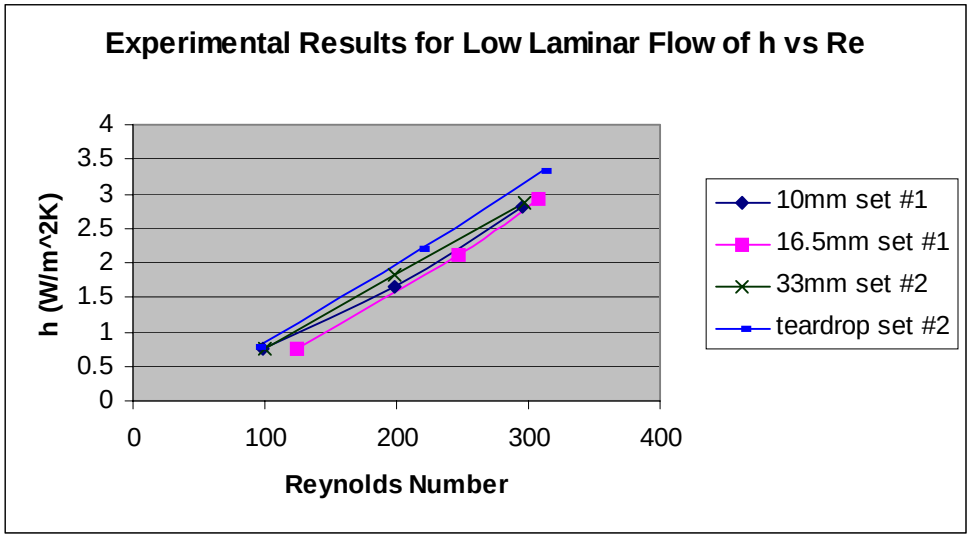

Figure 39. Plot of h vs. Re, top performers, low laminar

C. NUSSELT NUMBER (NU_{DH})

The Nusselt number is calculated with the equation in Appendix C and is equivalent to heat transfer coefficient times the hydraulic diameter divided by the thermal conductivity of the system. The Nusselt number is a dimensionless parameter that describes how efficient the convective heat transfer process is occurring. The convective heat transfer process is more productive with a higher Nusselt number. Figures (40-44) show the results of Nusselt number versus Reynolds number for all pin diameters and configurations.

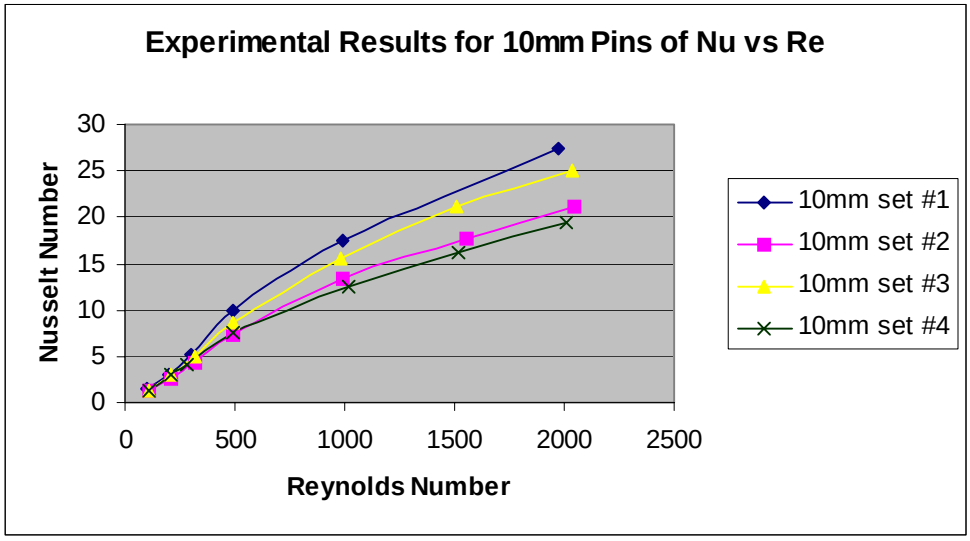

Figure 40. Plot of Nu vs. Re, 10mm pins

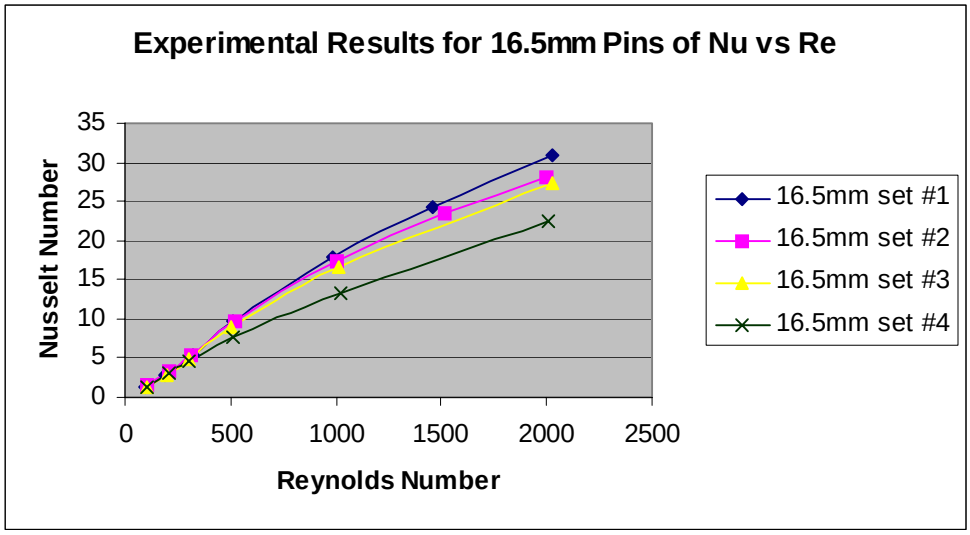

Figure 41. Plot of Nu vs. Re, 16.5mm pins

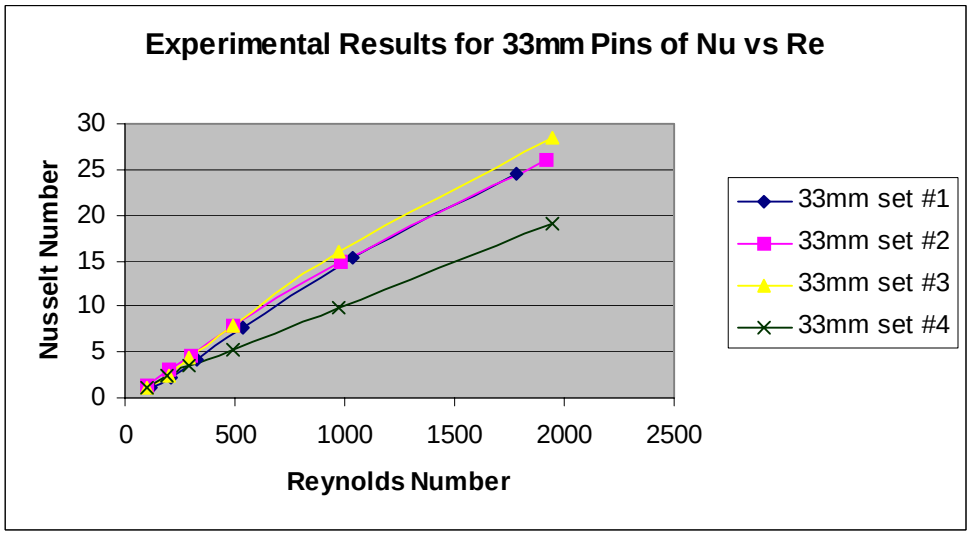

Figure 42. Plot of Nu vs. Re, 33mm pins

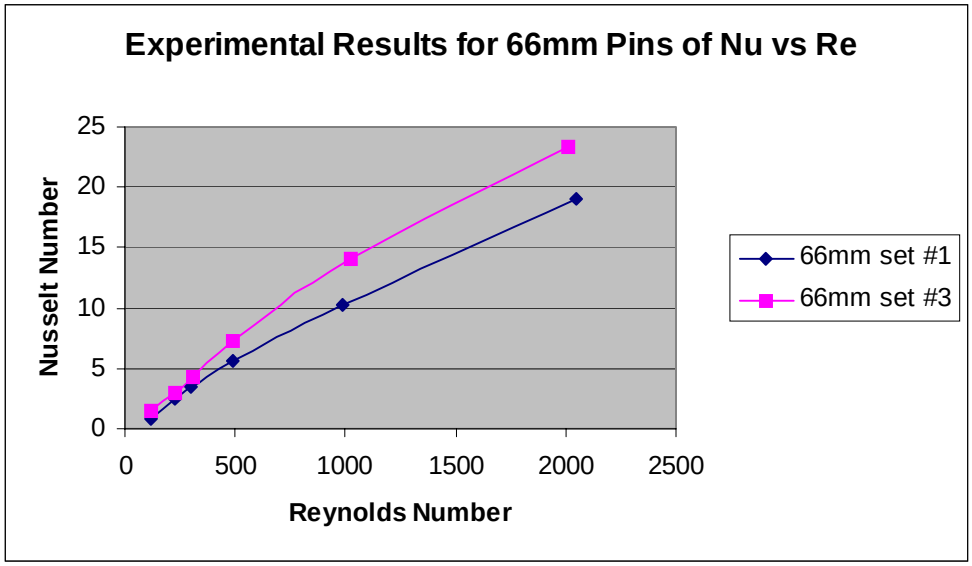

Figure 43. Plot of Nu vs. Re, 66mm pins

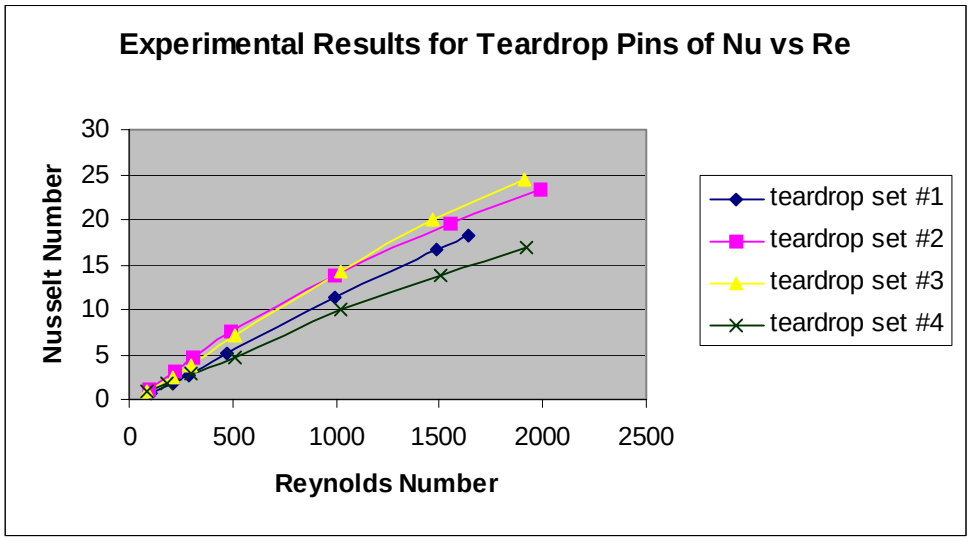

Figure 44. Plot of Nu vs. Re, teardrop pins

Due to the fact that the Nusselt number is directly proportional to the heat transfer coefficient, it would be expected that the results be similar to the previous section. For the 10mm and 16.5mm pins, the results were the same in that set #1 had the highest Nusselt number over the flow range. However, for the larger diameter pins the results were different. This is due to the fact that the larger diameter pin's hydraulic diameters are more susceptible to changes in pin configuration than the smaller diameter pins. Therefore, for the larger pins, the increase in hydraulic diameter overcomes the decrease in heat transfer coefficient, causing the configurations with fewer pins to be more

effective at convective heat transfer. This is true with the exception of set #4 for all pin diameters. Set #4 was the worst performer for all pin diameters. This is probably due to the actual configuration as shown in Appendix B. Set #4 doubles the S/D ratio while keeping X/D the same as set #1. As shown in Appendix B for all pin diameters, set #4 has two fairly unobstructed pathways for flow. The majority of the flow will take the path of least resistance and will therefore be a poor performer compared to the other configurations where these channels do not exist.

Figures (45-49) show the results of Nusselt number versus Reynolds number in the low laminar regime. The results for the low laminar analysis are similar to the upper laminar results with the exception that set #4 is not necessarily the poor performer for all pin diameters. This is probably due to the fact that the two channels in the set #4 configuration don't offer as significant relief to flow resistance as compared to higher flow rates. Set #2 stands out as the best performer for the teardrop and 33mm pins whereas in the upper laminar range, set #3 performed the best for these pins.

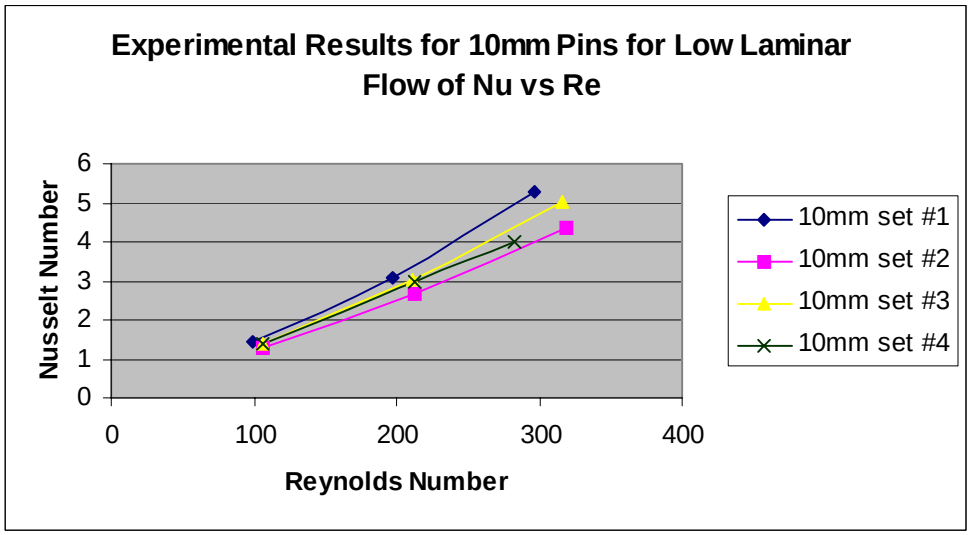

Figure 45. Plot of Nu vs. Re, 10mm pins, low laminar

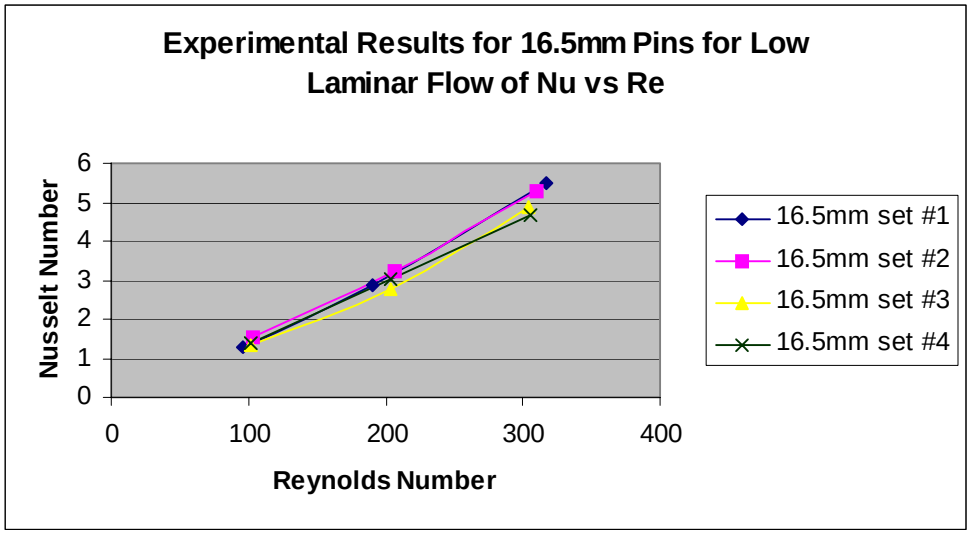

Figure 46. Plot of Nu vs. Re, 16.5mm pins, low laminar

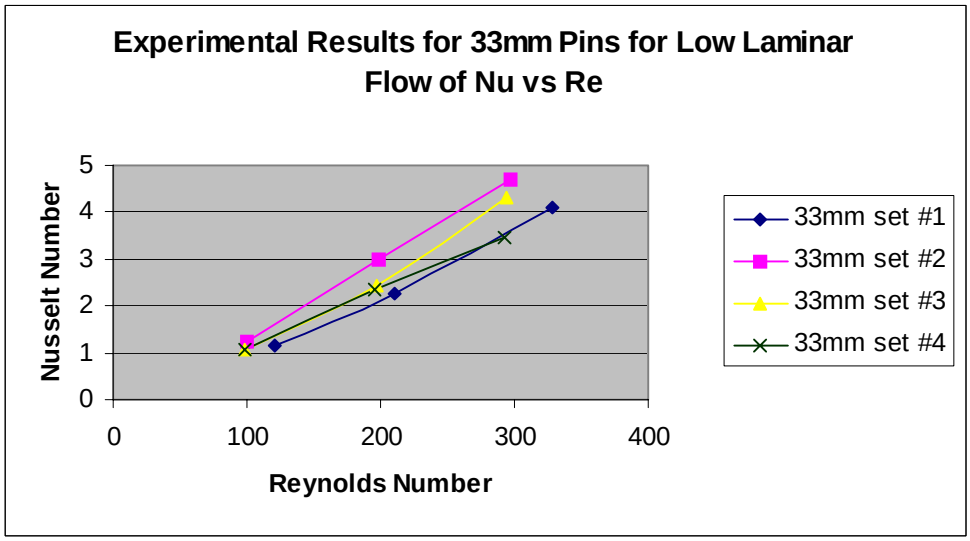

Figure 47. Plot of Nu vs. Re, 33mm pins, low laminar

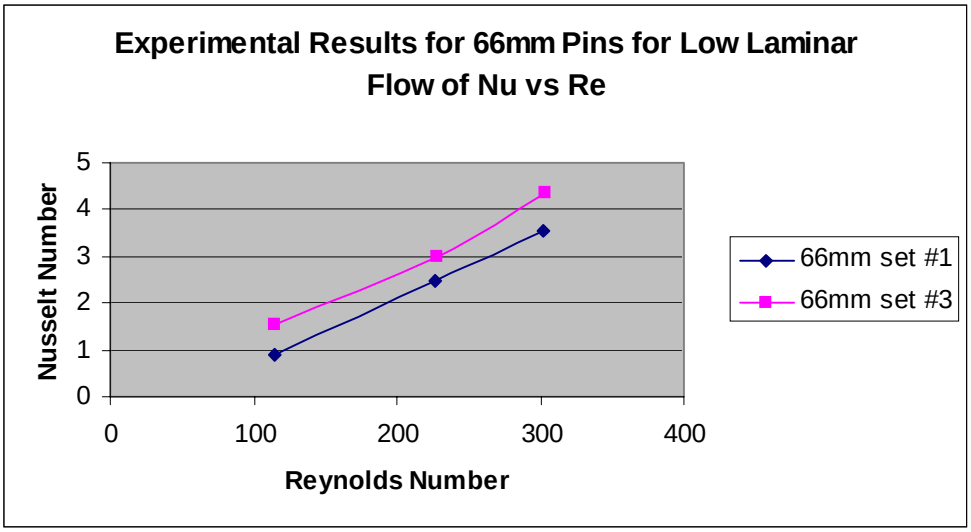

Figure 48. Plot of Nu vs. Re, 66mm pins, low laminar

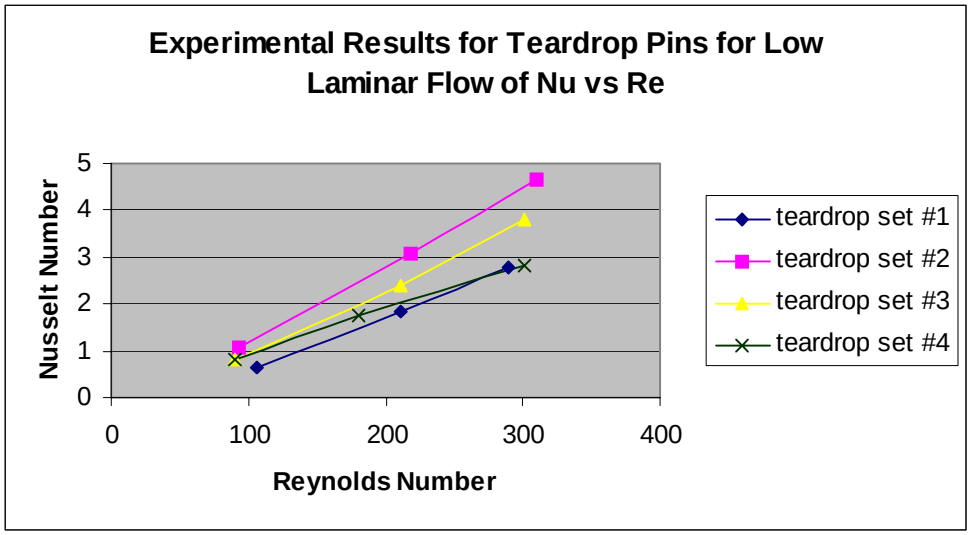

Figure 49. Plot of Nu vs. Re, teardrop pins, low laminar

Figure (50) compares the top performers for each pin diameter. The 16.5mm set #1 sets itself apart as the overall top performer in regards to convective heat transfer in the laminar regime. As far as the low laminar range (Figure 51), there is virtually no difference between the 10mm and the 16.5mm full set configuration. Ultimately, the 10mm would probably be the best choice in this range due to the significant decrease in material required to manufacture 10mm pins as compared to the 16.5mm pins.

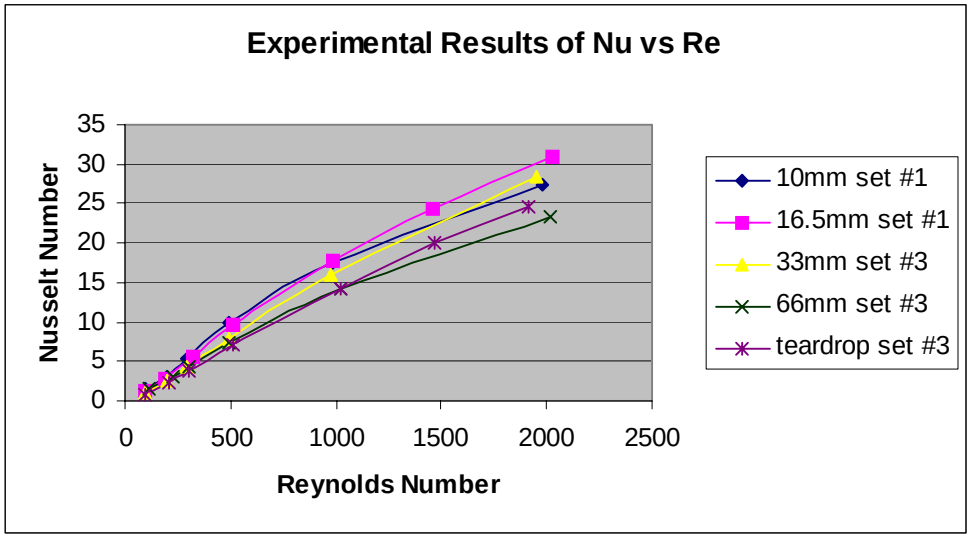

Figure 50. Plot of Nu vs. Re, top performers

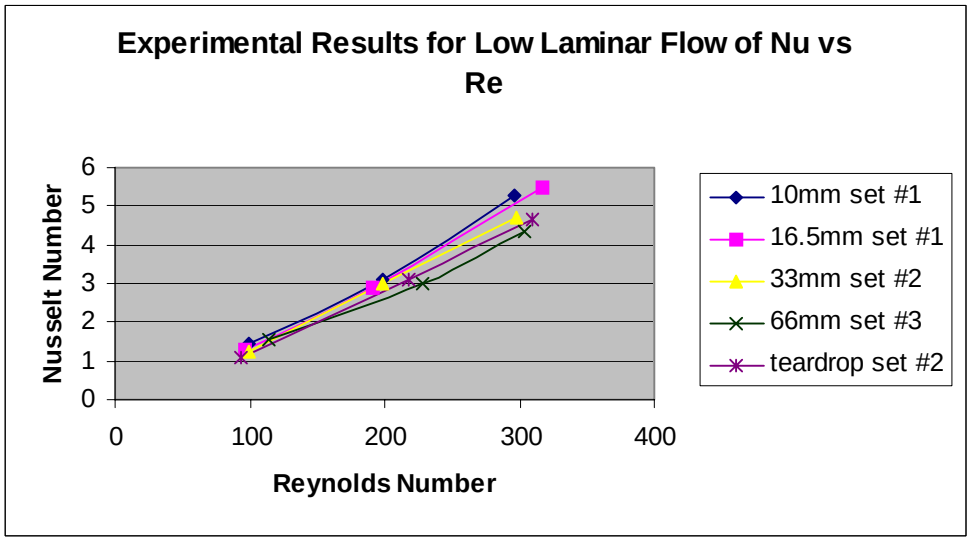

Figure 51. Plot of Nu vs. Re, top performers, low laminar

D. FRICTION FACTOR ANALYSIS

The friction factor is calculated with the equation in Appendix C and is proportional to the differential pressure across the heat exchanger and the hydraulic diameter, and inversely proportional to the density of the air passing through the heat exchanger, the average air velocity squared and the length of the heat exchanger. The friction factor is important to understanding the performance of a heat exchanger because it ultimately tells us how much energy the fluid loses as it passes through the heat exchanger.

The differential pressure across the heat exchanger is the input variable that affects the friction factor the most. The accuracy of the method of measuring the differential pressure across the heat exchanger is of utmost importance in order to have meaningful pressure drop data. Unfortunately, the precision of the two instruments that were used to measure differential pressure is not sufficient to measure the extremely small pressure drops associated with low laminar flow rates. For the upper laminar regime, for most pin diameters, there is sufficient pressure drop to measure it accurately, and the two instruments track with one another almost exactly. Figure (52) shows data collected for teardrop set #1 with a comparison of the micro-manometer and the differential pressure transducer. Figures (53-57) show the results for friction factor for all pin diameters and configurations.

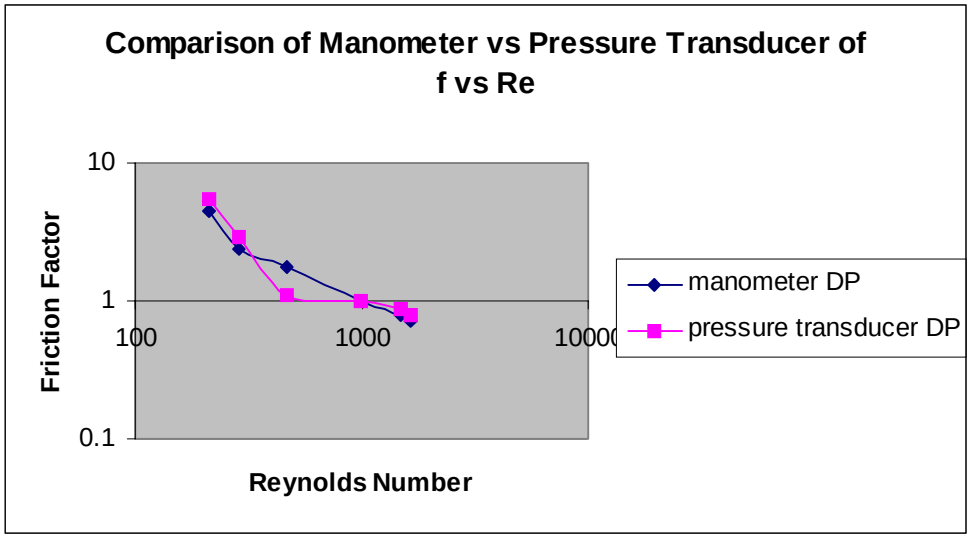

Figure 52. Plot of f vs. Re, manometer vs. pressure transducer

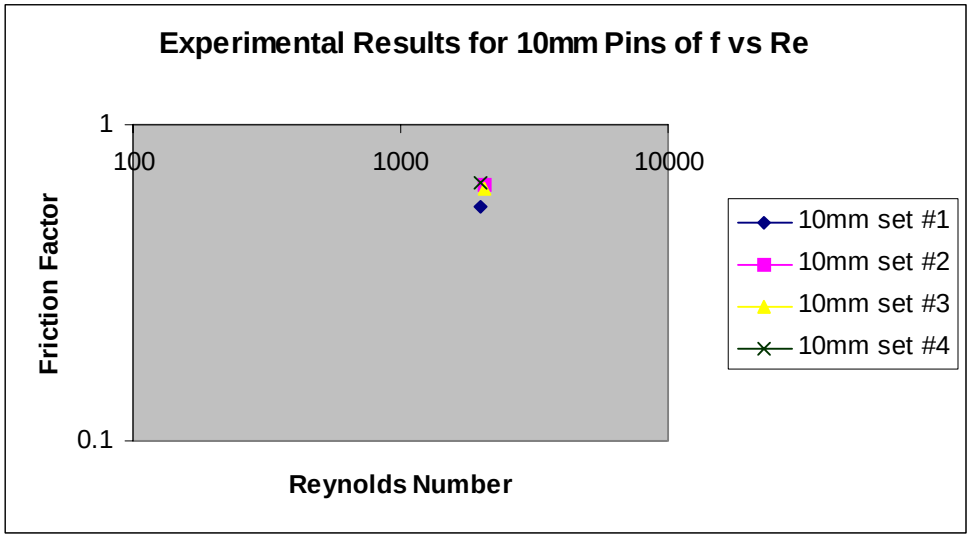

Figure 53. Plot of f vs. Re, 10mm pins

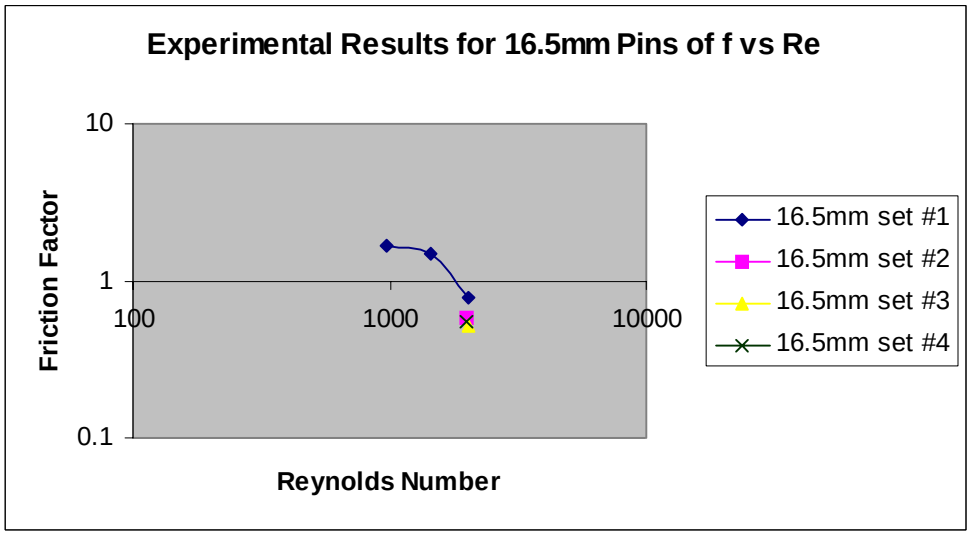

Figure 54. Plot of f vs. Re, 16.5mm pins

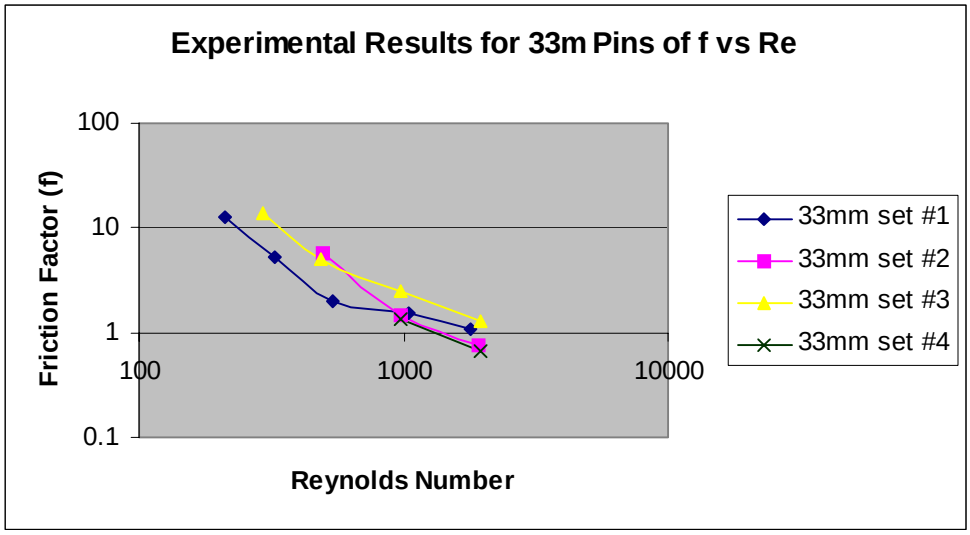

Figure 55. Plot of f vs. Re, 33mm pins

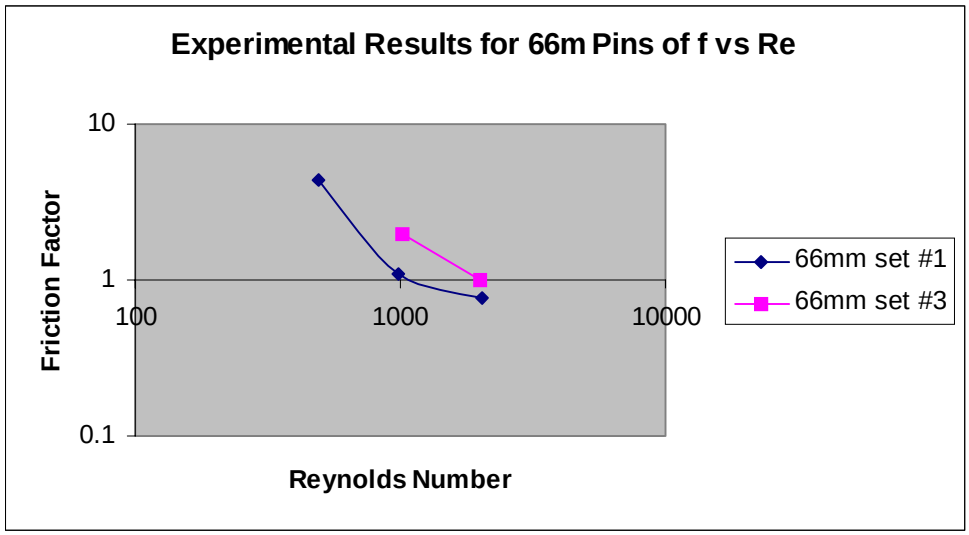

Figure 56. Plot of f vs. Re, 66mm pins

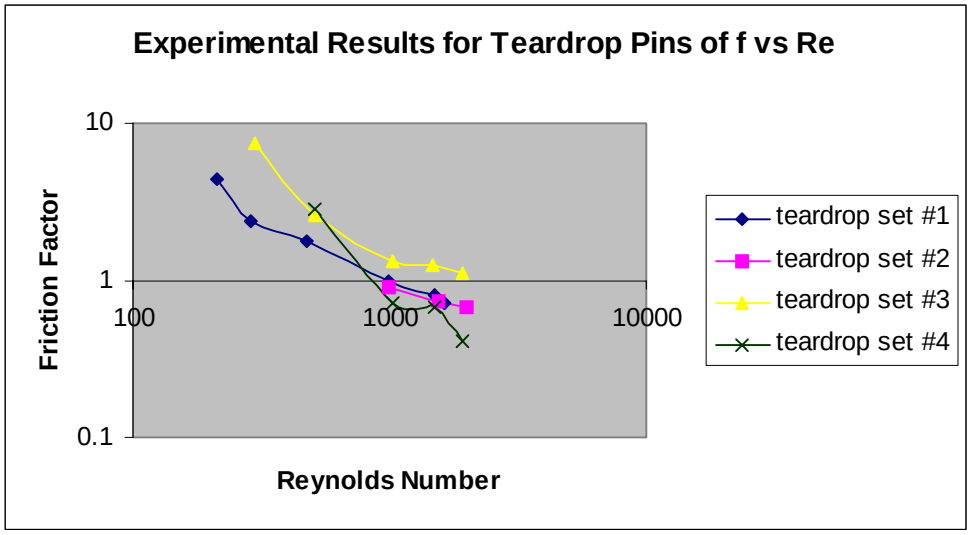

Figure 57. Plot of f vs. Re, teardrop pins

It can be seen in Figures (53 & 54) that the pressure drop was so small that there was effectively no useful data for these pin diameters. For both the 33mm pins and the teardrop pins, there is a distinctive crossover at around Reynolds number of 1000. At Reynolds number of 1000 and above, set #4 is the top performer for these pins, and below 1000, set #1 is the top performer. Figure (58) shows the top performers for Reynolds numbers of 1000 and greater. Figure (59) shows the top performers for Reynolds numbers of 1000 and lower.

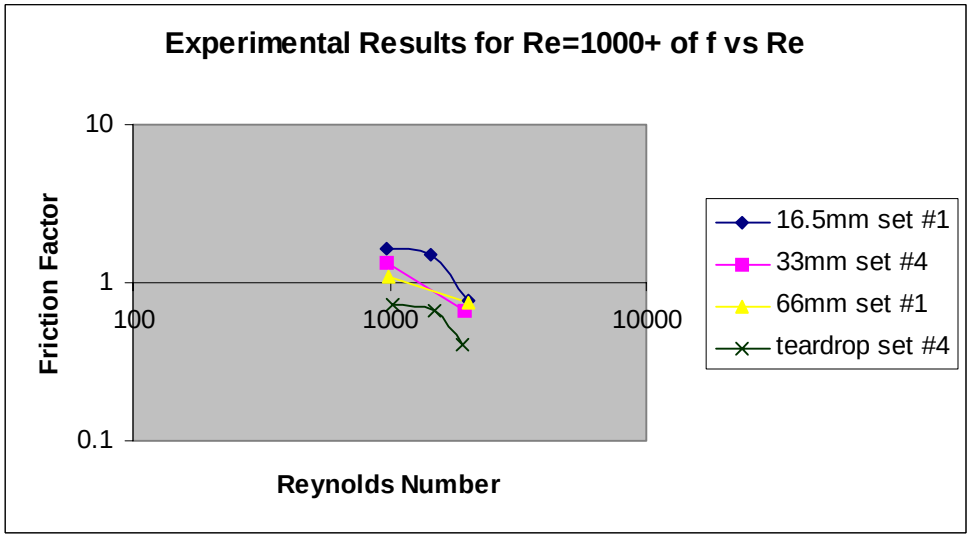

Figure 58. Plot of f vs. Re, top performers, Re=1000+

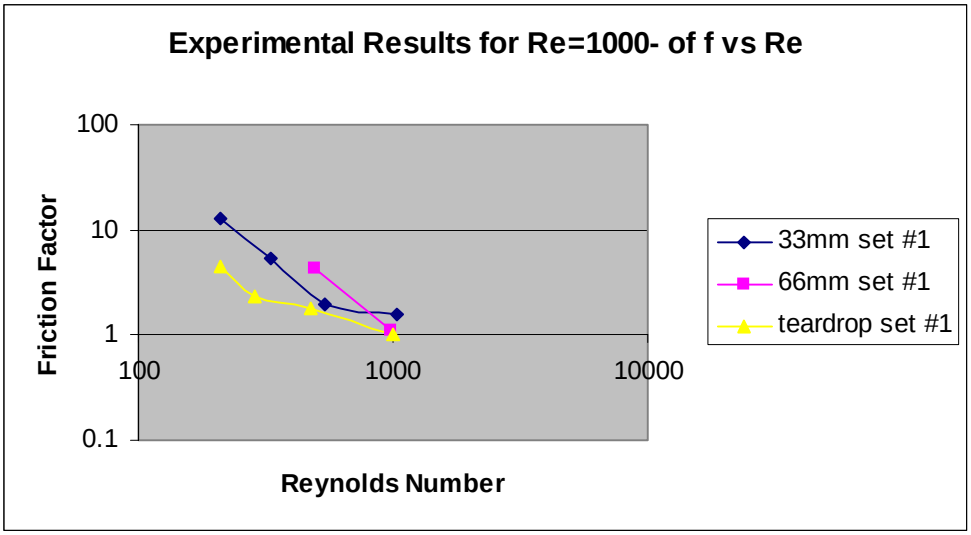

Figure 59. Plot of f vs. Re, top performers, Re=1000-

Figure (58) shows that teardrop set #4 performs best for Reynolds numbers of 1000 and greater. Figure (59) shows that teardrop set #1 performs best for Reynolds numbers of 1000 and lower. These results make sense in the fact that the teardrop shape is streamlined to help prevent flow separation and minimize the friction factor. For the lower Reynolds numbers, where there is significantly lower pressure drops, the full configuration of pins, i.e. set #1, don't provide significant pressure drop increases compared to configurations with fewer pins, therefore teardrop set #1 performed best in this region. Again, there is limited data due to the sensitivity of the instruments used to measure the differential pressure; therefore, the results are incomplete. The top performers for these two cases may ultimately not be if instruments with increased sensitivity were used.

Figures (60-64) show a comparison between some of the friction factor results of this research and the results of Summers (2003). The concern with Summers (2003) friction factor results was that the pressure drop data was corrupt due to leaks in the heat exchanger test section. The pressure drop data that is put into the calculation of friction factor is the most important input for this parameter. The results show that the concerns over the validity of Summers (2003) friction factor data were legitimate. In all of these cases Summers (2003) friction factor results were significantly below the results of this research, specifically for low Reynolds numbers. The lower the flow rates, the more a small leak will affect the pressure drop results.

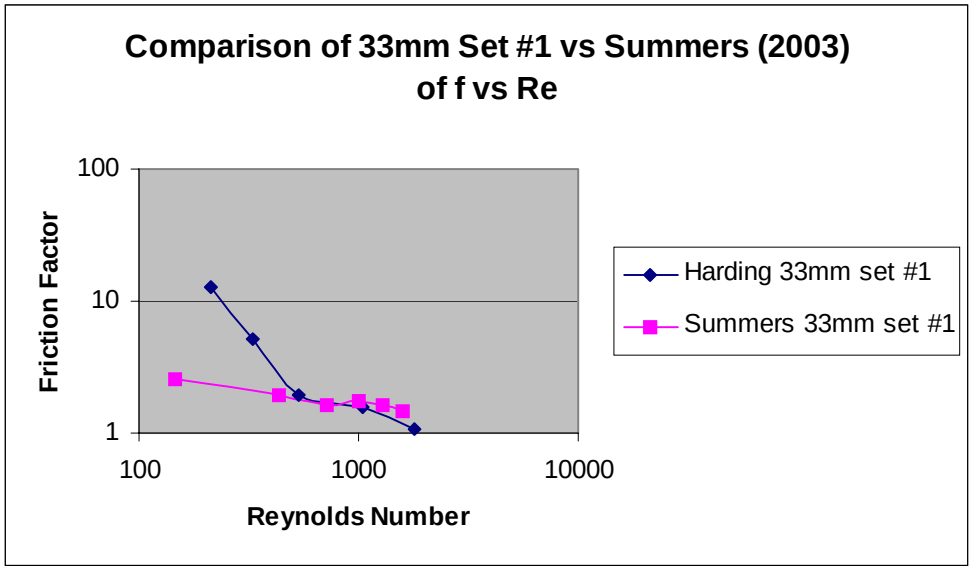

Figure 60. Plot of f vs. Re, 33mm set #1 vs. Summers (2003)

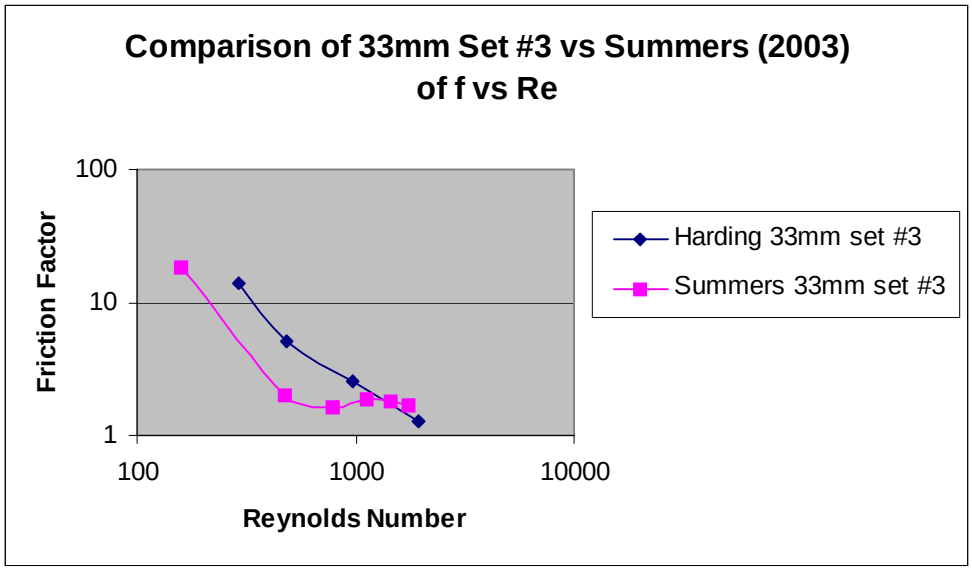

Figure 61. Plot of f vs. Re, 33mm set #3 vs. Summers (2003)

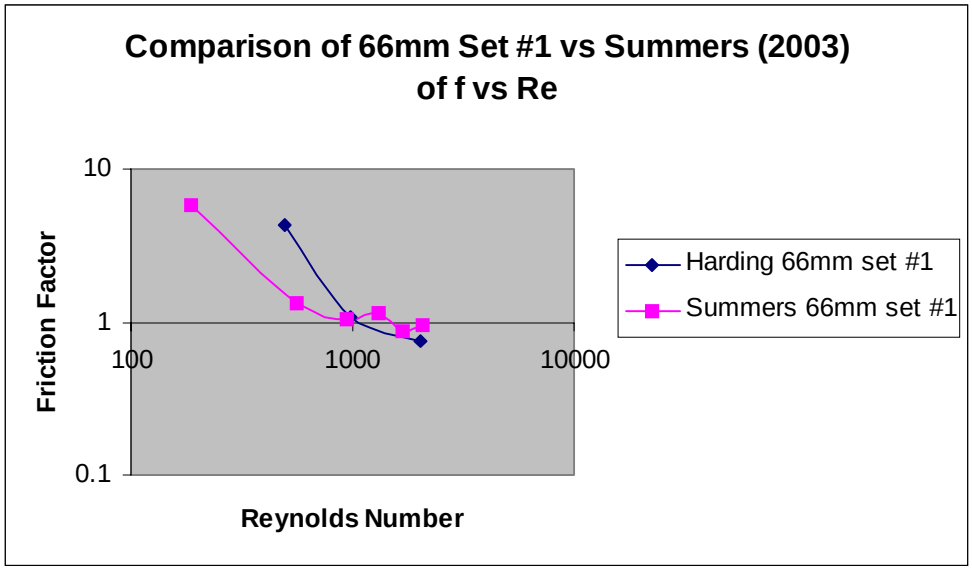

Figure 62. Plot of f vs. Re, 66mm set #1 vs. Summers (2003)

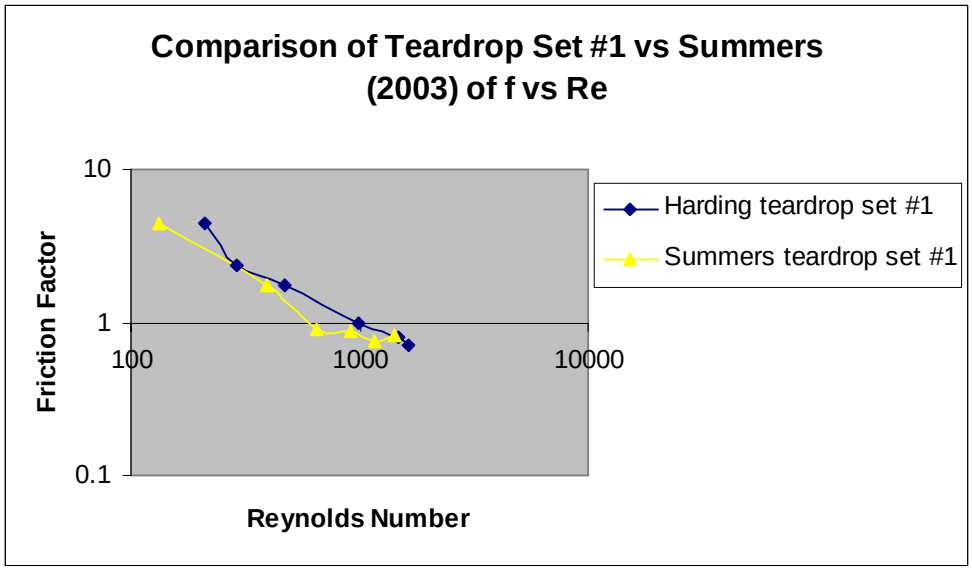

Figure 63. Plot of f vs. Re, teardrop set #1 vs. Summers (2003)

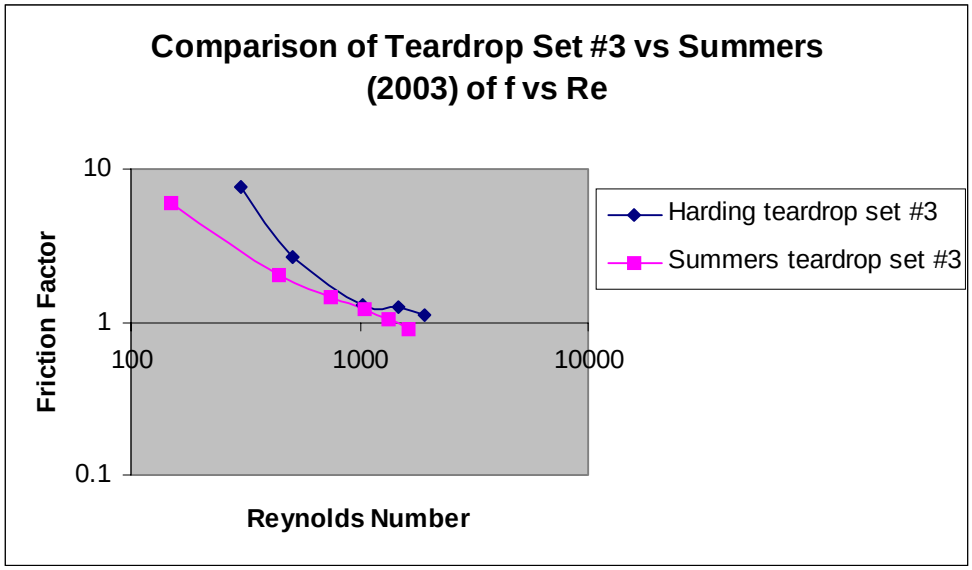

Figure 64. Plot of f vs. Re, teardrop set #3 vs. Summers (2003)

E. HEAT TRANSFER COEFFICIENT VS. FRICTION POWER (E)

The equation for frictional power expenditure (E) is located in Appendix C, and shows that E is equivalent to the heat transfer rate multiplied by the differential pressure across the heat exchanger divided by the wetted flow area. The frictional power expenditure is a parameter that, when plotted against heat transfer coefficient, can be used for optimization of pin diameters and configurations. Ultimately, a high heat transfer coefficient with low frictional power expenditure is desired. This shows that you can provide a high heat transfer with low fluid energy loses. A high heat transfer coefficient is worthless if the fluid loses all its energy while passing through the heat exchanger.

As shown in the previous section, differential pressure measurement is significant to friction factor as well as frictional power expenditure. The results will be incomplete for E as they were for f due to the lack of sensitivity of the differential pressure measuring devices in the lower laminar regime. Figures (65-69) show the results of heat transfer coefficient versus fluid friction power for all pin diameters and configurations.

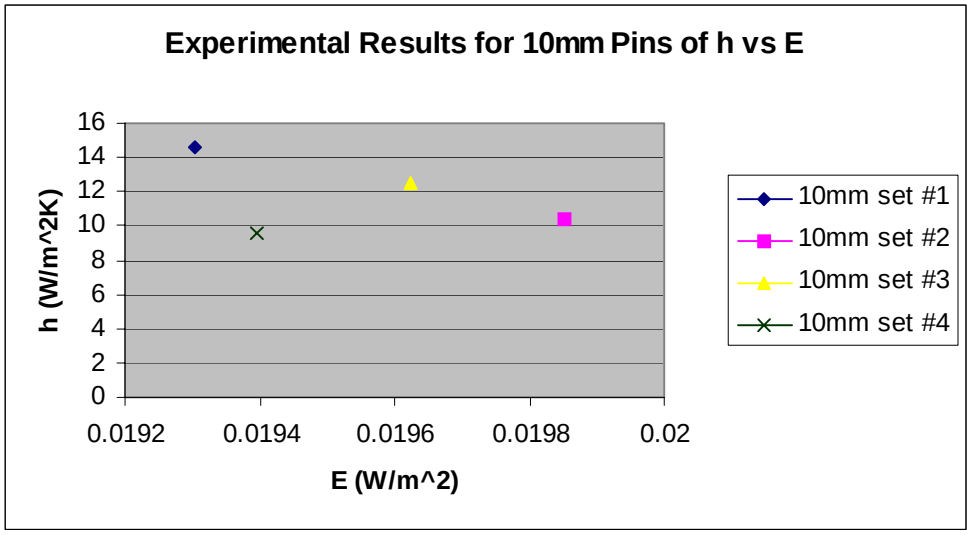

Figure 65. Plot of h vs. E, 10mm pins

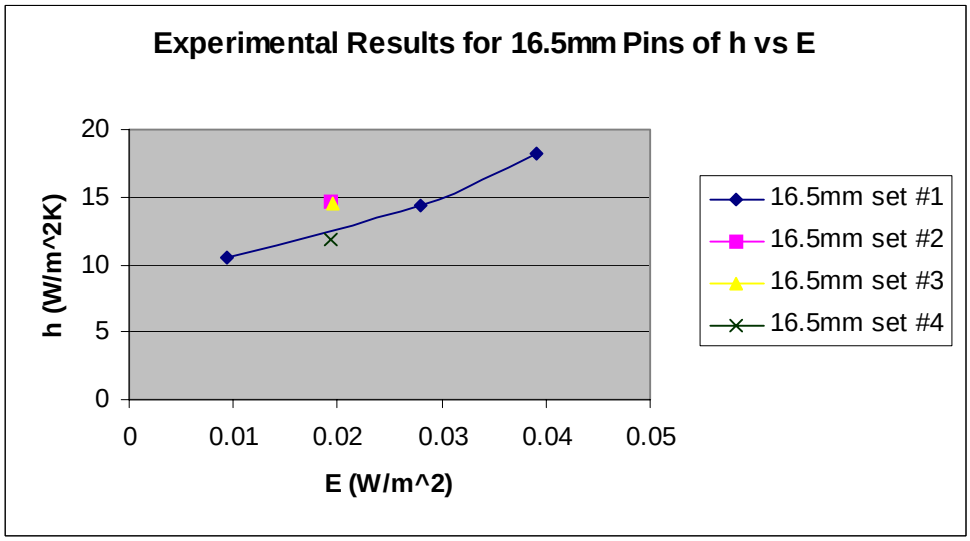

Figure 66. Plot of h vs. E, 16.5mm pins

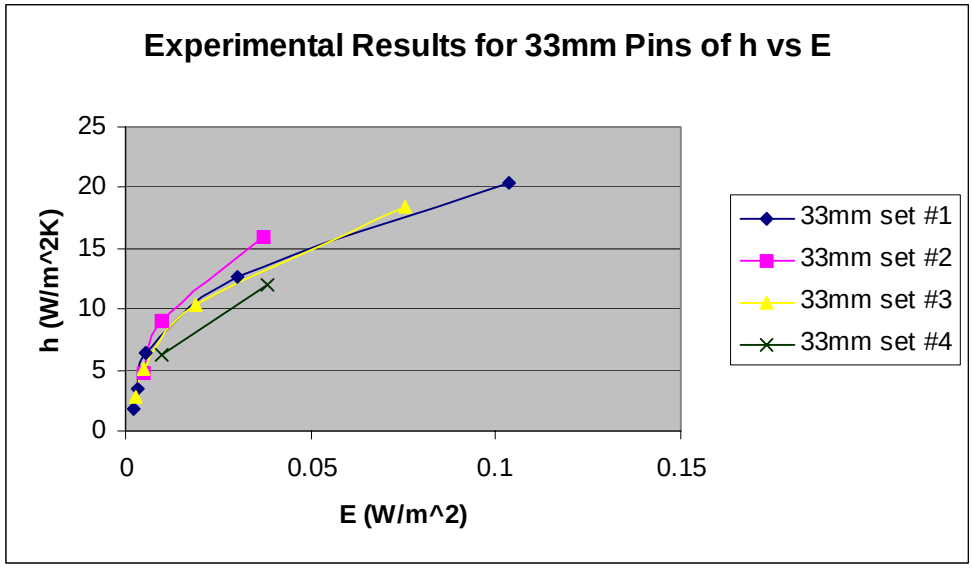

Figure 67. Plot of h vs. E, 33mm pins

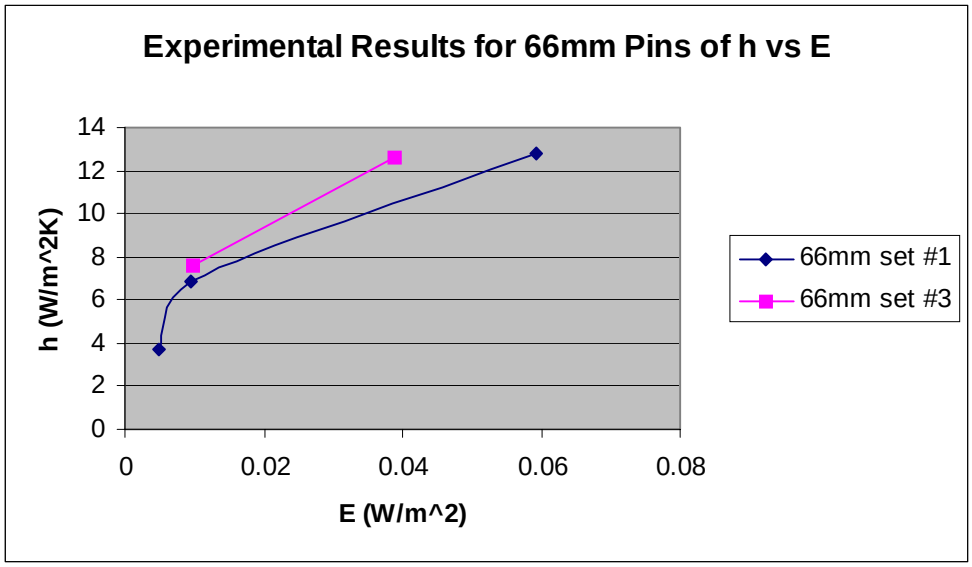

Figure 68. Plot of h vs. E, 66mm pins

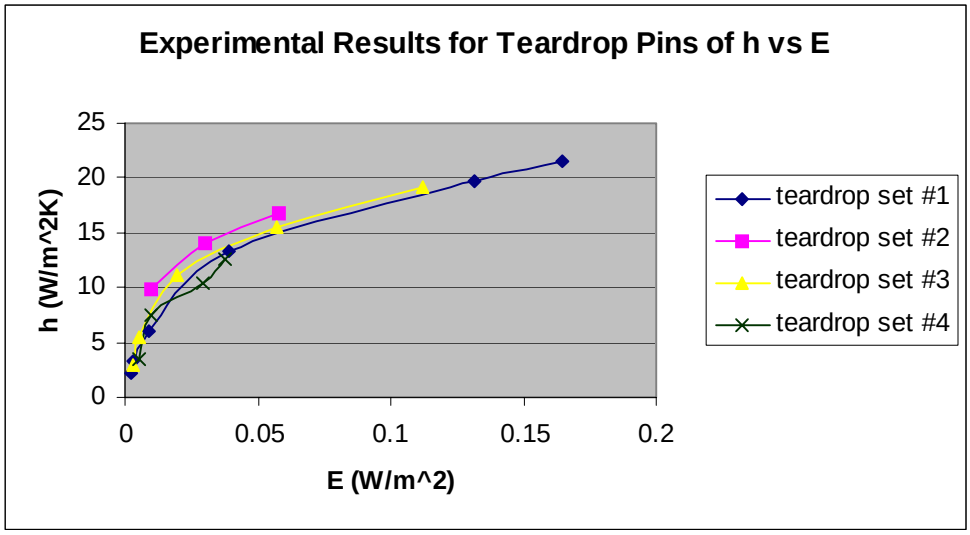

Figure 69. Plot of h vs. E, teardrop pins

Similar to friction factor, there is little useful information for the 10mm pins. The 16.5mm set #1 is the only useful information for this diameter pin. The 16.5mm set #2 is probably a better performer than the 16.5mm set #1, similarly to the 33mm and teardrop pins, but there is insufficient data to say for sure.

Figure (70) shows the results of the top performers for each pin diameter. The 16.5mm set #1 provides the highest heat transfer coefficient versus the frictional power expenditure for all cases where enough data was available. It is highly probable that either the 16.5mm set #2 or even a 10mm set could be the ultimate performer. A differential pressure measuring device with a higher sensitivity to the very small differential pressures associated with low laminar flow rates is required to make a definitive selection for optimum pin diameter and configuration. However, based on the data collected, the 16.5mm set #1 is the optimum choice.

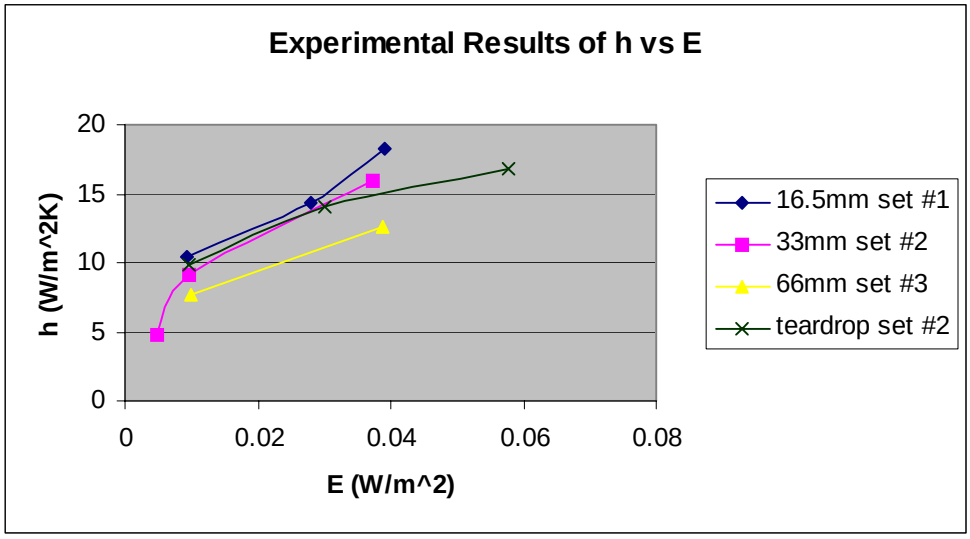

Figure 70. Plot of h vs. E, top performers

F. EFFECT OF CHANGING HEIGHT (H/D)

An analysis was conducted between two pin configurations to determine the effect of changing pin height, or H/D, while keeping the other ratios, X/D and S/D the same. 16.5mm set #1 and 33mm set #2 have the same S/D and X/D, with both equal to 3.0, but the 16.5mm set #1 has an H/D of 2.0, while the 33mm set #2 has an H/D of 1.0. Figures (71 & 72) show the results of heat transfer coefficient versus Reynolds number over the whole laminar range as well as the low laminar regime. The results show that increasing H/D causes a minimal increase in heat transfer coefficient over the whole laminar range, whereas there is virtually no effect on heat transfer coefficient in the low laminar regime. Figures (73 & 74) show similar results for Nusselt number versus Reynolds number. The results show that increasing H/D causes a minimal increase in Nusselt number over the entire laminar range, while there is no significant change in the low laminar regime.

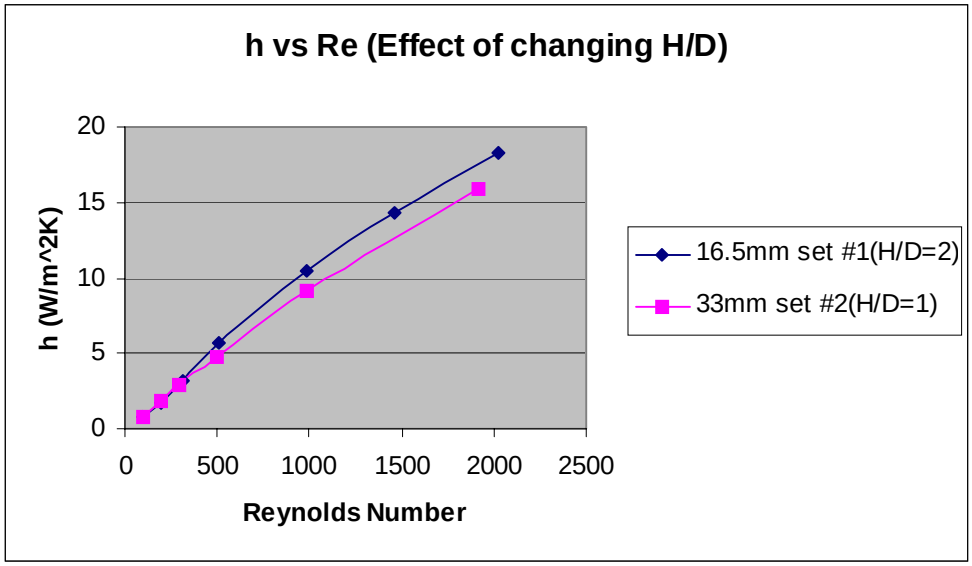

Figure 71. Plot of h vs. Re, effect of changing height

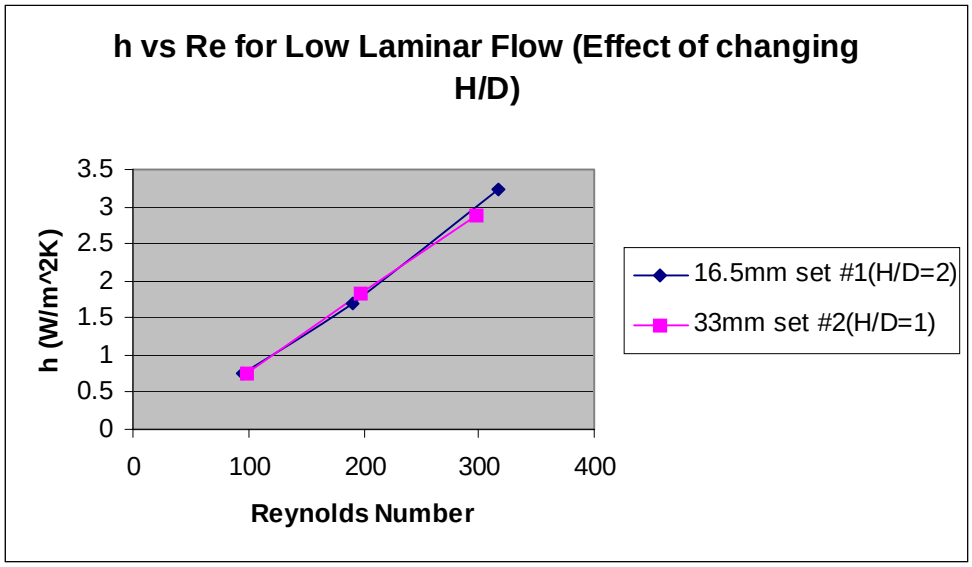

Figure 72. Plot of h vs. Re, effect of changing height, low laminar

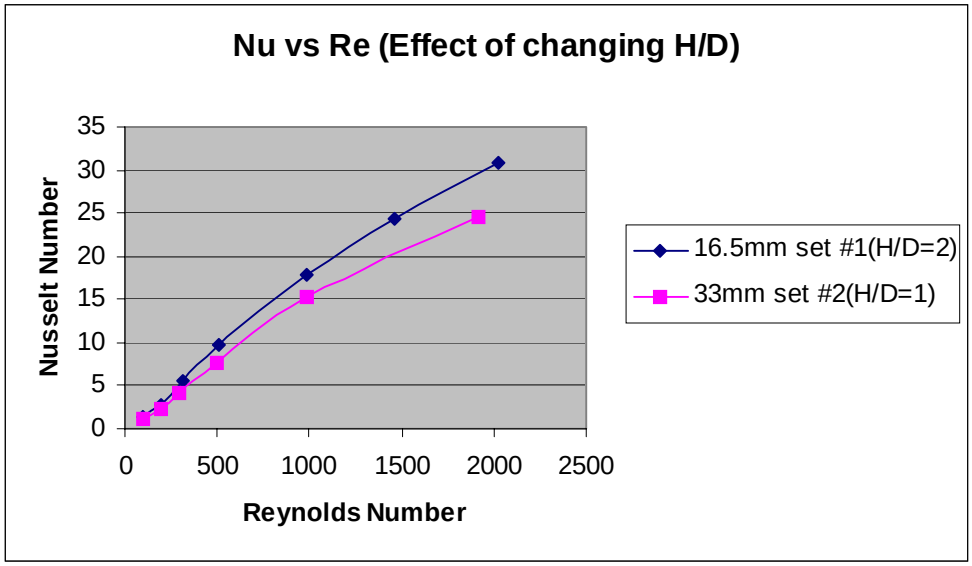

Figure 73. Plot of Nu vs. Re, effect of changing height

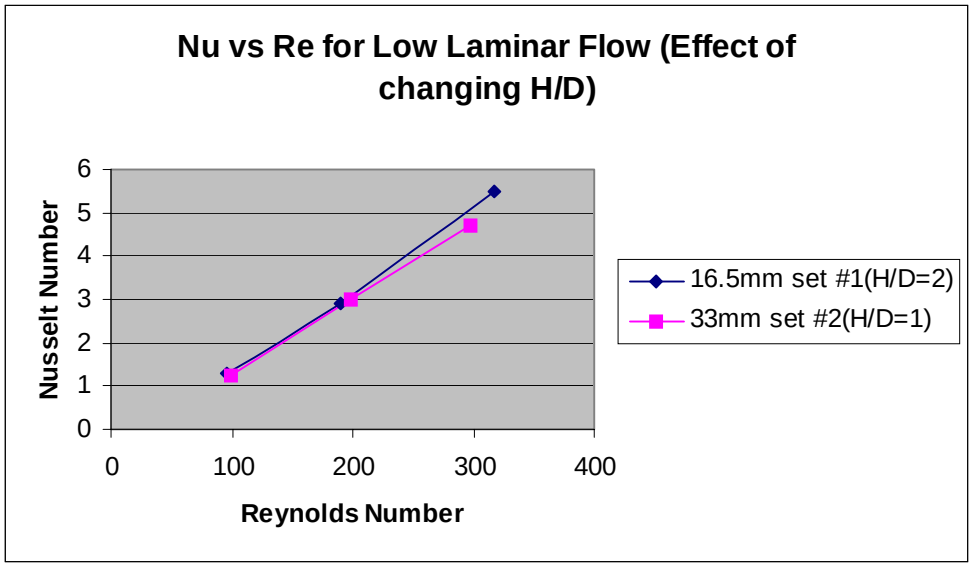

Figure 74. Plot of Nu vs. Re, effect of changing height, low laminar

Figure (75) shows the results of friction factor versus Reynolds number. The results indicate that there is little effect on friction factor when changing H/D. The 33mm set #2 shows minimal advantages over the 16.5mm set #1 in regards to friction factor. This indicates that the shorter the pin, the lower the frictional loses in the flow. Figure (76) shows the results of heat transfer coefficient versus frictional power expenditure. This plot shows that there is a marginal increase in heat transfer coefficient versus frictional power expenditure for an increased pin height. All the results indicate that

changing pin height has very marginal effects on the overall system performance. The results do indicate that increasing the pin height and keeping everything else constant does improve heat exchanger performance, however slight.

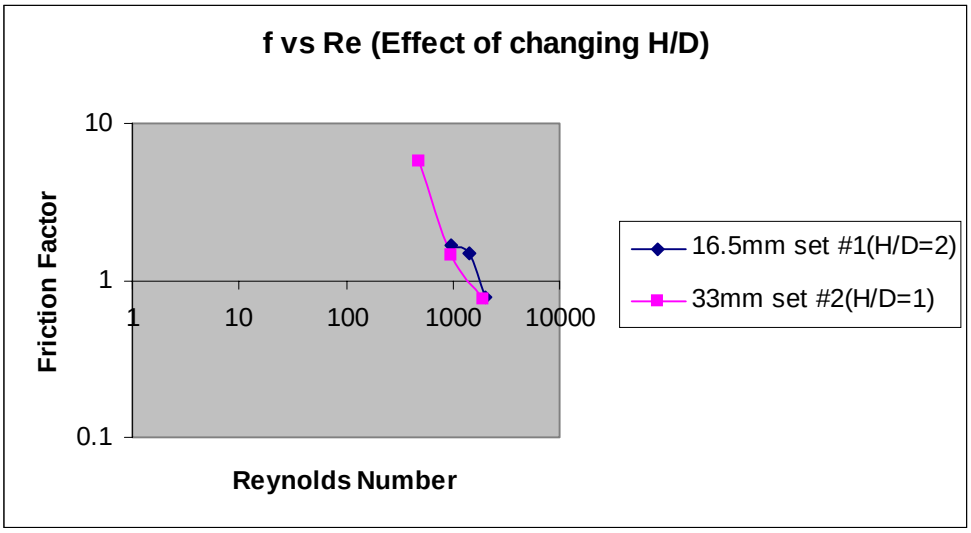

Figure 75. Plot of f vs. Re, effect of changing height

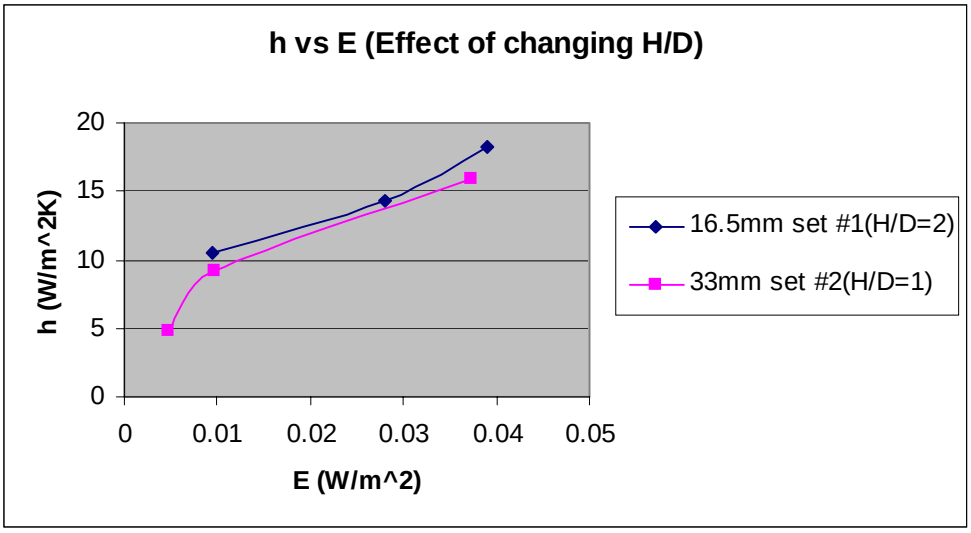

Figure 76. Plot of h vs. E, effect of changing height

G. NUMERICAL VS. EXPERIMENTAL

As stated earlier, Boulares (2003) conducted numerical model research with teardrop shaped pins. One of those numerical model runs was identical to the teardrop set #1 configuration for this research. An analysis was conducted to compare the numerical versus experimental results for this pin configuration. The results with

S/D=X/D=1.5 and H/D=1.0 are presented in Figures (77 & 78). Figure (77) shows the results of Nusselt number versus Reynolds number. The results show that the numerical model predicts a higher Nusselt number than the experimental results yield over the entire laminar range. Results are within 20% in the upper laminar range, with up to 50% deviation in the lower laminar regime. The experimental results appear to have a more uniform and stable linear characteristic. The numerical model curve appears to be less stable, specifically in the lower laminar regime.

Figure (78) shows the results of friction factor versus Reynolds number. The results show that there is a near linear trend for each curve as expected on a log-log plot. The smaller slope of the numerical curve compared to the experimental curve indicates that the numerical model is not as sensitive to the differential pressure across the heat exchanger as the experimental results suggest it should be. The experimental results shown were obtained by using the micro-manometer as the differential pressure monitoring device. Recall Figure (52) in which the results of teardrop set #1 were used to show the accuracy of both pressure monitoring devices, the micro-manometer and the differential pressure transducer. This gives credibility to the experimental results and indicates that the numerical model in not as sensitive to differential pressure as it should be.

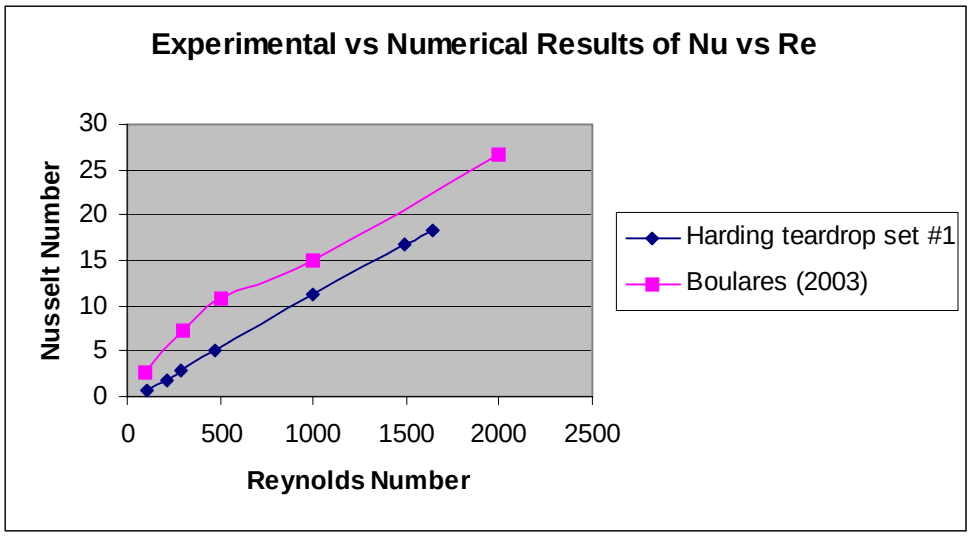

Figure 77. Plot of Nu vs. Re, experimental vs. numerical

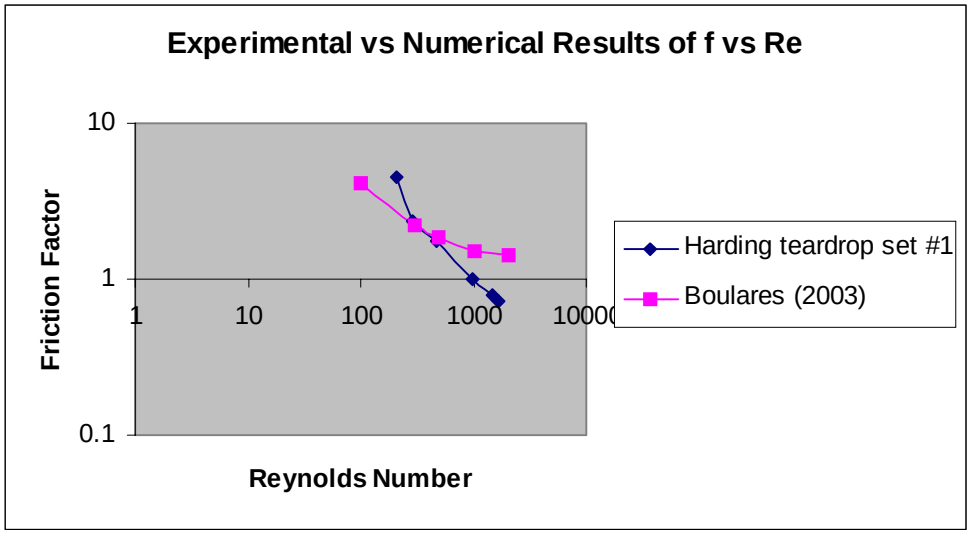

Figure 78. Plot of f vs. Re, experimental vs. numerical

There is currently no numerical modeling data collected for cylindrical pins in the laminar regime. Research in this field is expanding at the Naval Postgraduate School, and this research can be used to validate those future models.

H. MACRO VS. MICRO

As stated earlier, Rose (2004) and Roussakies (2004) designed, built and conducted experiments on micro-heat exchangers. All research conducted at the macro level can be scaled down to the micro level as long as the appropriate dimensionless numbers are based on hydraulic diameter, as they are in this research. Therefore, results can be directly compared between the two scales when dealing with heat exchangers with similar defining characteristics such as X/D, S/D and H/D.

The 33mm set #2 has similar dimensions to Roussakies' heat exchanger #1. Both heat exchangers have the same S/D and X/D, which are both equal to 3.0. The 33mm set #2 has an H/D of 1.0, which is almost the same as Roussakies' heat exchanger #1 H/D value of 0.8, and therefore a comparison of the two is valid. Figure (79) shows the results of Nusselt number versus Reynolds number for the two heat exchangers. The results show that the Nusselt number for both the macro and micro are very close to each other and within 20% across the range of Reynolds numbers analyzed.

Figure (80) shows the results of heat transfer coefficient versus Reynolds number for the two heat exchangers. Also, Figure (80) shows a curve that represents a scaled version of the heat transfer coefficient of this research. The hydraulic diameter for the

33mm set #2 is 43.13 mm which is about fifty times as much as the hydraulic diameter from Roussakies (2004) heat exchanger #1 which is 0.856 mm. Since the Nusselt number should be the same for each heat exchanger, the heat transfer coefficient should therefore scale up by fifty times for the micro-heat exchanger (since its hydraulic diameter is fifty times smaller). It is clear from Figure (80) that the scaled up curve from the current data is close, and always within the same order of magnitude, with the actual results of the micro-heat exchanger. This validates the assumption that results conducted at the macro level can be scaled down to the micro level. This means that all data collected at the macro level can be used to estimate expected heat transfer coefficients at the micro level for heat exchangers of similar ratios of X/D, S/D and H/D.

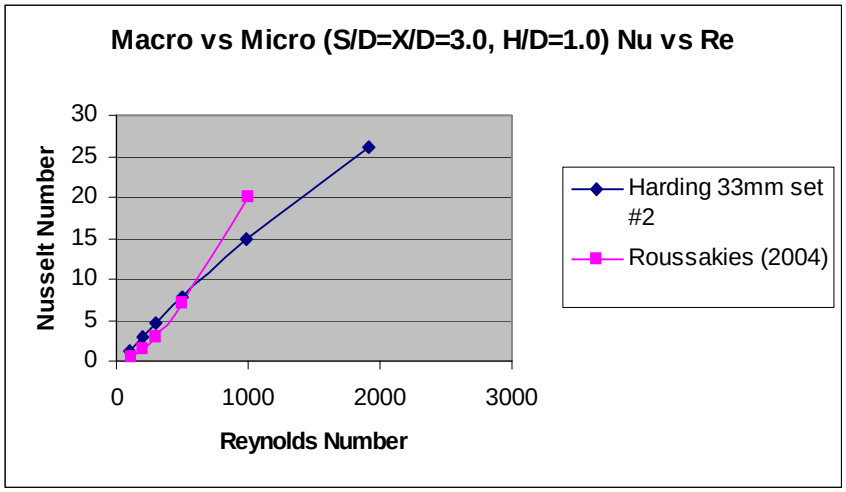

Figure 79. Plot of Nu vs. Re, macro vs. micro

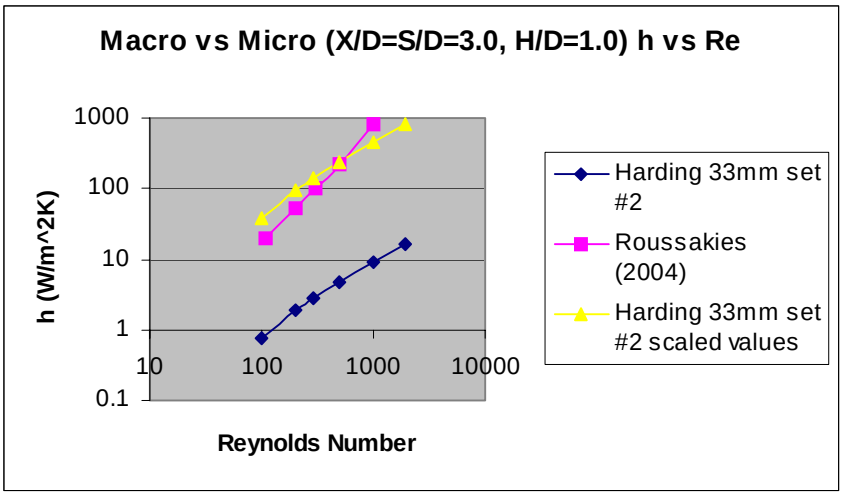

Figure 80. Plot of h vs. Re, macro vs. micro

VI. CONCLUSIONS AND FUTURE WORK

A. CONCLUSIONS

One of the primary objectives of this thesis was to redesign the heat exchanger rig to achieve a leak tight setup. The heat exchanger was rebuilt and enclosed with Plexiglas and has proven to be airtight thus far. The pressure drop data obtained appears reliable as two different pressure-monitoring devices tracked each other well throughout the work.

With the modified rig design significant amounts of data were collected to build upon the current database for the various pin diameters, shapes and configurations. One set of the current empirical data was compared to prior results from a numerical model and found to correlate well. The numerical model showed a relative lack of sensitivity to differential pressure compared to the experimental data.

It was also shown that the macro level data can be successfully scaled to the micro level in a consistent manner. This allows all data to be scaled down to the micro level to predict heat transfer coefficients of micro-heat exchangers.

The pressure drop and friction factor data from Summers (2003) was not consistent with the current results and is suspected to be corrupted due to leaks and other infidelities in the experimental equipment. It appears that his differential pressure data input into the friction factor calculation was lower than it should be, especially for low Reynolds numbers, due to small air leaks in the heat exchanger test section. This appears to be corrected by the heat exchanger's new design which appears to be airtight and providing good pressure drop data.

The differential pressure data that was gathered appears to be good; however, there is simply not enough data due to the very small pressure drops across the heat exchanger at very low flow rates. Differential pressure monitoring devices with increased sensitivity are required to accurately measure the pressure drops across the heat exchanger with very low flow rates. Based on the limited data obtained, the 16.5mm set #1 performed the best in regards to achieving the highest heat transfer coefficients with the least amount of fluid power expenditures. This may not actually be the optimum

configuration due to the incomplete nature of the differential pressure data for the low pressure drop configurations.

B. FUTURE WORK

The future of this research is going to focus on the micro-heat exchanger design. It has already been proven that the experiments conducted thus far at the macro level can be scaled down to the micro level. Micro-heat exchangers are becoming more and more important as technology continues to improve and components continue to get smaller. The need to remove high quantities of heat in a small volume is very high; therefore, the necessity to characterize such heat exchangers at the micro level is important.

Numerical models are increasingly important to extend the parameter space that can be tested. This is because numerical models are extremely cost and time effective and afford flexibility. However, numerical models must first be validated by quality empirical data, before they can be used for extended predictions.

APPENDIX A. NOMENCLATURE

$\bar{A}$	Average flow area (m^2)
A_{duct}	Duct area (m^2)
A_{wf}	Wetted area for flow (includes endwalls) (m^2)
A_{wh}	Wetted area for heat (no endwalls) (m^2)
HX	Heat exchanger
Cp	Specific heat capacity (J/kg-K)
D, d	Pin diameter (m)
D_h	Hydraulic diameter (m)
E	Fluid friction power per unit surface area (W/m^2)
f	Friction factor
h	Heat transfer coefficient (W/m^2 -K)
$\bar{h}$	Average heat transfer coefficient (W/m^2 -K)
H	Pin height (m)
k	Thermal conductivity (W/m-K)
L	Length of HX
$\dot{m}$	System mass flow rate (kg/sec)
N_p	Number of pins installed
Nu_{Dh}	Nusselt number based on hydraulic diameter
P_{dens}	Pressure for density (Pa)
P_{in}	Heat exchanger inlet pressure (Pa)
P_{man}	Manometer pressure (inch H_20)
P_{NOAA}	Reference pressure from NOAA (inch H_20)
P_{off}	Reference offset pressure (Pa)
P_{turb}	Heat Exchanger outlet pressure (Pa)
P_{vdc}	Voltage output of differential pressure transmitter (VDC)
ΔP, dp	Heat exchanger differential pressure or pressure drop (Pa)
q	Heat transfer rate (W)
$\dot{Q}$	Volumetric flow rate (m^3/s)
R	Gas constant (J/kg-K)
Re_{Dh}	Reynolds number based on hydraulic diameter
S	Span wise spacing (m)
T_{ave}	Average heat exchanger outlet temperature (K)
T_{in}	Heat exchanger inlet temperature (K)
T_{out}	Heat exchanger outlet temperature (K)
T_{wall}	Endwall temperature (K)
ΔT	Temperature change across heat exchanger (K)
ΔT_{lm}	Log mean bulk differential temperature (K)
$\bar{U}$	Average fluid velocity (m/sec)
V_{off}	Reference offset voltage, flow (VDC)
V_{open}	Open fluid volume in heat exchanger
X	Stream wise spacing (m)
W	Width of HX (m)

ρ	Density (kg/m^3)
μ	Dynamic viscosity (Pa-s)

APPENDIX B. PIN CONFIGURATIONS

(Flow is from left to right)

1. 10 mm Pin Configurations

Figures (81-84) show the various configurations tested for the 10 mm pins.

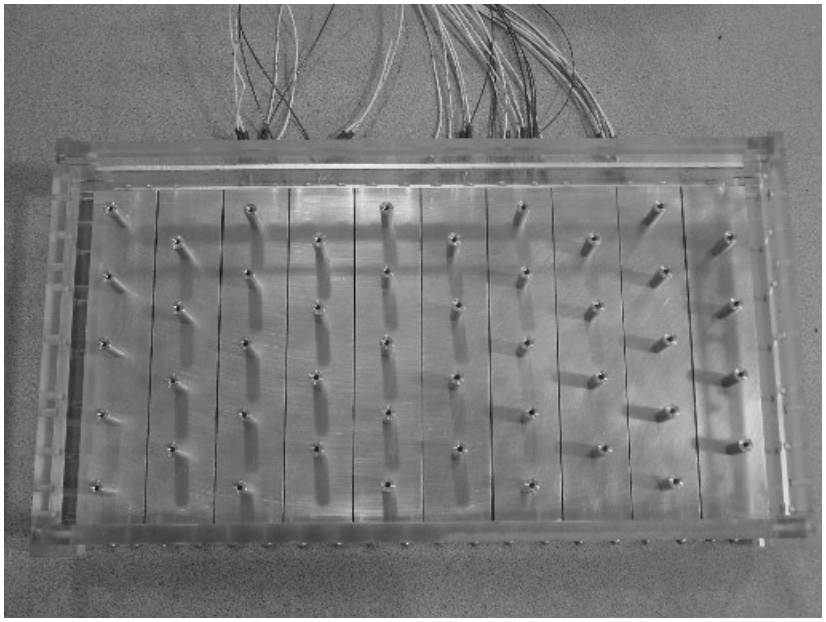

Figure 81. 10 mm set #1, S/D = 5.0 X/D = 5.0 H/D = 3.3

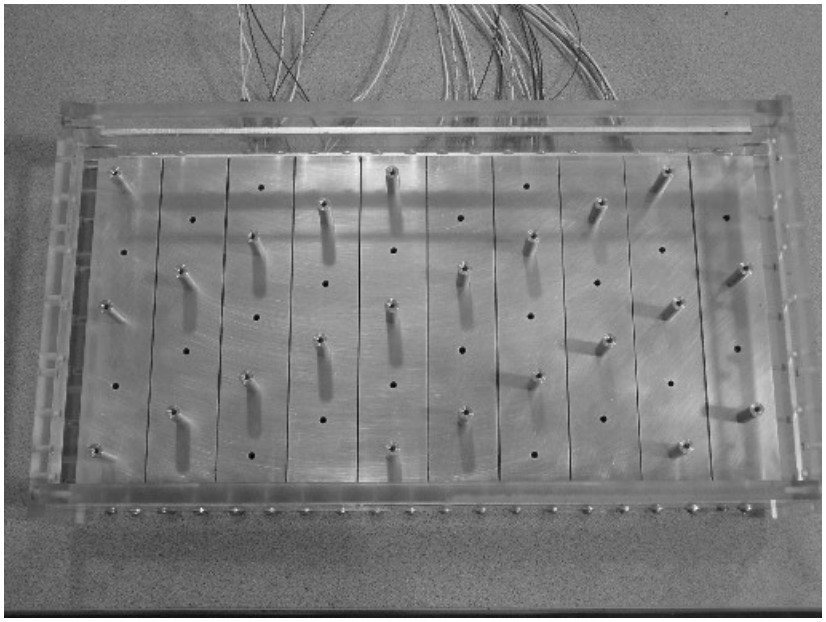

Figure 82. 10 mm set #2, S/D = 10.0 X/D = 10.0 H/D = 3.3

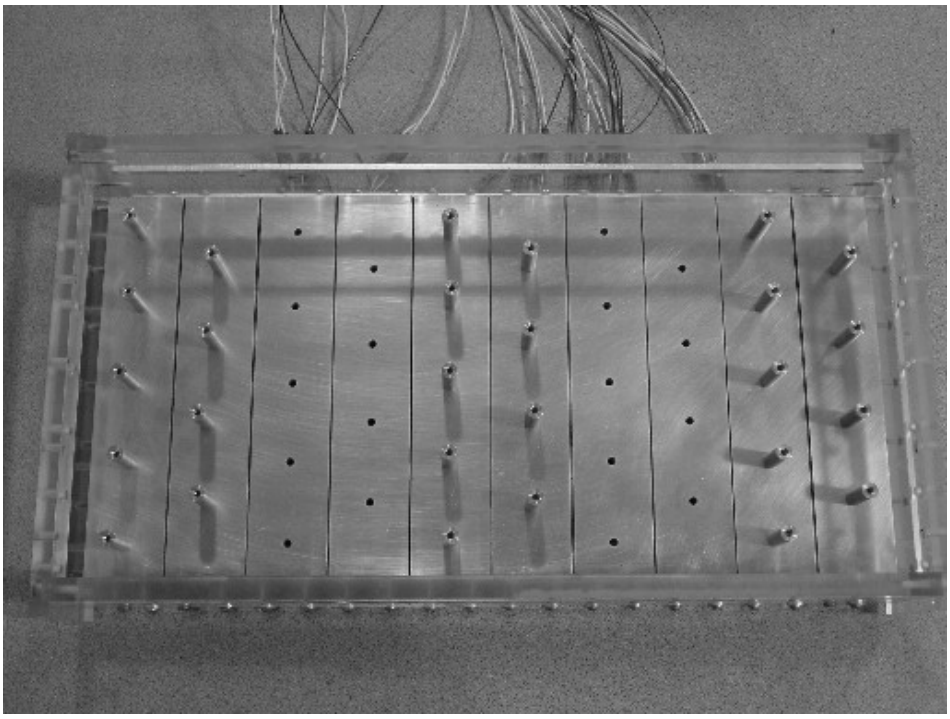

Figure 83. 10 mm set #3, S/D = 5.0 X/D = 10.0 H/D = 3.3

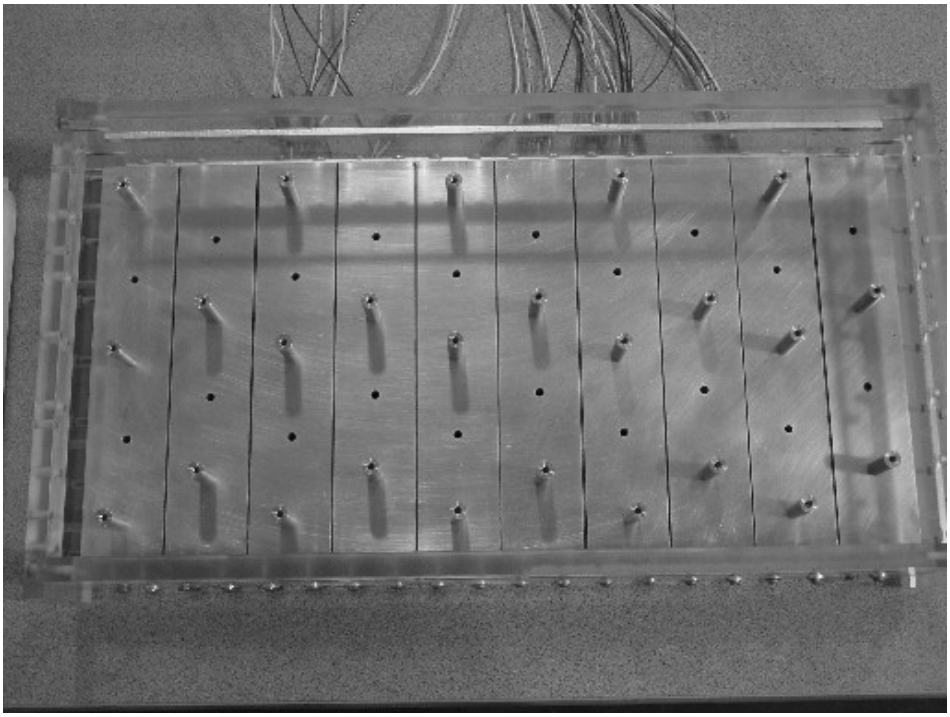

Figure 84. 10 mm set #4, S/D = 10.0 X/D = 5.0 H/D = 3.3

2. 16.5 mm Pin Configurations

Figures (85-88) show the various configurations tested for the 16.5 mm pins.

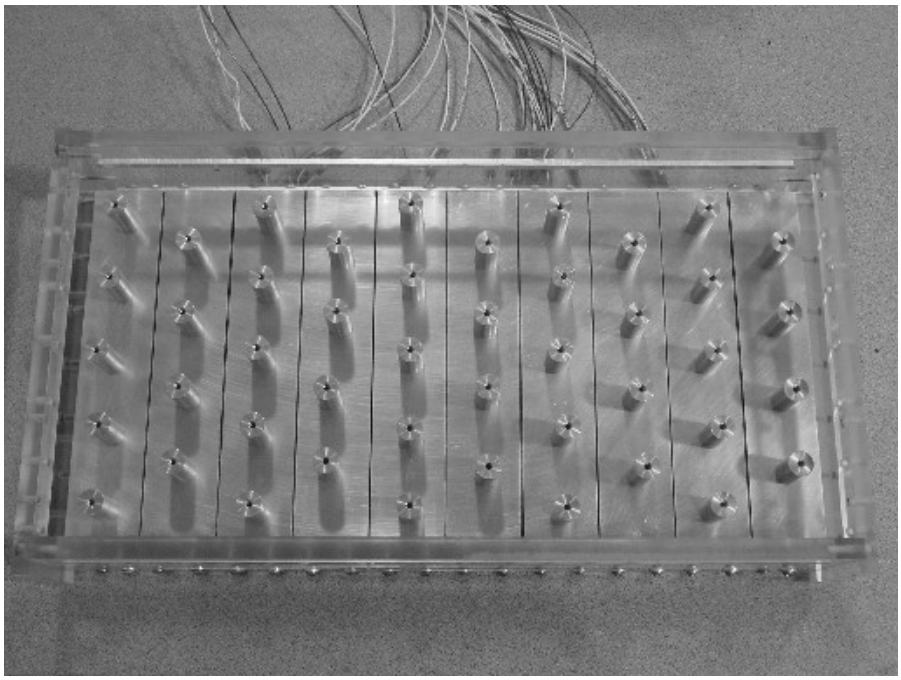

Figure 85. 16.5 mm set #1, S/D = 3.0 X/D = 3.0 H/D = 2.0

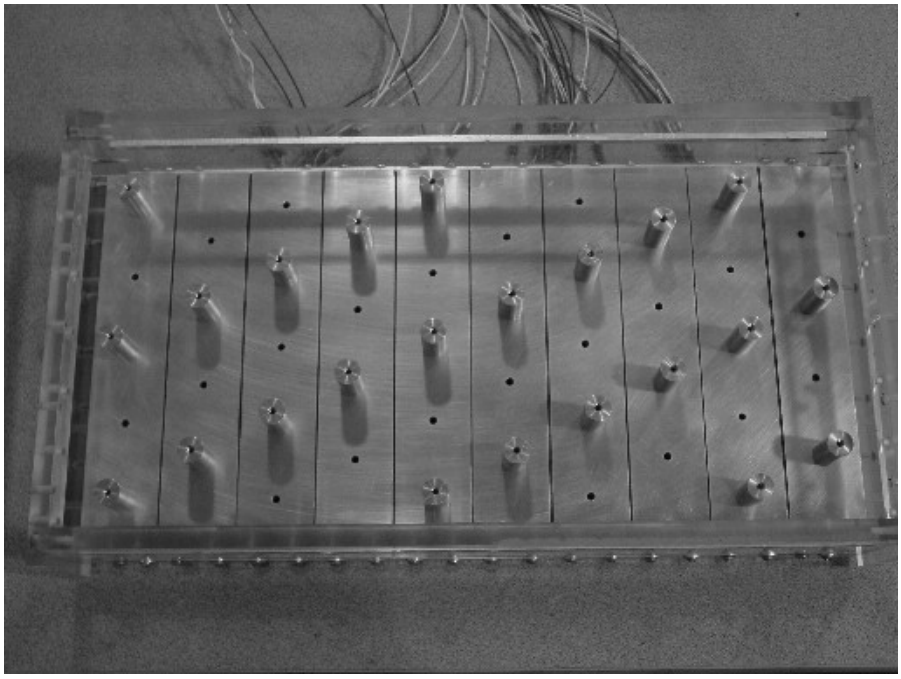

Figure 86. 16.5 mm set #2, S/D = 6.1 X/D = 6.1 H/D = 2.0

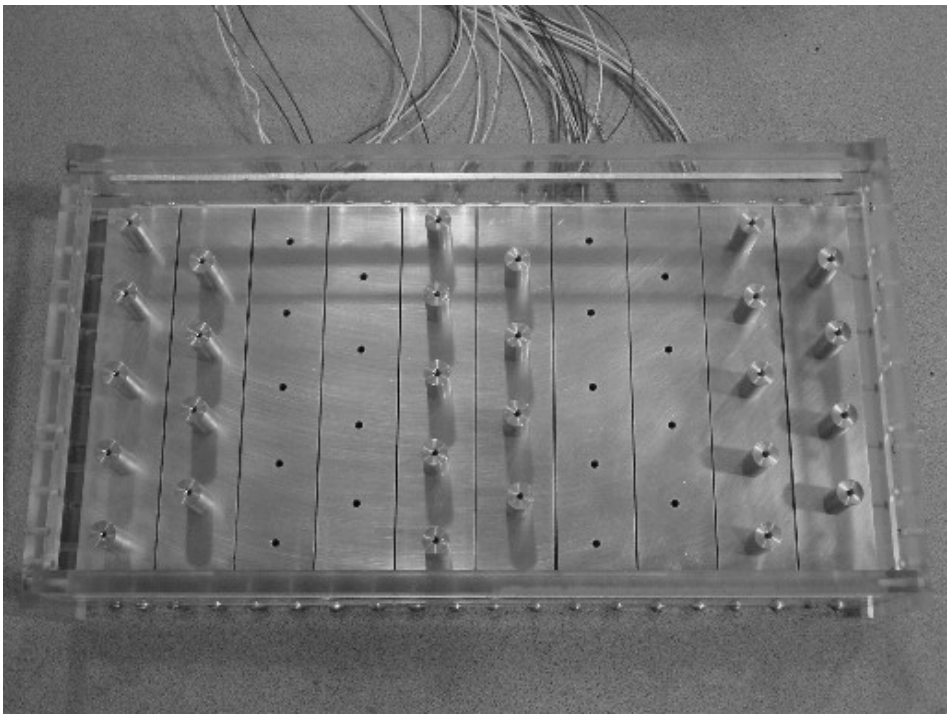

Figure 87. 16.5 mm set #3, S/D = 3.0 X/D = 6.1 H/D = 2.0

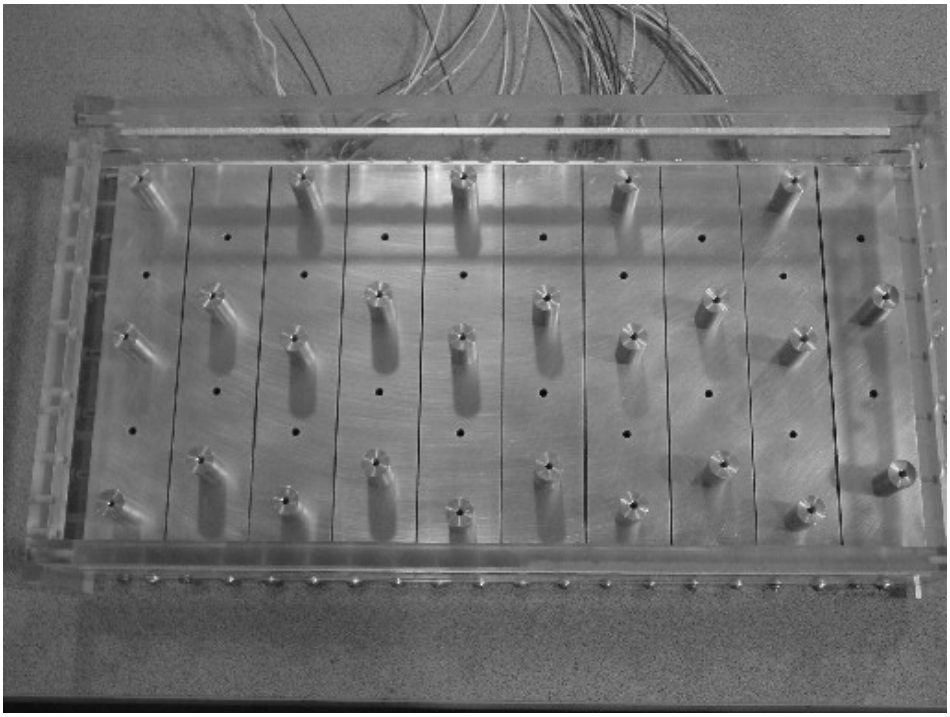

Figure 88. 16.5 mm set #4, S/D = 6.1 X/D = 3.0 H/D = 2.0

3. 33 mm Pin Configurations

Figures (89-92) show the various configurations tested for the 33 mm pins.

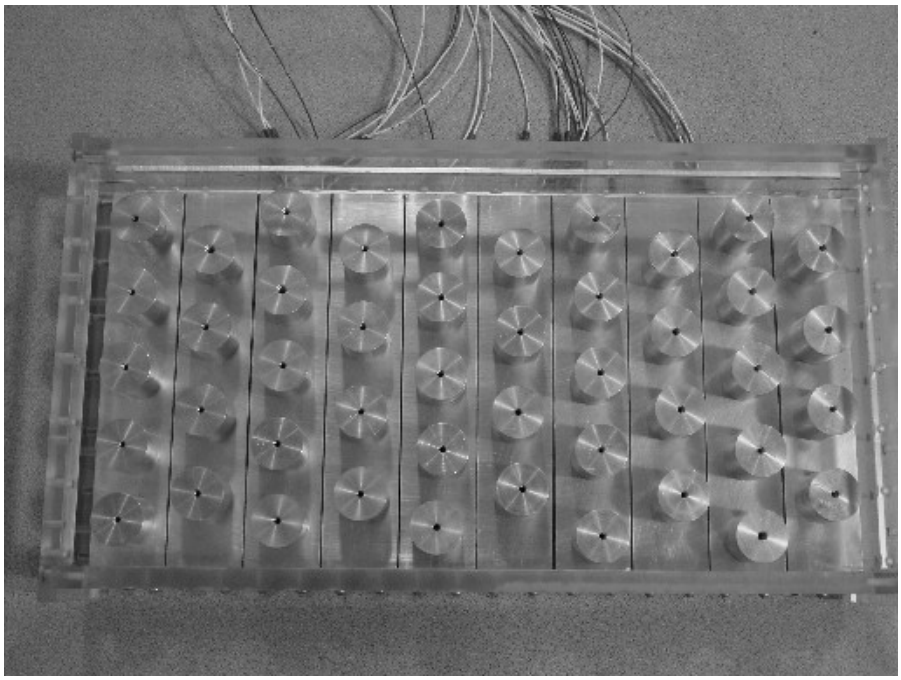

Figure 89. 33 mm set #1, S/D = 1.5 X/D = 1.5 H/D = 1.0

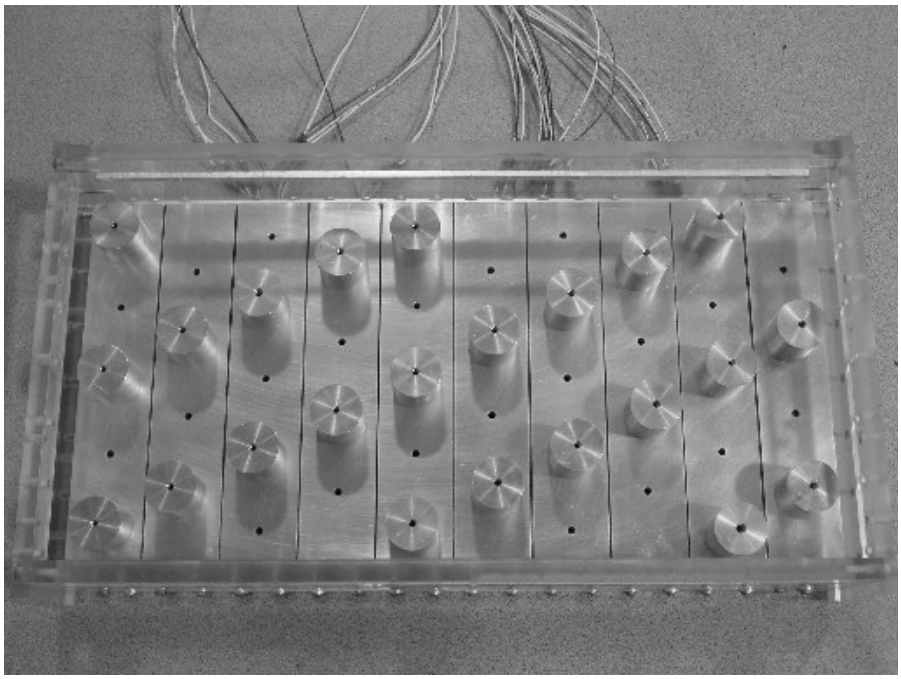

Figure 90. 33 mm set #2, S/D = 3.0 X/D = 3.0 H/D = 1.0

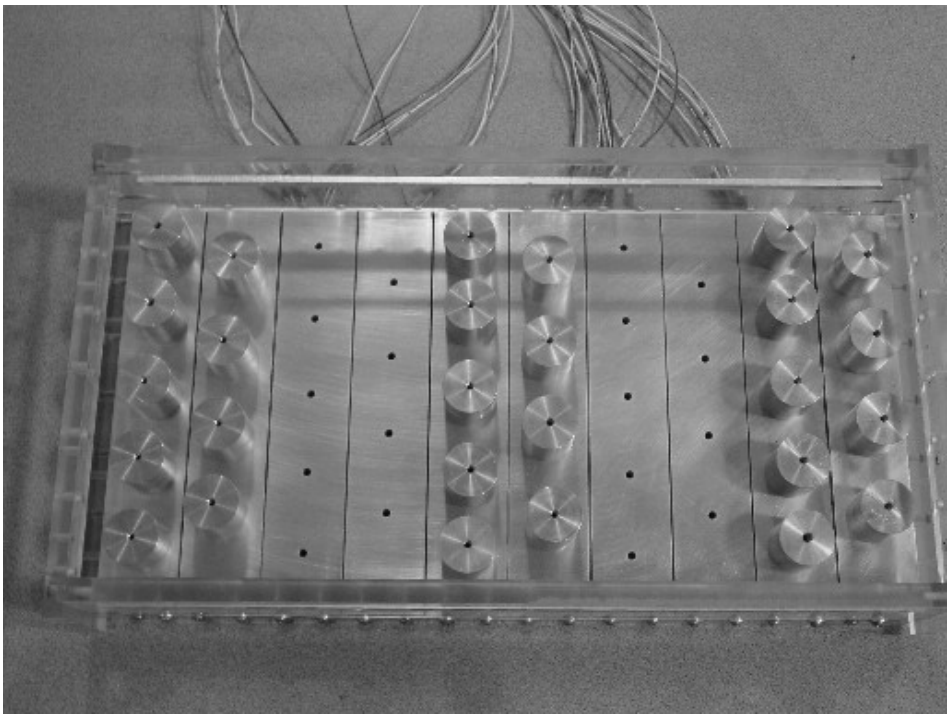

Figure 91. 33 mm set #3, S/D = 1.5 X/D = 3.0 H/D = 1.0

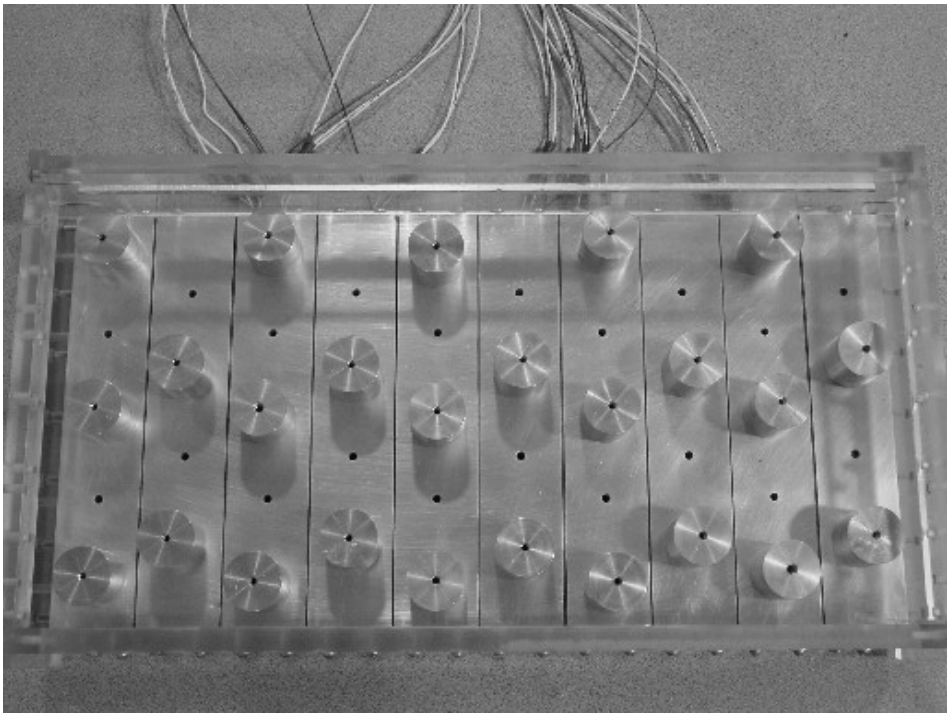

Figure 92. 33 mm set #4, S/D = 3.0 X/D = 1.5 H/D = 1.0

4. 66 mm Pin Configurations

Figures (93-94) show the various configurations tested for the 66 mm pins. Only set numbers one and three were completed due to the physical size constraints of the pins and the heat exchanger.

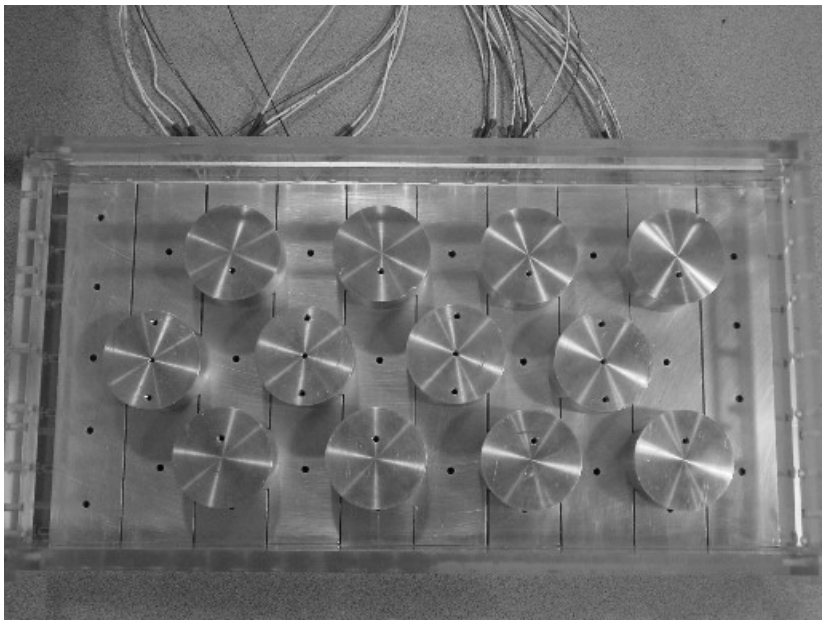

Figure 93. 66 mm set #1, S/D = 1.89 X/D = 0.76 H/D = 0.5

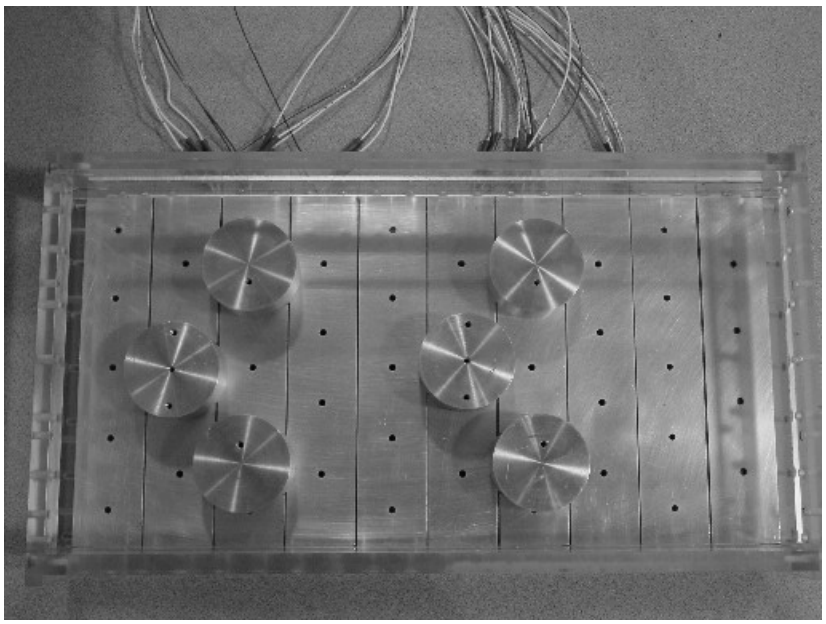

Figure 94. 66 mm set #3, S/D = 1.89 X/D = 1.52 H/D = 0.5

5. Teardrop Shape Pin Configurations

Figures (95-98) show the various configurations tested for the teardrop shaped pins. The last row is filled with 33 mm cylindrical pins to prevent the teardrop tails from extending into the exit duct.

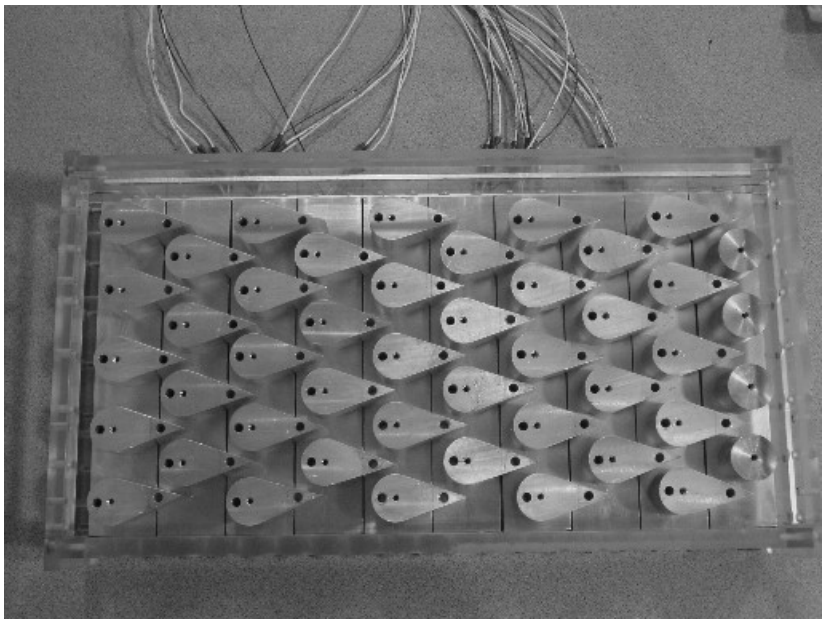

Figure 95. Teardrop set #1, S/D = 1.5 X/D = 1.5 H/D = 1.0

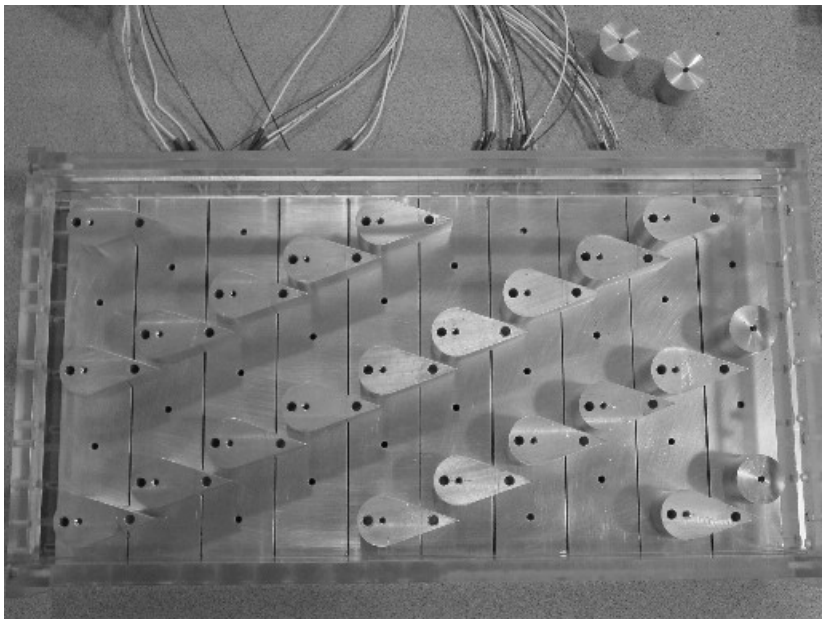

Figure 96. Teardrop set #2, S/D = 3.0 X/D = 3.0 H/D = 1.0

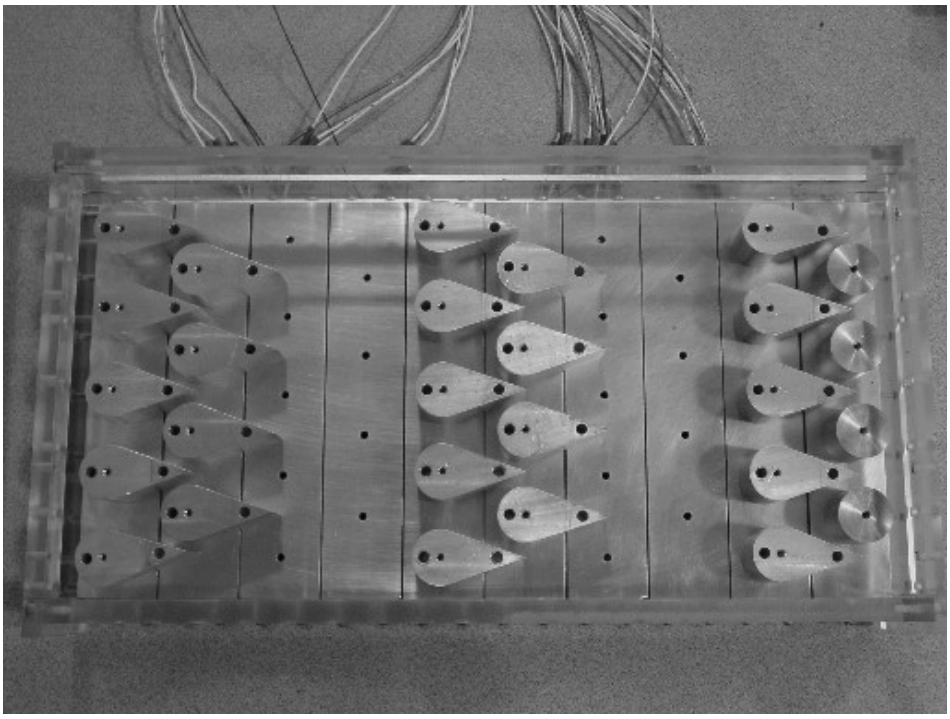

Figure 97. Teardrop set #3, S/D = 1.5 X/D = 3.0 H/D = 1.0

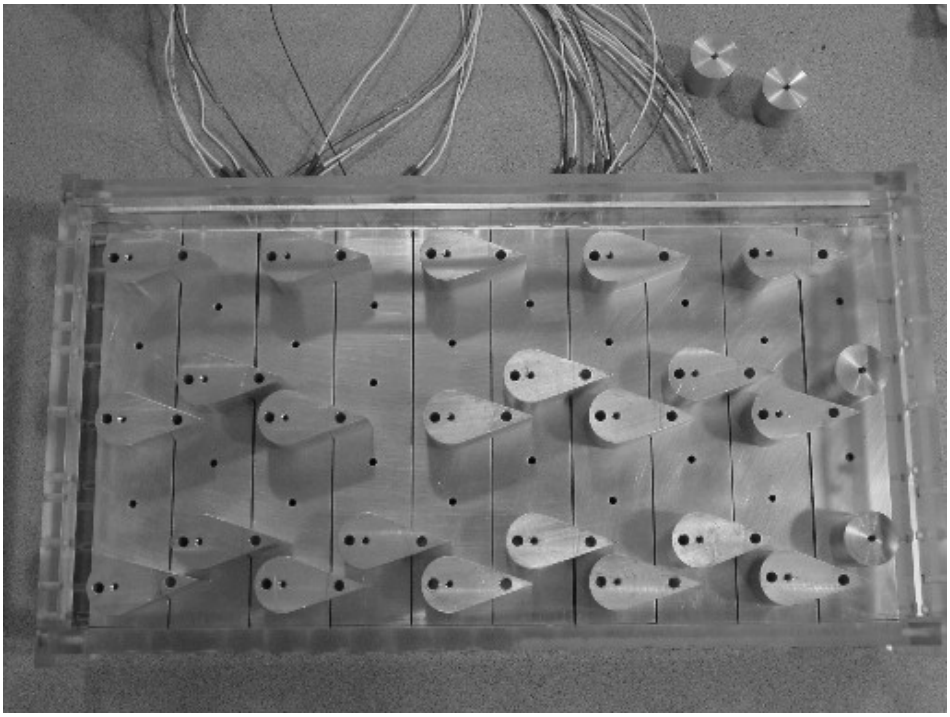

Figure 98. Teardrop set #4, S/D = 3.0 X/D = 1.5 H/D = 1.0

THIS PAGE INTENTIONALLY LEFT BLANK

APPENDIX C. EQUATIONS

1. Conversions

a. Volumetric flow - VDC to M^3/sec:

$$\dot{Q}\left[\frac{m^3}{s}\right] = (\dot{Q}_{VDC}\left[VDC\right] - \dot{Q}off\left[VDC\right])0.0204\left[\frac{m^3}{\sec - VDC}\right]$$

b. Volumetric flow – SLPM to M^3/sec:

$$\dot{Q}[\frac{m^3}{\sec}] = (\dot{Q}[\frac{Liters}{\min}])(\frac{1\min}{60\sec})(0.001\frac{m^3}{Liter})$$

c. Pressure – VDC to Pascals:

$$P[Pa] = (P_{VDC}[VDC] - P_{off\,[VDC]})(248.84[\frac{Pa}{inH_2O}])(6.25[\frac{inH\,2O]}{VDC}])$$

d. Pressure - Inches of water to Pascals:

$$P[Pa] = (P_{inH_2O})(248.84[\frac{Pa}{inH_2O}])$$

e. Pressure – Inches of Mercury to Pascals:

$$P[Pa] = (P_{inHg})(3386.388[\frac{Pa}{inHg}])$$

2. Reynolds Number ($Re_{Dh)}$

a. Reynolds number based on hydraulic diameter:

$$\mathrm{Re}_{D_h} = \frac{\rho \bar{U} D_h}{\mu}$$

b. Hydraulic diameter:

$$D_h[m] = \frac{4V_{open}}{A_{wf}}$$

c. Average fluid velocity:

$$\bar{U}[\frac{m}{\sec}] = \frac{\dot{m}}{\rho \bar{A}}$$

d. Dynamic viscosity using Sutherland Law:

$$\mu[Pa - \sec] = \mu_0 \left(\frac{(T_{in} + T_{out})/2}{T_0} \right)^{3/2} \left(\frac{T_0 + S}{(T_{in} + T_{out})/2 + S} \right)$$

where: $T_0 = 273.15K,\ S_{air} = 110.4K,\ \mu_0 = 1.71E-5\ \frac{kg}{m \cdot s}$

e. Density averaged over entire heat exchanger:

$$\rho[\frac{kg}{m^3}] = (\frac{P_{dens}}{R(T_{in} + T_{out})/2})$$

f. Open fluid volume of heat exchanger:

$$V_{open}[m^3] = (LWH) - (\frac{N_p \pi D_{pin}^2 H}{4})$$

* This equation is for the cylindrical shaped pins.

$$V_{open}[m^3] = (LWH) - N_p[(\frac{\pi D_{pin}^2 H}{8}) + (\frac{0.05 * DH}{2})]$$

* This equation is for the teardrop shaped pins.

g. Wetted area for flow (includes endwalls):

$$A_{wf}[m^2] = 2\left(LW + HL - \frac{45\pi D^2}{4} \right) + 45\pi DH$$

* This equation is for the cylindrical shaped pins.

$$A_{wf}[m^2] = 2\left(LW + HL - N_p[(\frac{\pi D^2}{8}) - (\frac{0.05D}{2})] \right) + N_p[(\frac{\pi DH}{2}) + (2H(0.5^2 * 0.0165^2)^{0.5})]$$

* This equation is for the teardrop shaped pins.

h. System mass flow rate:

$$\dot{m}[\frac{kg}{\sec}] = \dot{Q}_{measured} \rho$$

i. Average flow area:

$$\bar{A}[m^2] = \frac{V_{open}}{L}$$

j. Final Reynolds number after substitution:

$$\mathrm{Re}_{D_h} = \frac{P_{turb}\dot{Q}_{measured}D_h}{R((T_{in}+T_{out})/2)\bar{A}\mu}$$

3. Heat Transfer Coefficient (h)

a. Heat transfer coefficient:

$$h[\frac{W}{m^2-K}] = \frac{q}{(\Delta T_{lm})(A_{wh})}$$

b. Heat transfer rate:

$$q[Watts] = \dot{m}C_p(T_{outave} - T_{in})$$

c. Log mean bulk differential temperature:

$$\Delta T_{lm}[K] = \frac{(T_{wall}-T_{in})-(T_{wall}-T_{out})}{\ln\left(\frac{T_{wall}-T_{in}}{T_{wall}-T_{out}}\right)}$$

d. Wetted area for heat calculations (no endwalls):

$$A_{wh}[m^2] = 2\left(LW - \frac{N_p\pi D^2}{4}\right) + N_p\pi DH$$

* This equation is for the cylindrical shaped pins.

$$A_{wh}[m^2] = 2\left(LW - N_p[(\frac{\pi D^2}{8}) + (\frac{0.05D}{2})]\right) + N_p[(\frac{\pi DH}{2}) + (2H(0.5^2 * 0.0165^2)^{0.5})]$$

* This equation is for the teardrop shaped pins.

e. System mass flow rate:

$$\dot{m}[\frac{kg}{\sec}] = \dot{Q}_{measured}\rho$$

4. Nusselt Number (Nu_{Dh})

a. Nusselt number based on hydraulic diameter

$$Nu_{D_h} = \frac{\overline{h}_{array} D_h}{k}$$

b. Average heat transfer coefficient for the heat exchanger array:

$$\overline{h}_{array}[\frac{watts}{m^2 - K}] = \frac{q}{A_{wh}\Delta T_{lm}}$$

c. Hydraulic diameter, D_h, is the same as for Reynolds number:

$$D_h[m] = \frac{4V_{open}}{A_{wf}}$$

d. Open fluid volume of heat exchanger:

$$V_{open}[m^3] = (LWH) - (\frac{N_p \pi D_{pin}^2 H}{4})$$

* This equation is for the cylindrical shaped pins.

$$V_{open}[m^3] = (LWH) - N_p[(\frac{\pi D_{pin}^2 H}{8}) + (\frac{0.05 * DH}{2})]$$

* This equation is for the teardrop pins.

e. Wetted area for flow (includes endwalls):

$$A_{wf}[m^2] = 2\left(LW + HL - \frac{45\pi D^2}{4}\right) + 45\pi DH$$

* This equation is for the cylindrical shaped pins.

$$A_{wf}[m^2] = 2\left(LW + HL - N_p[(\frac{\pi D^2}{8}) + (\frac{0.05D}{2})]\right) + N_p[(\frac{\pi DH}{2}) + (2H(0.5^2 * 0.0165^2)^{0.5})]$$

* This equation is for the teardrop shaped pins.

f. Log mean bulk differential temperature:

$$\Delta T_{lm}[K] = \frac{(T_{wall} - T_{in}) - (T_{wall} - T_{out})}{\ln\left(\frac{T_{wall} - T_{in}}{T_{wall} - T_{out}}\right)}$$

g. Wetted area for heat calculations (no endwalls):

$$A_{wh}[m^2] = 2\left(LW - \frac{N_p \pi D^2}{4}\right) + N_p \pi DH$$

* This equation is for the cylindrical shaped pins.

$$A_{wh}[m^2] = 2\left(LW - N_p[(\frac{\pi D^2}{8}) + (\frac{0.05D}{2})]\right) + N_p[(\frac{\pi DH}{2}) + (2H(0.5^2 * 0.0165^2)^{0.5})]$$

* This equation is for the teardrop shaped pins.

h. System mass flow rate:

$$\dot{m}[\frac{kg}{\sec}] = \dot{Q}_{measured}\rho$$

5. Friction Factor (f)

a. Friction factor:

$$f = \frac{\Delta P_{HX} D_h}{\frac{1}{2}\rho \bar{U}^2 L}$$

b. Differential pressure across CHE:

$$\Delta P_{HX} = \Delta P_{measured} - P_{off}$$

c. Hydraulic diameter, D_h, is the same as for Reynolds number:

$$D_h[m] = \frac{4V_{open}}{A_{wf}}$$

d. Open fluid volume of CHE:

$$V_{open}[m^3] = (LWH) - (\frac{N_p \pi D_{pin}^2 H}{4})$$

* This equation is for the cylindrical shaped pins.

$$V_{open}[m^3] = (LWH) - N_p[(\frac{\pi D_{pin}^2 H}{8}) + (\frac{0.05 * DH}{2})]$$

* This equation is for the teardrop pins.

e. Wetted area for flow (includes endwalls):

$$A_{wf}[m^2] = 2\left(LW + HL - \frac{45\pi D^2}{4}\right) + 45\pi DH$$

* This equation is for the cylindrical shaped pins.

$$A_{wf}[m^2] = 2\left(LW + HL - N_p[(\frac{\pi D^2}{8}) + (\frac{0.05D}{2})]\right) + N_p[(\frac{\pi DH}{2}) + (2H(0.5^2 * 0.0165^2)^{0.5})]$$

* This equation is for the teardrop shaped pins.

f. Density taken at exit of heat exchanger:

$$\rho[\frac{kg}{m^3}] = (\frac{P_{dens}}{RT})$$

g. Average fluid velocity:

$$\bar{U}[\frac{m}{\sec}] = \frac{\dot{m}}{\rho \bar{A}}$$

h. System mass flow rate:

$$\dot{m}[\frac{kg}{\sec}] = \dot{Q}_{measured}\rho$$

i. Average flow area:

$$\bar{A}[m^2] = \frac{V_{open}}{L}$$

6. Frictional Power Expenditure (E)

a. Frictional power expenditure:

$$E[\frac{watts}{m^2}] = \frac{\dot{Q}_{measured}\Delta P_{HX}}{A_{wf}}$$

b. Differential pressure across heat exchanger:

$$\Delta P_{HX} = \Delta P_{measured} - P_{off}$$

c. Wetted area for flow (includes endwalls):

$$A_{wf}[m^2] = 2\left(LW + HL - \frac{45\pi D^2}{4} \right) + 45\pi DH$$

* This equation is for the cylindrical shaped pins.

$$A_{wf}[m^2] = 2\left(LW + HL - N_p[(\frac{\pi D^2}{8}) - (\frac{0.05D}{2})] \right) + N_p[(\frac{\pi DH}{2}) + (2H(0.5^2 * 0.0165^2)^{0.5})] *$$

* This equation is for the teardrop shaped pins.

THIS PAGE INTENTIONALLY LEFT BLANK

APPENDIX D. UNCERTAINTY ANALYSIS

The method from Kline and McClintock (1953) was used to determine the uncertainty of measured and calculated parameters. The analysis will be calculated for the Reynolds number, Nusselt number, and friction factor. The governing equation is as follows:

$$W_R = \left[\left(\frac{\partial R}{\partial x_1} W_1 \right)^2 + \left(\frac{\partial R}{\partial x_2} W_2 \right)^2 + \cdots + \left(\frac{\partial R}{\partial x_n} W_n \right)^2 \right]^{1/2}$$

Where:

R is a given function of the independent variables x_1, x2,…x_n.

W_R is the uncertainty.

1. Reynolds Number

$$\mathrm{Re}_{D_h} = \frac{\rho \bar{U} D_h}{\mu}$$

$$\frac{W \mathrm{Re}_{D_h}}{\mathrm{Re}_{D_h}} = \sqrt{\left(\frac{W_\rho}{\rho} \right)^2 + \left(\frac{W_{Dh}}{D_h} \right)^2 + \left(\frac{W_{\bar{U}}}{\bar{U}} \right)^2}$$

The uncertainty associated with the Reynolds number is based on density, average fluid velocity, hydraulic diameter, and dynamic viscosity. The dynamic viscosity will be treated as a constant and the other three variables will be analyzed.

a. Density

$$\frac{W_\rho}{\rho} = \left[\left(\frac{W_p}{p} \right)^2 + \left(\frac{W_T}{T} \right)^2 \right]^{1/2} = \left[\left(\frac{1.0025}{101325} \right)^2 + \left(\frac{0.5}{310} \right)^2 \right]^{1/2} = 0.0016$$

- 1.0025 represents the 0.25% error associated with the pressure transducer.

- 0.5 K represents the error associated with the thermocouples.
- 101325 Pascals represents maximum pressure.
- 310 K represents max heater temperature.

b. Hydraulic Diameter

$$\frac{W_{Dh}}{D_h} = \left[\left(\frac{W_{Vopen}}{V_{open}} \right)^2 + \left(\frac{W_{Aw}}{A_w} \right)^2 \right]^{1/2}$$

Where,

$$\frac{W_{Vopen}}{V_{open}} = \left[\left(\frac{W_x}{x} \right)^2 + \left(\frac{W_y}{y} \right)^2 + \left(\frac{W_z}{z} \right)^2 \right]^{1/2} = \left[\left(\frac{3}{500} \right)^2 + \left(\frac{1}{250} \right)^2 + \left(\frac{0.5}{33} \right)^2 \right]^{1/2} = 0.017$$

and

$$\frac{W_{Aw}}{A_w} = \left[\left(\frac{W_x}{x} \right)^2 + \left(\frac{W_y}{y} \right)^2 \right]^{1/2} = \left[\left(\frac{3}{500} \right)^2 + \left(\frac{1}{250} \right)^2 \right]^{1/2} = 0.007$$

therefore,

$$\frac{W_{Dh}}{D_h} = \left[\left(\frac{W_{Vopen}}{V_{open}} \right)^2 + \left(\frac{W_{Aw}}{A_w} \right)^2 \right]^{1/2} = 0.018$$

- 3mm/500mm represents the uncertainty in length in the X-direction.
- 1mm/250mm represents the uncertainty in length in the Y-direction.
- 0.5mm/33mm represents the uncertainty in length in the Z-direction.

c. Average Fluid Velocity

$$\frac{W_{\bar{U}}}{\bar{U}} = \left[\left(\frac{W_{\dot{Q}}}{\dot{Q}} \right)^2 + \left(\frac{W_{\bar{A}}}{\bar{A}} \right)^2 \right]^{1/2}$$

where,

$$\frac{W_{\dot{Q}}}{\dot{Q}} = \left[\left(\frac{W_V}{V_f} \right)^2 \right]^{1/2} = \left[\left(\frac{0.015}{300} \right)^2 \right]^{1/2} = 0.00005$$

and

$$\frac{W_{\bar{A}}}{\bar{A}} = \left[\left(\frac{W_{Vopen}}{V_{open}} \right)^2 + \left(\frac{W_L}{L} \right)^2 \right]^{1/2} = \left[(0.017)^2 + (0.006)^2 \right]^{1/2} = 0.018$$

therefore,

$$\frac{W_{\bar{U}}}{\bar{U}} = \left[\left(\frac{W_{\dot{Q}}}{\dot{Q}} \right)^2 + \left(\frac{W_{\bar{A}}}{\bar{A}} \right)^2 \right]^{1/2} = \left[(0.00005)^2 + (0.018)^2 \right]^{1/2} = 0.018$$

- 0.015 represent the 1.5% uncertainty associated with the Omega FMA-1844 mass flow meter.
- 0.017 represents the total uncertainty of the open volume.
- 0.018 represents the total uncertainty of the average flow area.

d. Reynolds Number Uncertainty

$$\frac{W_{\mathrm{Re}_{Dh}}}{\mathrm{Re}_{Dh}} = \left[\left(\frac{W_\rho}{\rho} \right)^2 + \left(\frac{W_{Dh}}{D_h} \right)^2 + \left(\frac{W_{\bar{U}}}{\bar{U}} \right)^2 \right]^{1/2} = \left[(0.0016)^2 + (0.018)^2 + (0.018)^2 \right]^{1/2} = 0.0255$$

- Based on maximum flow the max uncertainty is 2.55%. This number would decrease as flow decreased.

2. Nusselt Number

$$Nu_{Dh} = \frac{hD_h}{k},$$

Where,

$$h = \frac{q}{A_w \Delta T_{lm}}$$

therefore,

$$\frac{W_{Nu_{Dh}}}{Nu_{Dh}} = \left[\left(\frac{W_h}{h} \right)^2 + \left(\frac{W_{Dh}}{D_h} \right)^2 \right]^{1/2}$$

and

$$\frac{W_h}{h} = \left[\left(\frac{W_q}{q} \right)^2 + \left(\frac{W_{Aw}}{A_w} \right)^2 + \left(\frac{W_{\Delta T_{lm}}}{\Delta T_{lm}} \right)^2 \right]^{1/2}$$

The uncertainties for hydraulic diameter, heat transfer rate, wetted surface area and bulk log mean differential temperature must be determined. Thermal conductivity will be assumed constant and the values of hydraulic diameter and wetted surface area will be the same as for the Reynolds number.

$$\frac{W_{Dh}}{D_h} = \left[\left(\frac{W_{Vopen}}{V_{open}} \right)^2 + \left(\frac{W_{Aw}}{A_w} \right)^2 \right]^{1/2} = 0.018$$

and

$$\frac{W_{Aw}}{A_w} = \left[\left(\frac{W_x}{x} \right)^2 + \left(\frac{W_y}{y} \right)^2 \right]^{1/2} = \left[\left(\frac{3}{500} \right)^2 + \left(\frac{1}{250} \right)^2 \right]^{1/2} = 0.007$$

a. Heat Transfer Rate

$$\frac{W_q}{q} = \left[\left(\frac{W_q}{q} \right)^2 \right]^{1/2} = \frac{8.387}{600} = 0.014$$

- 8.387 is based on how long each heater is on during a given cycle. The total run time is 10 minutes or 600 seconds.

b. Bulk Differential Log Mean Temperature

$$\frac{W \Delta T_{lm}}{\Delta T_{lm}} = \frac{0.5K}{10.5} = 0.0476$$

- 0.5 (k) represents the uncertainty of each thermocouple and the max bulk differential temperature observed was approximately 10.5K.

c. Nusselt Number Uncertainty

$$\frac{W_{Nu_{Dh}}}{Nu_{Dh}} = \left[\left(\frac{W_q}{q} \right)^2 + \left(\frac{W_{Aw}}{A_w} \right)^2 + \left(\frac{W_{\Delta T_{lm}}}{\Delta T_{lm}} \right)^2 + \left(\frac{W_{Dh}}{D_h} \right)^2 \right]^{1/2} =$$

$$\left[(0.007)^2 + (0.007)^2 + (0.0476)^2 + (0.018)^2 \right]^{1/2} = 0.0518$$

- The overall uncertainty for the Nusselt number is 5.18%. This number can increase as the bulk differential mean temperature decreases.

3. Friction Factor

$$f = \frac{2\Delta p D_h}{\rho \bar{U}^2 L},$$

$$\frac{W_f}{f} = \left[\left(\frac{W_{\Delta p}}{\Delta p} \right)^2 + \left(\frac{W_{Dh}}{D_h} \right)^2 + \left(\frac{W_\rho}{\rho} \right)^2 + \left(\frac{W_L}{L} \right)^2 \right]^{1/2}$$

The uncertainty of friction factor is based on heat exchanger differential pressure, hydraulic diameter, density, heat exchanger length, and average fluid velocity. All except the differential pressure have been determined and are as follows:

$$\frac{W_{Dh}}{D_h} = \left[\left(\frac{W_{Vopen}}{V_{open}} \right)^2 + \left(\frac{W_{Aw}}{A_w} \right)^2 \right]^{1/2} = 0.018$$

$$\frac{W_\rho}{\rho} = \left[\left(\frac{W_p}{p} \right)^2 + \left(\frac{W_T}{T} \right)^2 \right]^{1/2} = \left[\left(\frac{1.0025}{101325} \right)^2 + \left(\frac{0.5}{310} \right)^2 \right]^{1/2} = 0.0016$$

$$\frac{W_L}{L_x} = \left[\left(\frac{W_x}{x} \right)^2 \right]^{1/2} = \left[\left(\frac{3}{500} \right)^2 \right]^{1/2} = 0.006$$

$$\frac{W_{\bar{U}}}{\bar{U}} = \left[\left(\frac{W_{\dot{Q}}}{\dot{Q}} \right)^2 + \left(\frac{W_{\bar{A}}}{\bar{A}} \right)^2 \right]^{1/2} = \left[(0.00005)^2 + (0.018)^2 \right]^{1/2} = 0.018$$

a. Differential Pressure

$$\frac{W_{\Delta p}}{\Delta p} = \left[\left(\frac{0.498Pa}{\Delta p}\right)^2\right]^{1/2} = \frac{0.498Pa}{\Delta p}$$

b. Friction Factor Uncertainty

$$\frac{W_f}{f} = \left[\left(\frac{W_{\Delta p}}{\Delta p}\right)^2 + \left(\frac{W_{Dh}}{D_h}\right)^2 + \left(\frac{W_\rho}{\rho}\right)^2 + \left(\frac{W_L}{L}\right)^2 + \frac{W_{\bar{U}}}{\bar{U}}\right]^{1/2} =$$

$$\left[\left(\frac{1.24Pa}{\Delta p}\right)^2 + (0.018)^2 + (0.0016)^2 + (0.006)^2 + (0.018)^2\right]^{1/2}$$

$$= 0.145 - 1.00$$

- The uncertainty for friction factor can be from 14.5% at the high end to 100% at the low end of the flow range.

APPENDIX E. EQUIPMENT LIST

1) Omega differential pressure transducer, model PX653-25D5V
2) Omega mass flow meter, model FMA-1844 with attached LCD display
3) Pentium III IBM compatible computer with Microsoft Windows 2000 based operating system
4) PC to HP 3852A interface card
5) Hewlett Packard 3852A data acquisition unit
6) HP3852A control modules
7) G Relay board and Relays by Grayhill; 24 channel rack, # 70GRCQ24 and G5 Modules, #70G-OAC5
8) HP interface ribbon cable for relay board
9) SOLA Electric 120VAC constant voltage power supply, model LR 44590
10) Bush Samos 10 hp, 388 cfm regenerative blower, model FBC3388.6
11) The Merriam Instrument Company 0-4” inclined manometer, model 40HA10
12) National Instruments LabVIEW software
13) Omega precision Type E fine wire thermocouples
14) Watlow 120 VAC 50 Watt heaters, part number 0241C-14
15) Digital power meter by Brand Electronics, Model 20-1850/CI
16) 6061 T6 aluminum metal for plates and pin construction
17) Plexiglas ducting
18) PVC piping and transition pieces (0.5” to 2.5”)
19) Stainless steel piping and fittings (0.5”)
20) 3/16 inch non-fluted wooden dowel

THIS PAGE INTENTIONALLY LEFT BLANK

APPENDIX F. EQUIPMENT SPECIFICATIONS AND CALIBRATION DATA

1. Blower

Figure (99) shows the Busch Samos Regenerative Blower model FBC 3388.6. Normal operating parameters are 450 VAC, 10 amps, and 0 hp with a max capacity of 388 CFM. Figure (100) shows the pump curve for this blower.

Figure 99. Busch Samos regenerative blower

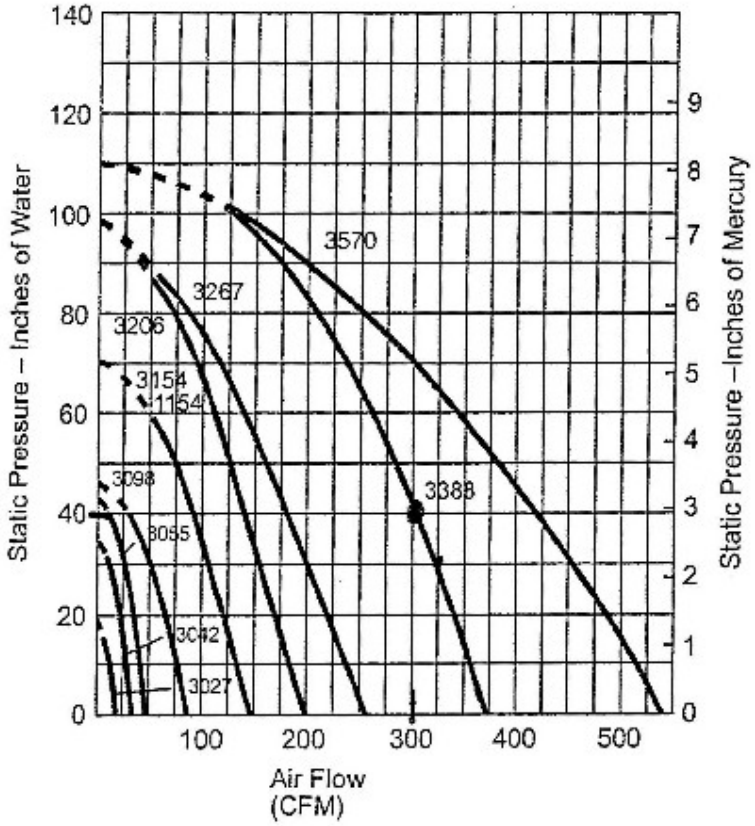

Figure 100. Blower pump curve, manufacturer data

2. Mass Flow Meter: Omega FMA-1844

The normal range of operation is 0 – 500 SLPM. The meter operated on a 12 VDC power supply and is accurate to 1.5% of full scale. Data was read directly off of the LCD display mounted on the flow meter (Figure 101) and input into LabVIEW. Omega Engineering performed the initial calibration.

Figure 101. Typical Omega FMA-1800 series flow meter with LCD display

3. Differential Pressure Transmitter: Omega PX653-25D5V

The differential pressure transducer shown in Figure (102) operates on a 24 VDC power supply and has an accuracy of 0.25% full scale. Omega Engineering performed the initial calibration and a calibration was performed locally using an inclined manometer. Figure (103) shows the relationship between differential pressure measured in inches of water and the differential pressure transducer output shown in VDC.

Figure 102. Omega PX653-25D5V differential pressure transducer

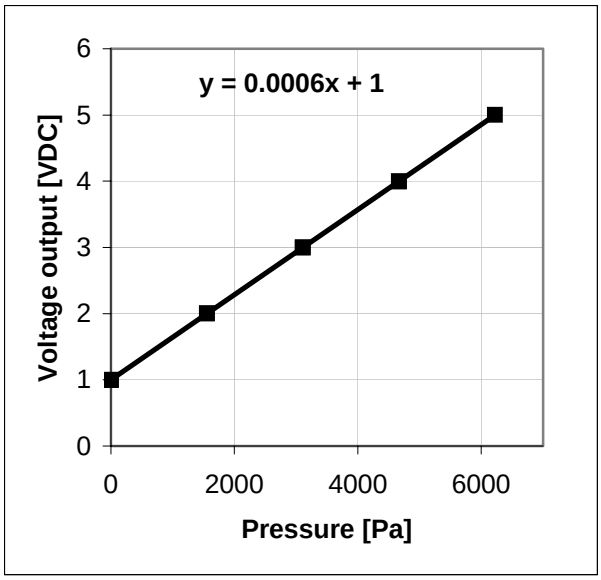

Figure 103. Plot of calibration data for differential pressure transducer

4. Thermocouples, Heaters and Digital Power Meter

There were a total of 20 heaters used for the heat exchanger. Watlow manufactured each 50-watt heater. Each heater was calibrated separately and then as a unit against a power meter made by Brand Electronics. The power meter (Figure 104) monitored the power supply to the heater assembly and showed that each heater used 50 watts of power and when all were energized that 1000 watts were consumed.

Figure 104. Digital power meter

The most efficient way to measure the accuracy of the thermocouple, heaters, (Figure 105) and relays was to gather the empirical data of various sub-runs and calculate the heat transfer rate based on mass flow rate, specific heat capacity, and differential

temperature across the heat exchanger. The heat transfer rate calculated by the method above should equal the heat transfer rate calculated by multiplying the average time the heaters were on by the number of heaters that were on by 50 watts per heater ($q_{electric}$). In order to compare the two numbers a no-load sub-run was performed to determine the losses to ambient. Once the losses were determined then the no-load number was subtracted from $q_{electric}$ and compared to the calculated heat transfer rate. On the vast majority these methods agreed within eight percent, which was acceptable. Table (6) shows results from the 16.5mm set #1 data run. This agreement gives confidence to the overall system performance as well as the heat transfer characteristics derived.

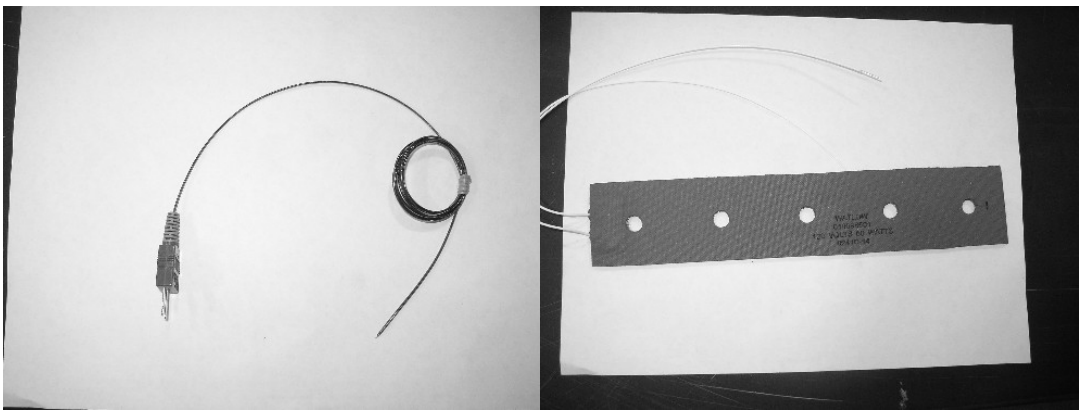

Figure 105. Omega type E thermocouple and Watlow 50-watt heater

.

Table 6. Comparison of heat rate calculations, 16.5mm set #1

Reynolds number	Channel 20 inlet temperature K	Channel 21-24 outlet temperature K	Specific heat capacity J/kg K	Mass flow rate kg/sec	Calculated heat rate	No load heat rate	heat rate electric	Net electric heat rate (electric - no load)	%difference between net electric heat rate and calculated heat rate
15	294.18714	301.164931	1005	0.0003	2.065424	34.2782	36.331	2.052759	0.6131608
30	294.42996	301.840819	1005	0.0006	4.3774	34.2782	39.0165	4.738259	8.2436821
50	294.51347	302.455392	1005	0.001	7.802585	34.2782	42.0955	7.817259	0.1880677
80	294.59422	302.97	1005	0.0016	13.14629	34.2782	45.0897	10.81144	17.760575
155	294.78343	302.78	1005	0.003	24.31688	34.2782	57.0524	22.77417	6.344213
230	295.014	302.49	1005	0.0045	33.78664	34.2782	65.4636	31.18541	7.6989809
320	295.33033	302.23	1005	0.0063	43.32933	34.2782	78.1319	43.85363	1.2100313

APPENDIX G. REPEATABILITY ANALYSIS

An analysis was conducted to verify that results obtained were repeatable. Two data runs were repeated after all runs per Table (1) were completed. 33mm set #1 and set #2 were repeated to verify that results were repeatable and reliable. Figures (106-109) show the results of the repeatability check for 33mm set #1. As can be seen, the data collected for the repeat run fell almost perfectly on top of the original data. Figures (110-113) show the repeatability results for 33mm set #2. Again, the results are very encouraging and give confidence to the fact that results are repeatable, and results obtained are very reliable.

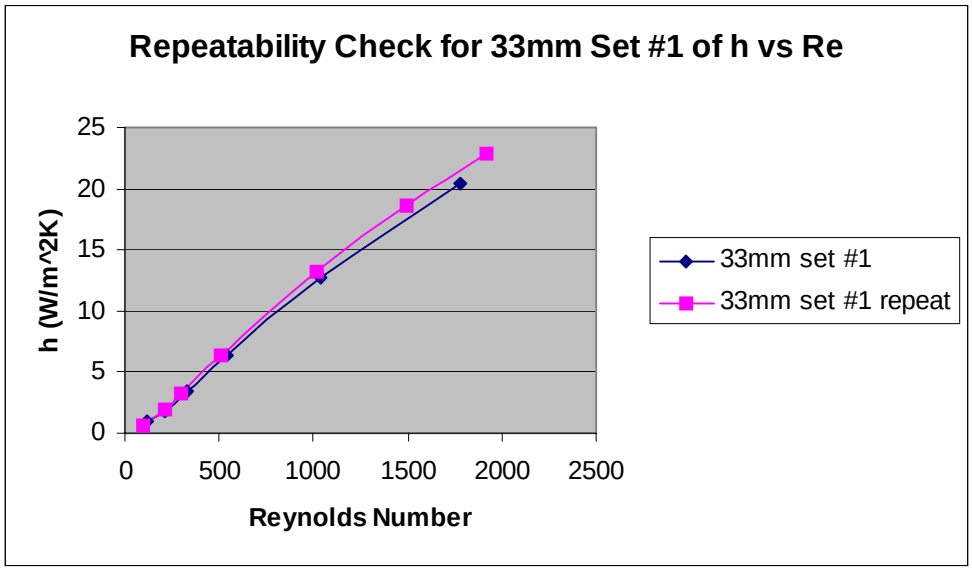

Figure 106. Plot of h vs. Re, 33mm set #1, repeatability check

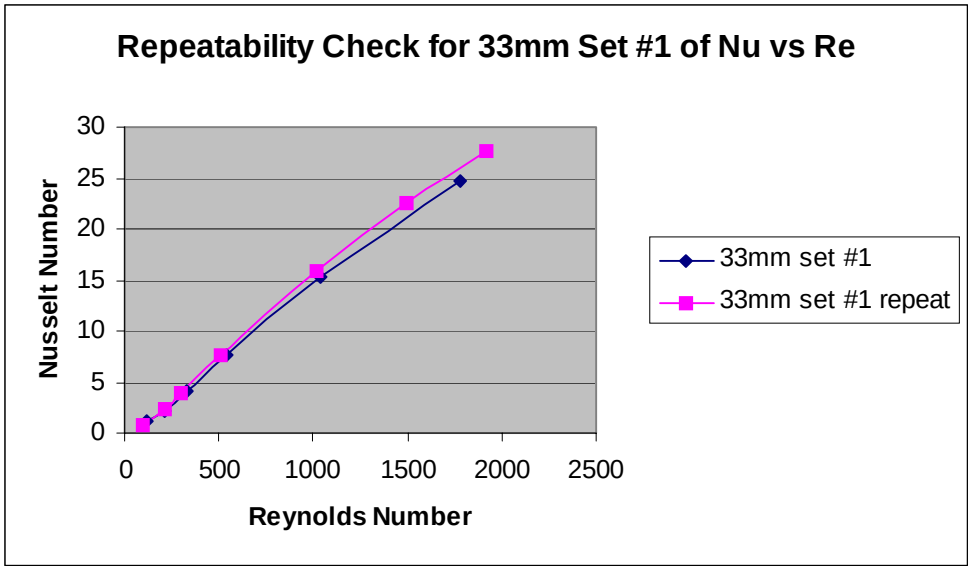

Figure 107. Plot of Nu vs. Re, 33mm set #1, repeatability check

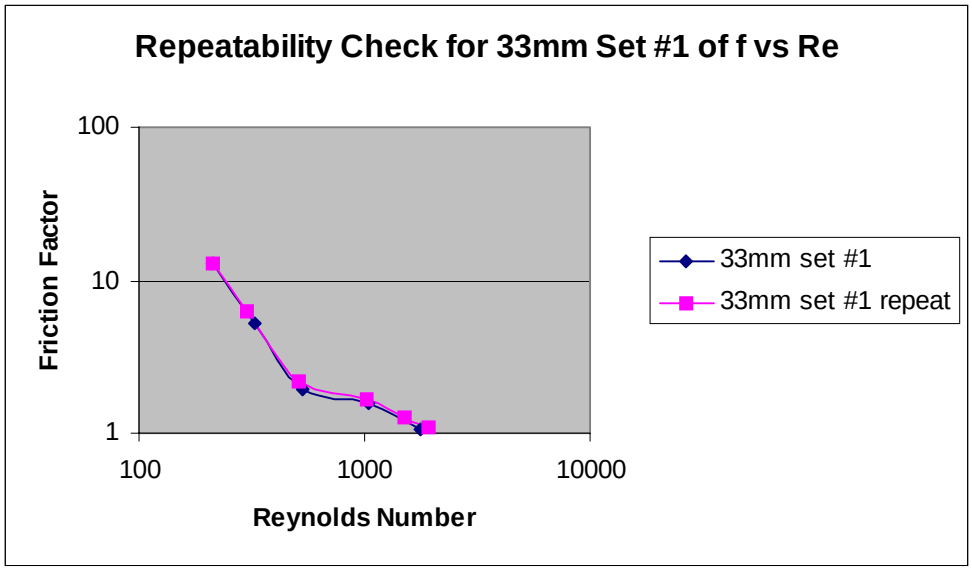

Figure 108. Plot of f vs. Re, 33mm set #1, repeatability check

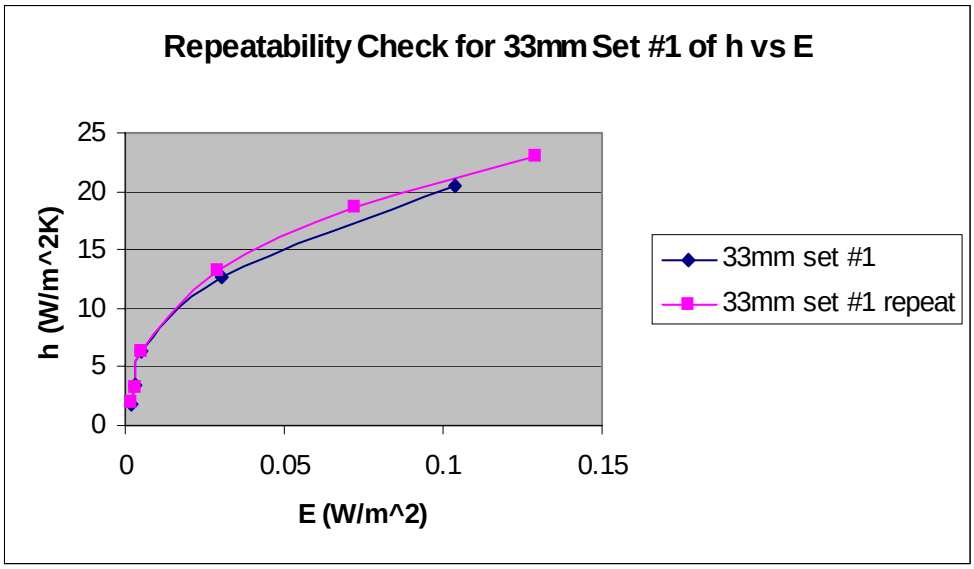

Figure 109. Plot of h vs. E, 33mm set #1, repeatability check

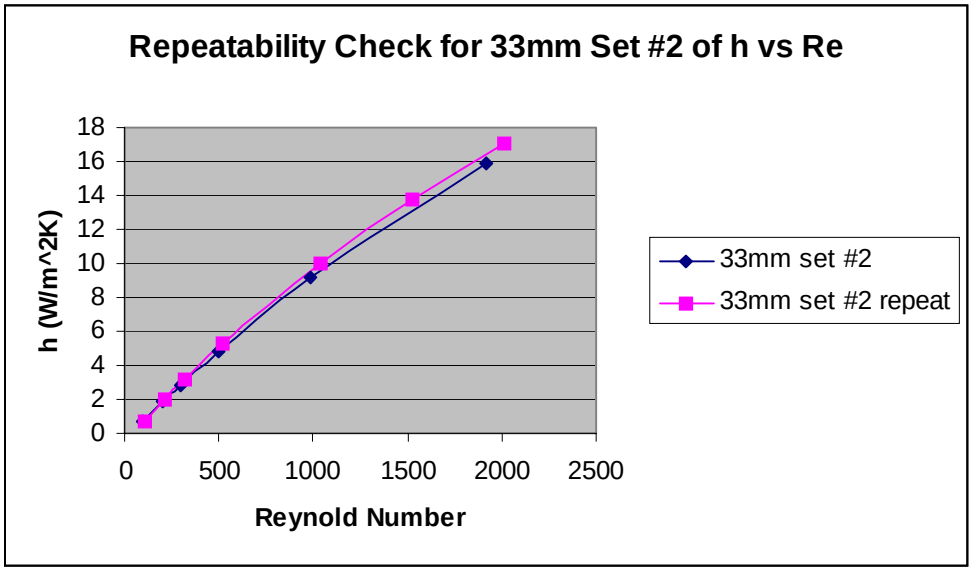

Figure 110. Plot of h vs. Re, 33mm set #2, repeatability check

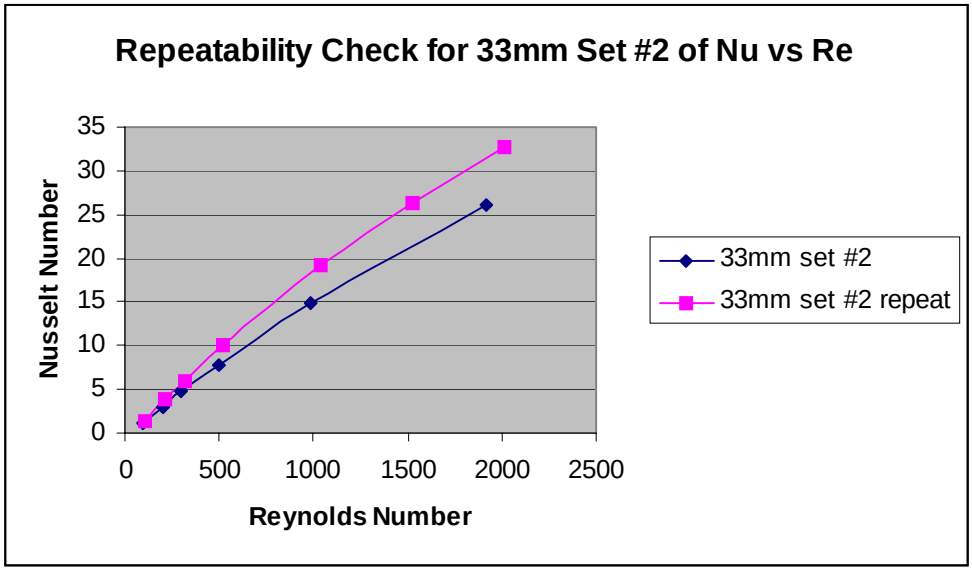

Figure 111. Plot of Nu vs. Re, 33mm set #2, repeatability check

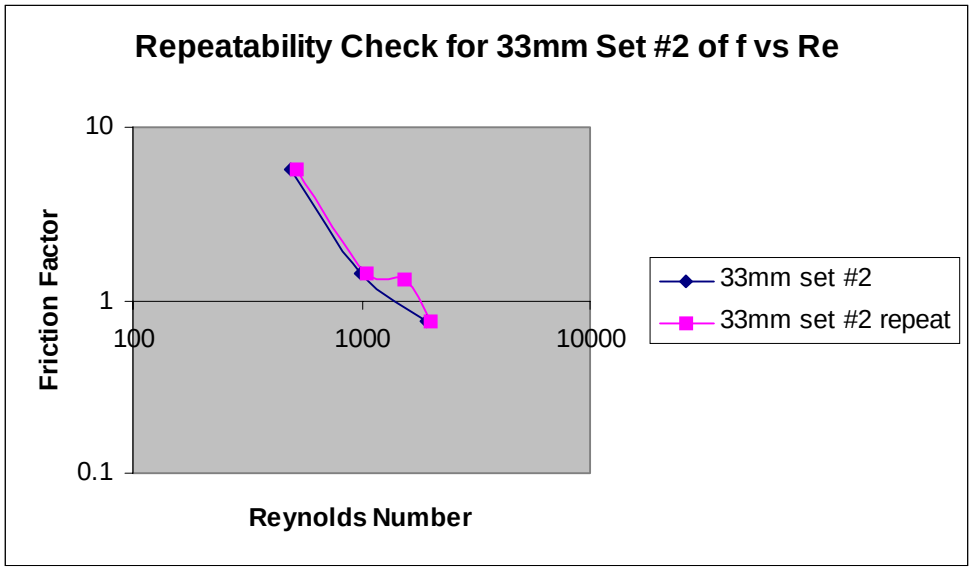

Figure 112. Plot of f vs. Re, 33mm set #2, repeatability check

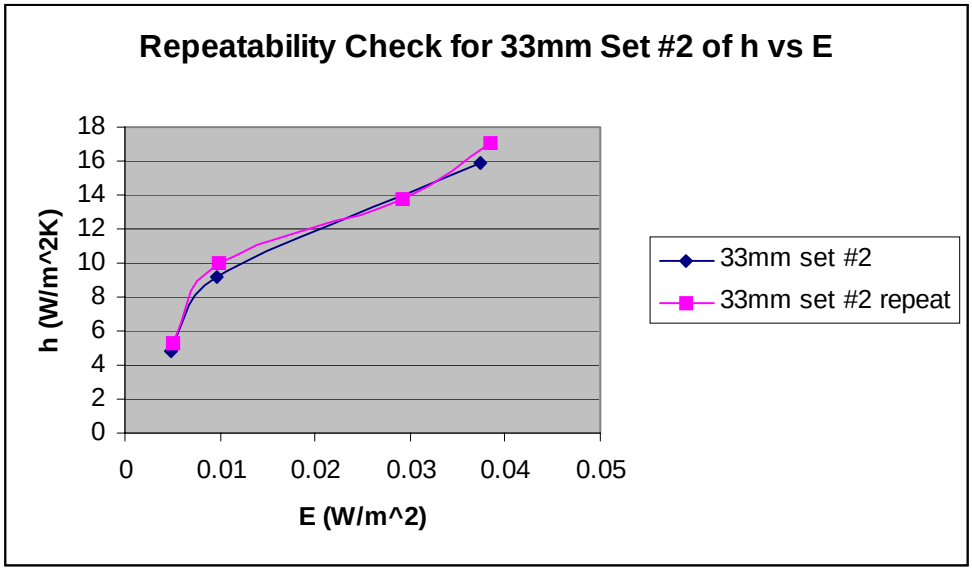

Figure 113. Plot of h vs. E, 33mm set #2, repeatability check

THIS PAGE INTENTIONALLY LEFT BLANK

LIST OF REFERENCES

Adametz, D.S., *Numerical Analysis of Heat Exchanger Performance for a Staggered Short Pin-Fin Array*, Naval Postgraduate School, Monterey, California, 2001.

Al Dabagh, A. M., and Andrews, G.E., "Pin-Fin Heat Transfer: Contributions of the Wall and the Pin to the Overall Heat Transfer," ASME Paper No. 92-GT-242, 1992.

Arora, S.C., and Abdel-Messeh, W., "Pressure Drop and Heat Transfer Characteristics of Circular and Oblong Low Aspect Ratio Pin Fins," AGARD Conference Proceedings, pp.4-1-4-15, 1985.

Boulares, J., *Numerical And Experimental Study Of The Performance Of A Drop-Shaped Pin Fin Heat Exchanger*, Naval Postgraduate School, Monterey, California, 2003.

Chyu, M.K., "Heat Transfer and Pressure Drop for Short Pin-Fin Arrays with Pin-Endwall Fillet," *ASME J. of Heat Transfer*, Vol. 112, pp. 926-932, 1990.

Chyu, M.K., Hsing, Y.C., Shih, T. I.-P., and Natarajan, V., "Heat Transfer Contributions of Pins and Endwall in Pin-Fin Arrays: Effects of Thermal Boundary Condition Modeling," *ASME J. of Turbomachinery*, Vol. 121, pp. 257-263, 1999.

Donahoo, E.E., Camci, C., Kulkarni, A.K., and Belegundu, A.D., "Determination of Optimal Row Spacing for a Staggered Cross-Pin Array in a Turbine Blade Cooling Passage," *Enhanced Heat Transfer*, Vol. 8, pp. 41-53, 2001.

Hamilton, L.J., *Numerical Analysis of the Performance of a Staggered Cross-Pin Array Heat exchanger*, Naval Postgraduate School, Monterey, California, 2003.

Incropera, F.P. and DeWitt, D.P., *Introduction to Heat Transfer*, 3rd Ed., Wiley, New York, 1996.

Jubran, B.A., Hamdan, M.A., Abdualh, R.M., "Enhanced Heat Transfer, Missing Pin, and Optimization for Cylindrical Pin Fin Arrays", *ASME J. of Heat Transfer*, Vol. 115, pp. 576-583, 1993.

Kline, S.J. and McClintock, F.A., "Describing Uncertainties in Single Sample Experiments," *Mechanical Engineering*, Vol. 75, pp. 3 - 8, 1953.

Li, Q., Chen, Z., Flechtner, U., Warnecke, H.-J., "Heat Transfer and Pressure Drop Characteristics in Rectangular Channels with Elliptic Pin Fins," *Int. J. of Heat and Fluid Flow*, Vol 19, pp. 245-250, 1998.

Metzger, D.E., Berry, R.A., Bronson, J.P., "Developing Heat Transfer in Rectangular Ducts With Staggered Arrays of Short Pin Fins," *ASME J. of Heat Transfer*, Vol. 104, pp. 700-706, 1982.

Ramthun, D., *An Experimental Study of a Pin-Fin Heat Exchanger,* Naval Postgraduate School, Monterey, California, 2003.

Rose, G.D., *Design and Fabrication of a Short Pin-Fin Micro-Heat Exchanger*, Naval Post Graduate School, Monterey, California, 2004.

Roussakies, J.C., *An Experimental Study of the Performance of a Pin-Fin Micro-Heat Exchanger,* Naval Post Graduate School, Monterey, California, 2004.

Shah, R. K., "Advances in Numerical Analysis of Heat Transfer and Flow Friction Characteristics of Compact Heat Exchangers Surfaces," International Centre for Heat and Mass Transfer, Session 13, www.ichmt.org/abstracts/CHT-97/session13.html.

Sparrow, E.M., Stahl, T.J., and Traub, P., "Heat Transfer Adjacent to the attached end of a Cylinder in Crossflow," *Int. J. of Heat and Mass Transfer*, Vol. 25, pp. 233-242, 1984

Summers, J.W., *An Empirical Study of a Pin-Fin Heat Exchanger in Laminar and Turbulent Flow,* Naval Post Graduate School, Monterey, California, 2003.

VanFossen, G.J., "Heat Transfer Coefficient for Staggered Arrays of Short Pin Fins," *ASME J. of Engineering for Power*, Vol. 104, pp. 268-274, 1982.

White, F. M., *Fluid Mechanics*, McGraw-Hill, Inc., 4th Ed., 1999.

INITIAL DISTRIBUTION LIST

1. Defense Technical Information Center
   Ft. Belvoir, Virginia

2. Dudley Knox Library
   Naval Postgraduate School
   Monterey, California

3. Professor Ashok Gopinath
   Naval Postgraduate School
   Monterey, California

4. LT Matthew T. Harding
   Naval Postgraduate School
   Monterey, California